5-3-2016

Real-Time Hybrid Substructuring For System Level Vibration Testing Of Mechanical Equipment

Joseph A. Franco III
University of Connecticut, joseph.franco@uconn.edu

Real-Time Hybrid Substructuring For System Level Vibration Testing Of Mechanical Equipment

Joseph A Franco III, PhD

University of Connecticut, 2016

Vibration of mechanical equipment in structures can result in fatigue, detection, and/or environmental concerns. Numerical simulation of these mechanical/structural systems to verify the system meets these performance requirements can be difficult and can require full system testing. During the design phase of a system, however, the mechanical portion of the system may be pre-existing and can be physically tested while the support structure is still existent as a computer aided design concept which can be numerically simulated. The challenge in verifying the full system meets performance requirements is to accurately combine the physical and numerical substructures. One forma of substructuring, where physical and numerical substructures are combined for dynamic testing in real-time as a feedback loop, is called real-time hybrid substructuring. This research proposes to extend and demonstrate RTHS for the system level vibration testing of mechanical equipment.

The overall approach to extend RTHS for system level vibration testing of mechanical equipment involves the analysis of the dynamics of a notional multiple degree of freedom (MDOF) mechanical system to demonstrate the need and application of RTHS for mechanical equipment and the implementation of compensation techniques for a uni-directional MDOF servo-hydraulic shake table serving as the transfer system to interface between the physical and numerical substructures. These research efforts will specifically address the unique challenges encountered in the application of RTHS to mechanical equipment including nonlinearities of the transfer system actuator dynamics due to low amplitude high bandwidth demands and the application of RTHS to lightly damped substructures. Experimental results demonstrate that RTHS accurately captures the system-level response and allows for repeatable tests of various dynamic conditions and potential system improvements to be efficiently examined.

Real-Time Hybrid Substructuring For System Level Vibration Testing Of Mechanical Equipment

Joseph Anthony Franco III

B.S., Clarkson University, 2006

M.E., Clarkson University, 2007

A Dissertation

Submitted in Partial Fulfillment of the

Requirements for the Degree of

Doctor of Philosophy

at the

University of Connecticut

2016

APPROVAL PAGE

Doctor of Philosophy Dissertation

Real-Time Hybrid Substructuring For System Level Vibration Testing Of Mechanical Equipment

Presented by

Joseph Anthony Franco III, B.S., M.E.

Major Advisor _____
Richard Christenson

Associate Advisor _____
Shinae Jang

Associate Advisor _____
Michael Accorsi

Associate Advisor _____
Jiong Tang

University of Connecticut
2016

ACKNOWLEDGEMENTS

In 2011, the opportunity to start as a doctoral student at the University of Connecticut became available to me through my employment at General Dynamics Electric Boat. Before this point, I hadn't given much thought to achieving higher levels of education than a Master's degree. Initially, I wasn't sure I was up to the challenge but through the encouragement of my family, friends, and colleagues I decided to take on this once in a lifetime challenge. I will never forget this experience and will always be grateful to all the people that made this happen due to their unwavering support.

I can't express enough of my sincere thanks to my advisor, Professor Richard Christenson, for his guidance and advice over the years. Throughout my time as a graduate student, he has been nothing but encouraging and re-assuring, which kept me going. His enthusiastic interest and dedication to scientific research is inspiring. I want to also thank the rest of advisory committee, Professor Michael Accorsi, Shinae Jang, and Jiong Tang for the endless encouragement, support, and patience throughout my graduate studies.

This research was made possible by the support of the Office of Naval Research (ONR), particularly the Structural Acoustics program under Deborah Nalchajian as well as Dr. John Muench from ONR. Thanks to them for their support and encouragement, as well as their patience. Without them, this research would not be possible.

I especially want to thank my colleagues and management at General Dynamics Electric Boat for being exceptionally tolerant and supportive with me over these years. My colleagues have provided endless advice and guidance over the years. Also, my department management over the years has allowed me to work a flexible part time schedule while I split my time and focus between school and work over the years. This thesis would have never been possible without their continued support and assistance. I can't express how appreciative I am of all their help over the years.

Most importantly, I want to acknowledge my wife for her endless love, encouragement, support, and understanding. Through all the long nights and weekends, she not only put-up with me but also continuingly encouraged me; never letting me become discouraged or give-up. Without her, this wouldn't have been possible.

TABLE OF CONTENTS

LIST OF FIGURES

LIST OF TABLES

1 INTRODUCTION

1.1 Background

Vibration of mechanical equipment in certain mechanical systems can result in fatigue, detection, and/or environmental concerns. Quantification of transmitted vibration energy through these systems to verify the system meets fatigue, detection, and/or environmental performance requirements can be a critical aspect in the design of these systems with mechanical equipment. The design of the system, as a whole, consists of satisfying various requirements imposed on the vibration transmission of mechanical equipment to the support structure. Based on the transmissibility of the support structure, the mechanical portion of the system might have vibratory design restrictions that need to be identified early in the development or selection of these mechanical components.

During the design phase of a system, the mechanical portion of the system, (i.e. an engine, a fluid pump or valve, an electric motor, etc.) may be pre-existing or may have to be developed and it is important to understand the requirements of this mechanical equipment early on so an appropriate component can be selected. Once this component is determined, it can be physically tested to quantify the vibration energy that will be transmitted to the support structure. The mechanical vibration energy is typically measured and analyzed in the frequency domain. Frequency response functions and power spectral density (PSD) functions are used to quantify and characterize the mechanical vibration energy. Frequency response functions are a relative measure of the output normalized by the input to the system. Because mechanical components are typically complex and can have multiple sources of vibration energy, it can be difficult to quantify the correct representative input to use for the calculation of the frequency response function. PSDs are absolute measures of the output of the system and, in most cases are of ultimate interest. As such, PSDs are typically used to quantify the amount of energy transmitted by the mechanical equipment throughout the remainder of the structure.

During the design process, the support structure is not pre-existing and is iteratively designed to withstand as well as mitigate as much as possible the vibration energy transmitted by the mechanical equipment. The support structure usually only exists as a computer aided design (CAD) concept which can be used to construct a finite element model (FEM) to analyze and determine the transmissibility (or inversely the effectiveness) of the foundation structure. In the frequency domain, this transmissibility is typically quantified as a frequency response function. The challenge in substructuring is to combine these two substructures in order to accurately verify the system meets performance requirements. Further, it is advantageous to do this analysis early in the design phase while there is still time to iterate on the design if necessary. One form of substructuring, called real-time hybrid substructuring (RTHS), is examined here to address the challenges and needs of current vibration testing for mechanical equipment.

Early research concerning vibration energy transmission in mechanical systems including multi-stage mechanical systems, which consist of multiple substructures representing the various levels of isolation within a general system is (Sykes, 1956), (Wright, 1958) and (Akey, J G, 1963). A practical method to combining the experimentally obtained PSD data of the mechanical equipment and the numerically computed FRF of the support structures was developed by (Darby R. A., 1964) to quantify the vibration energy transmitted through a real world mechanical system and is referred to as the *Darby Method* in industry.

Other existing methods, in the field of substructuring, known as Transfer Path Analysis (TPA) are frequency response functions (FRF) based techniques that describe the dynamics of the mechanical system by the multiplication of the FRFs of the system substructures. Variations of TPA methods are known as Frequency Based Substructuring (FBS) methods which allow for the calculation of the entire mechanical system dynamic response based on the FRFs of the system substructures using various methods. Primary developments of FBS methods are (Crowley, Klosterman, Rocklin, & Vold, 1984), (Jetmundsen, Bielawa, & Flannelly, 1998), (Imregun, Robb, & Ewins, 1987) and later on (Gordis, Bielawa, & Flannelly, 1991) and (de Klerk, Rixen, & de Jong, 2006). Generally, this work demonstrated a

wide variety of methods to couple substructures based on either numerically computed or experimentally measured FRFs. There are many other variations of FBS methods including (Su & Juang, 1994) and later on (Sjovall & Abrahamsson, 2007) which developed state-space based methods to couple structural substructures together. These methods provide a dynamic substructuring framework to couple numerical and experimental substructures together in the frequency-domain. Recently (Rixen & van derValk, 2013) who developed a time-domain based substructuring technique which is analogous to the aforementioned frequency-domain techniques. This method takes advantage of either numerically or experimentally measured impulse response functions (IRF). (de Klerk, Rixen, & Voormeeren, 2008) provides an extensive overview and survey of the mathematical formulations for these and other methods for both model reduction and experimental dynamic substructuring.

Real-time hybrid substructuring, also known as real-time hybrid simulation, (RTHS) is a cyber-physical method of testing that provides the capability to isolate and physically test the critical components of a mechanical system, similar to the blocked component level test, while including the full dynamic interaction with a numerical representation of the support structure. RTHS is a relatively new test method, made more practical in recent years due to advances in computer power, digital signal processing hardware/software, and hydraulic control hardware. RTHS shows promise to accurately represent the dynamics of the mechanical system at the time of the mechanical equipment qualification testing. Early research in RTHS focused on seismic evaluation of building components (Nakashima & Masaoka, 1999), (Darby, Blakeborough, & Williams, 1999), (Dimig, Shield, French, Bailey, & Clark, 1999), and (Horiuchi, Inoue, Konno, & Namita, 1999). These applications generally consisted of support structures dominated by low fundamental frequencies with relatively highly damped physical substructures including linear and nonlinear base isolators and damping devices. More recently, (Christenson & Lin, 2008) describes the RTHS test setup at the University of Colorado Boulder NEES and (Jiang, Kim, Plude, & Christenson, 2013) describes the RTHS testing at the Lehigh University NEES facility. As well as (Phillips & Spencer Jr., 2012) and (Gao, Castaneda, & Dyke, 2013) which have recently expanded the use

of RTHS to multi-actuator multiple degree of freedom coupling of the numerical and physical substructures. Generally, all of these RTHS studies done were exclusively in the field of Earthquake Engineering. Recently, (Botelho R. , 2015) expanded the use of RTHS to mechanical systems which also included numerically fluid-loaded marine systems. All of these studies consist of systems with large amplitude, highly damped vibration as well as known system loads which were numerically opposed on the RTHS test. This dissertation attempts to continue this work and expand the capabilities of RTHS to include system level vibration testing of lightly damped, small vibration mechanical systems especially those with unknown mechanical loads.

A similar cyber-physical test method to real-time hybrid substructuring is hardware-in-the-loop (HWIL) testing. HWIL testing is typically used in mechanical applications to test electrical control systems. In this hybrid substructuring test method, since the physical substructure is typically an electrical component, the interface between the numerical and physical substructures is achieved through the direct transfer of electrical signals and therefore doesn't require displacement commanded servo-hydraulic control systems, as in RTHS. Some examples of HWIL research done in design of electro-mechanical systems are (Hanselmann, 1993), who early on pioneered the method for the study and testing of engine control units (ECU)'s in automobiles as well as its subsequent extensions by (Isermann, Schaffnit, & Sinsel, 1999) in the testing of ECUs and (Carmeli, Castelli-Dezzaa, Mauri, & Marchegiani, 2013) who expanded to use of HWIL testing into the design of distributed renewable energy generating systems. Similar research topics that used a mechanical automotive engine as the physical substructure, referred to as engine-in-the-loop, are (Fathy, Ahlawat, & Stein, 2005), (Filipi, et al., 2006) and (Filipi & Kim, 2010). Similar to HWIL, as a part of engine-in-the-loop research, the interface between the numerical and physical substructures is achieved through the direct transfer of electrical signals.

1.2 Research Objective

The objective of this research is to extend and demonstrate real-time hybrid substructuring (RTHS) as a solution to solve the challenge of accurately combining the dynamics of mechanical components with the

predicted performance of the supporting structure, known as system-level vibration characterization of mechanical systems. This research specifically addresses the unique challenges encountered in the application of RTHS to mechanical systems including potential instability of the transfer system actuator dynamics and the lightly damped substructures. To accomplish this objective, the following research tasks have been conducted:

- Comparison of the linear superposition approximation of system level dynamics with the exact solution in order to illustrate improvements using RTHS and determine the applications when RTHS offers improved accuracy over the linear superposition approximation.
- Implementation of actuator dynamic compensation for stable closed-loop RTHS testing of lightly damped systems.
- Construction and testing of representative case studies for demonstrating RTHS for system level vibration testing of mechanical equipment.

1.3 Outline of Dissertation

This dissertation is organized into 6 chapters and 2 appendices. This first chapter provides the introduction including literature review and motivation for this research. Chapters 2 through 5 are self-contained manuscripts that will be submitted for journal publication. Chapter 6 provides conclusions including a summary of the significant findings and key contributions of this research as well as potential directions for future research. Summaries of Chapters 2 through 5 are provided in this section.

Chapter 2 presents the use of real-time hybrid substructuring (RTHS) to directly interface a physical test of a piece of mechanical equipment to a numerical model of the support structure. First, a numerical example is used to illustrate the effects of neglecting the phase interaction and thus the dynamic interaction between the mechanical equipment and the support structure. Experimental data is used to verify the numerical example. Next, a RTHS case study is performed and is verified by the experimental testing of the mechanical system. It is shown that RTHS can provide an improved method for system-

level vibration testing of mechanical equipment to accurately predict the vibration transmission of mechanical equipment into the support structure. The results of this case study are used to show the validity to extend RTHS for system level vibration testing of mechanical equipment.

Chapter 3 presents a control based hybrid substructuring approach to Transfer Path Analysis by recognizing the similarities between feedback control and dynamic substructuring. It is shown that this approach can accurately predict the coupled dynamic system response of multiple substructured systems including operating mechanical equipment with a complex vibration source. The main advantage of this method is that it uses blocked force measurements in the form of a power spectral density matrix measured uncoupled from the rest of the system. This substructuring method is demonstrated using a simplified case study comprised of a two-stage vibration isolation system and excited by operating mechanical equipment.

Chapter 4 presents a methodology to achieve effective control of a multi degree-of-freedom (MDOF) shake table and describes the corresponding multiple input multiple output (MIMO) system identification and model-based feedforward feedback compensation to facilitate both stable and accurate RTHS testing of lightly damped mechanical systems. The results are used for the following MDOF RTHS case study.

Chapter 5 capitalizes on the previous research that presents effective control of a MDOF shake table for RTHS applications to facilitate both stable and accurate RTHS testing of lightly damped mechanical systems. The results show that the proposed compensation methods allow for successful MDOF RTHS experiments that capture the coupled dynamics of the full system.

1.4 REFERNCES

Akey, J G. (1963). Transfer-Matrix Method and Computer Program for the Vibration Analysis of Series Plane-Frame Structures Having Material Damping and Complex Terminations. *Defense Technical Information Center.*

Botelho, R. (2015). *Real-Time Hybrid Substructuring for Marine Application of Vibration Control and Structural Acoustics.* University of Connecticut.

Carmeli, M. S., Castelli-Dezzaa, F., Mauri, M., & Marchegiani, G. (2013). Novel Mechanical Hardware in the Loop Platform for Distributed Generation Systems. *Distributed Generation and Alternative Energy Journal, 28*(3), 7-27.

Christenson, R., & Lin, Y. Z. (2008). Real Time Hybrid Simulation of a Siesmically Excited Structure With Large Scale Magneto Rheological Fluid Dampers. In *Hybrid Simulation Theory, Implementation and Applications.*

Crowley, J., Klosterman, A., Rocklin, G., & Vold, H. (1984). Direct Structural Modification using Frequency Response Functions. *Proceedings of the Second International Modal Analysis Conference.* Orlando, FL.

Darby, A. P., Blakeborough, A., & Williams, M. S. (1999). Real Time Substructure Test Using Hydraulic Actuator. *Journal of Engineering Mechanics, 125*(10), 1133-1139.

Darby, R. A. (1964). A Practical Method for Predicting Acoustic Radiation or Shock Excursions of Navy Machinery. *The Shock and Vibration Bulletin, 3*.

de Klerk, D., Rixen, D., & de Jong, J. (2006). The Frequency Based Substructuring Method Reformulation According to the Dual Domain Decomposition Method. *Proceedings of the Fifteenth International Modal Analysis Conference.* St. Louis, MO.

de Klerk, D., Rixen, D. J., & Voormeeren, S. N. (2008). General Framework for Dynamic Substructuring: History, Review and Classification of Techniques. *AIAA Journal, 46*(5), 1169-1181.

Dimig, J., Shield, C., French, C., Bailey, F., & Clark, A. (1999). Effective Force Testing: A Method of Siesmic Simulation for Structural Testing. *Journal of Structural Engineering, 125*(9), 1028-1037.

Fathy, H. K., Ahlawat, R., & Stein, J. L. (2005). Proper powertrain modeling for engine-in-the-loop simulation. *ASME 2005 International Mechanical Engineering Congress and Exposition*, 1195-1201.

Filipi, Z., & Kim, Y. J. (2010). Hydraulic hybrid propulsion for heavy vehicles: Combining the simulation and engine-in-the-loop techniques to maximize the fuel economy and emission benefits. *il & Gas Science and Technology–Revue de l'Institut Francais du Petrole, 65*(1), 155-178.

Filipi, Z., Fathy, H., Hagena, J., Knafl, A., Ahlawat, R., Liu, J., . . . Stein, J. (2006). Engine-in-the-loop testing for evaluating hybrid propulsion concepts and transient emissions-HMMWV case study. *AE Technical Paper*.

Gao, X., Castaneda, N., & Dyke, S. J. (2013). Experimental validation of a generalized procedure for MDOF real-time hybrid simulatio. *Journal of Engineering Mechanics, 140*(4).

Gordis, J. H. (1994). Structural synthesis in the frequency domain: a general formulation. *Shock and Vibration, 1*(5), 461-471.

Gordis, J., Bielawa, R., & Flannelly, W. (1991). A Generalized Theory for Frequency Domain Structural Synthesis. *Journal of Sound & Vibration, 150*, 139-158.

Hanselmann, H. (1993). *Hardware-in-the loop simulation as a standard approach for development, customization, and production test of ECU's.* SAE Technical Paper.

Horiuchi, T., Inoue, M., Konno, T., & Namita, Y. (1999). Real Time Hybrid Experimental System With Actuator Delay Compensation and It's Applications to a Piping System With Energy Absorber. *Earthquaker Engineering and Structural Dynamics, 28*(10), 1121-1141.

Imregun, M., Robb, D., & Ewins, D. (1987). Structural Modifications and Coupling Dynamic Analysis Using Measured FRF Data. *Proceedings of the Fifth International Modal Analysis Conference.* London, UK.

Isermann, R., Schaffnit, J., & Sinsel, S. (1999). Hardware-in-the-loop simulation for the design and testing of engine-control systems. *Control Engineering Practice, 7*(5), 643-655.

Jetmundsen, B., Bielawa, R. L., & Flannelly, W. G. (1988). Generalized frequency domain substructure synthesis. *Journal of the American Helicopter Society, 33*(1), 55-64.

Jiang, Z., Kim, S. J., Plude, S., & Christenson, R. (2013). Real Time Hybrid Simulation of a Complex Bridge Model with MR Dampers Using the Convolution Integral Method. *Journal of Smart Materials and Structures, 22*(10).

Nakashima, M., & Masaoka, N. (1999). Real Time On-Line Test for MDOF Systems. *Earthquake Engineering and Structural Dynamics, 28*, 393-420.

Phillips, B. M., & Spencer Jr., B. F. (2012). Model-based multiactuator control for real-time hybrid simulation. *Journal of Engineering Mechanics, 139*(2), 219-228.

Rixen, D. J., & van derValk, P. L. (2013). An Impulse Base Substructuring Approach for Impact Analysis and Load Case Simulation. *Journal of Sound and Vibration*, 7174-7190.

Sjovall, P., & Abrahamsson, T. (2007). State Space Model Identification for Component Synthesis. *Porcedding of the 25th International Modal Analysis Conference.* Society for Experimental Mechanics.

Su, T. J., & Juang, J. N. (1994). Substructure System Identification and Synthesis. *Journal of Guidance, Control and Dynamics*, 1087-1095.

Sykes, A. O. (1956). The Evaluation of Mounts Isolating Nonrigid Machines From Nonrigid Foundations. *ASME Applied Machanics Division Conference.*

Wright, D. V. (1958). Impedance Analysis of Distributed Mechanical Systems. *Colloquim on Mechanical Impedance Methods fro Mechanical Vibrations.* ASME.

2 SINGLE DEGREE OF FREEDOM SYSTEM LEVEL VIBRATION TESTING OF MECHANICAL EQUIPMENT USING REAL-TIME HYBRID SUBSTRUCTURING

2.1 Abstract

In the design of mechanical systems, there can be constraints imposed on the vibration levels mechanical equipment transmits into the supporting structure. To assess the mechanical equipment performance early in the design process it is important to predict system-level dynamics responses through component level testing. The mechanical equipment can have highly complex vibration sources that require physical testing in the laboratory. The support structure is typically more readily modeled using well established numerical methods such as lumped mass models or the finite element method. To assess the system performance, well-established Transfer Path Analysis (TPA) methods are typically used to combine the measured interface forces of the mechanical equipment with the model-based frequency response functions of the support structure to determine the level of vibration transmission through the full system. The TPA methods, however, neglect the phase interaction between the equipment and the support structure, which can lead to inaccuracies and overly conservative predictions of vibration levels transmitted at frequencies approaching the resonant frequencies of the mechanical equipment and support structure. This paper proposes the use of real-time hybrid substructuring (RTHS) to directly interface a physical test of mechanical equipment to a numerical model of the support structure. First, a numerical example is used to illustrate the effect of neglecting the phase interaction and thus the dynamic interaction between the mechanical equipment and the support structure. Experimental data is used to verify the numerical example. Next, a RTHS case study is performed and is verified by the experimental testing of the mechanical system. It is shown that RTHS can provide an improved method for system-level vibration testing of mechanical equipment to accurately predict the vibration transmission of mechanical equipment into the support structure.

2.2 Introduction

Vibration of mechanical equipment can result in fatigue, detection, and/or environmental concerns for a support structure. A critical aspect of the design of systems with mechanical equipment is quantifying the level of transmitted vibration energy through the supporting structure. The system design typically consists of strict constraints imposed on the vibration transmission of the mechanical equipment through the full system. During the design phase of a system, the mechanical equipment, (i.e. an engine, a fluid pump or valve, an electric motor, etc.) is often pre-existing and can be physically tested to quantify the vibration energy produced and also to qualify the system level performance. Mechanical equipment is typically designed through a process where equipment requirements are defined and the design, in accordance with these requirements, is completed. Upon initial testing, a series of improvements are made to the mechanical equipment and qualification testing is conducted. In a somewhat parallel process, the support structure is also designed through identifying requirements, including allowable levels of vibration energy transmission into various surrounding environments. A design is conducted and improvements to the design are made. It is at the end of both of these processes that the combined system is first test to ensure qualification of the coupled full system. Figure 2.1 shows a general timeline of this design procedure of a mechanical system.

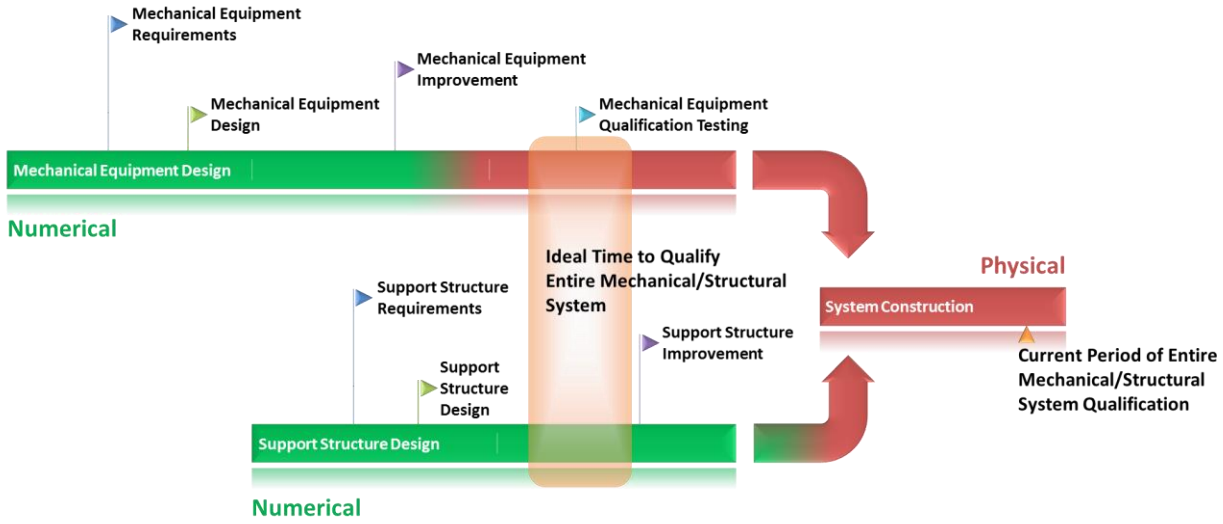

Figure 2.1 – General Timeline of Design Procedure for a Mechanical System

From Figure 2.1, it is clear that the system level vibration testing is conducted too late in the design process for substantial improvements to the support structure to be realized. Ideally, the system level vibration testing would be conducted early enough in the design process of the support structure so that necessary improvements can be made. This timing is proposed in Figure 2.1.

Current practice is to experimentally quantify the vibration transmission of mechanical equipment through blocked component level tests (Darby R. A., 1964). In these tests, qualification of the critical components of a mechanical system are mounted directly to the ground, i.e. blocked boundary conditions, and physically tested. Measured responses are then used to calculate, in the frequency domain, the auto power spectral density (PSD) of the forces at the base of the mechanical equipment. At the time of the mechanical equipment qualification testing, the support structure may not be physically built and therefore cannot be tested with the mechanical equipment. However, a numerical model of the support structure is likely available. From this numerical model the frequency response function (FRF) can be computed as a frequency domain representation of the dynamics behavior of the support structure. The combination of the experimentally determined PSD data and the numerically computed FRF is used to quantify the vibration energy of the full system through what is referred to as Transfer Path Analysis (TPA).

Early research concerning vibration energy transmission in mechanical systems including multi-stage mechanical systems, which consist of multiple substructures representing the various levels of isolation within a general system is (Sykes, 1956), (Wright, 1958) and (Akey, J G, 1963). A practical method to combining the experimentally obtained PSD data of the mechanical equipment and the numerically computed FRF of the support structures was developed by (Darby R. A., 1964) to quantify the vibration energy transmitted through a real world mechanical system and is referred to as the *Darby Method* in industry. Frequency based substructuring (FBS) methods developed by (Jetmundsen, Bielawa, & Flannelly, 1988), (Gordis J. H., 1994) and (de Klerk, Rixen, & de Jong, 2006) provide a dynamic substructuring framework to couple numerical and experimental substructures together in the frequency-

domain as well as (de Klerk, Rixen, & Voormeeren, 2008) which provides an extensive overview and survey of the mathematical formulations for these and other TPA methods for both model reduction and experimental dynamic substructuring.

While the method for testing mechanical equipment proposed by (Darby R. A., 1964), is quite effective and accurate in general, there are certain conditions where the dynamic interaction between the equipment and the support structure must be fully accounted to ensure accurate results. The *Darby Method* approximates the dynamics of the combined system by multiplying the frequency response function magnitudes of the two independent systems. This method preserves the resonances of either the independent systems into the dynamics of the coupled system and is often a conservative approximation of the magnitude of the coupled system dynamics. Multiplying the magnitudes assumes an in-phase relationship between the two systems across all frequencies. This assumption causes the magnitude of the coupled system's frequency response function to be over predicted at frequencies where the relationship between the two systems is out-of-phase. Further, since the coupled system has its own resonant frequency, separate from the resonant frequencies of the two independent systems, by multiplying the magnitudes of the two systems, will under-predict the coupled response of the system at the coupled system at its resonant frequencies.

Real-time hybrid substructuring, also known as real-time hybrid simulation, (RTHS) is a cyber-physical method of testing that provides the capability to isolate and physically test the critical components of a mechanical system, similar to the blocked component level test, while including the full dynamic interaction with a numerical representation of the support structure. RTHS is a relatively new test method, made more practical in recent years due to advances in computer power, digital signal processing hardware/software, and hydraulic control hardware. RTHS shows promise to accurately represent the dynamics of the mechanical system at the time of the mechanical equipment qualification testing. Early research in RTHS focused on seismic evaluation of building components (Nakashima & Masaoka, 1999), (Darby, Blakeborough, & Williams, 1999), (Dimig, Shield, French, Bailey, & Clark, 1999), and

(Horiuchi, Inoue, Konno, & Namita, 1999). These applications generally consisted of support structures dominated by low fundamental frequencies with relatively highly damped physical substructures including linear and nonlinear base isolators and damping devices. More recently, (Christenson & Lin, 2008) describes the RTHS test setup at the University of Colorado Boulder NEES and (Jiang, Kim, Plude, & Christenson, 2013) describes the RTHS testing at the Lehigh University NEES facility. As well as (Phillips & Spencer Jr., 2012) and (Gao, Castaneda, & Dyke, 2013) which have recently expanded the use of RTHS to multi-actuator multiple degree of freedom coupling of the numerical and physical substructures. Generally, all of these RTHS studies done were exclusively in the field of Earthquake Engineering. Recently, (Botelho R. , 2015) expanded the use of RTHS to mechanical systems which also included numerically fluid-loaded marine systems. All of these studies consist of systems with large amplitude, highly damped vibration as well as known system loads which were numerically opposed on the RTHS test. This paper attempts to continue this work and expand the capabilities of RTHS to include system level vibration testing of lightly damped, small vibration mechanical systems especially those with unknown mechanical loads.

A similar cyber-physical test method to real-time hybrid substructuring is hardware-in-the-loop (HWIL) testing. HWIL testing is typically used in mechanical applications to test electrical control systems. In this hybrid substructuring test method, since the physical substructure is typically an electrical component, the interface between the numerical and physical substructures is achieved through the direct transfer of electrical signals and therefore doesn't require displacement commanded servo-hydraulic control systems, as in RTHS. Some examples of HWIL research done in design of electro-mechanical systems are (Hanselmann, 1993), who early on pioneered the method for the study and testing of engine control units (ECU)'s in automobiles as well as its subsequent extensions by (Isermann, Schaffnit, & Sinsel, 1999) in the testing of ECUs and (Carmeli, Castelli-Dezzaa, Mauri, & Marchegiani, 2013) who expanded to use of HWIL testing into the design of distributed renewable energy generating systems. Similar research topics that used a mechanical automotive engine as the physical substructure, referred to as engine-in-the-loop,

are (Fathy, Ahlawat, & Stein, 2005), (Filipi, et al., 2006) and (Filipi & Kim, 2010). Similar to HWIL, as a part of engine-in-the-loop research, the interface between the numerical and physical substructures is achieved through the direct transfer of electrical signals.

This paper proposes a RTHS systematic approach for the system level vibration testing of mechanical equipment to provide direct system level response predictions of lightly damped, small amplitude system vibration while using physical system excitation and a displacement based transfer system. This paper also examines the potential limitations of the TPA and the *Darby Method* of vibration testing for mechanical equipment. Real-time hybrid substructuring requires accurate tracking of desired displacements using servo-hydraulic actuators due to the tendency of the frequency dependent dynamics of these servo hydraulic actuators to cause instabilities in the hybrid feedback loop, therefore this paper also examines the compensation and stability methods of RTHS.

2.3 System Level Vibration Testing of Mechanical Equipment

2.3.1System Level Vibration Testing of Mechanical Equipment

Component level testing of mechanical equipment to provide information on the system level behavior of a support structure was first proposed back in the 1950s, Sykes, 1956 (Sykes, 1956). Transfer Path Analysis (TPA) is an approximation used to combine measured interface forces with the model-based structural frequency response functions to determine vibration transmission of a multiple stage mechanical system. The TPA method proposed by (Darby R. A., 1964) is an open loop method that combines the dynamics of the mechanical equipment written in the frequency domain as $H_1(i\omega)$, with the dynamics of the foundation system, $H_2(i\omega)$. The dynamics of each of these systems are determined as independent systems. The dynamics of the combined system are approximated by multiplying the frequency response functions of the two independent systems. This method preserves the resonances of either the independent systems into the dynamics of the coupled system which can be inaccurate and

overly conservative. Figure 2.2 shows a simple control system diagram demonstrating the calculation of the force transmitted, F_T through the entire system using the *Darby Method.*

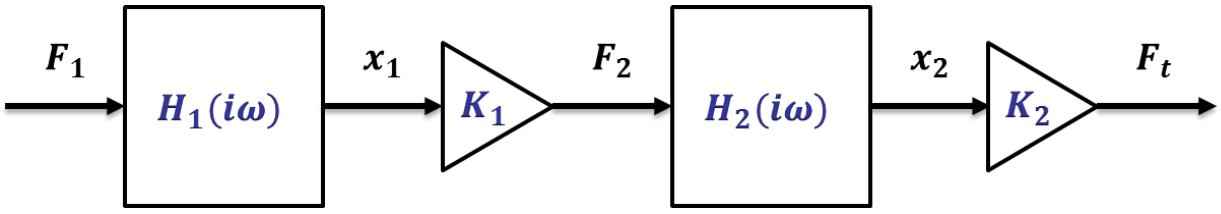

Figure 2.2 – System Diagram of the Darby Method

Where $F_{1,2}$ are the forces exerted on each respective system, $K_{1,2}$ are each respective system's inherent stiffness, and $x_{1,2}$ are the respective reactant displacements of each system. The equation for the *Darby Method* system's force transmissibility,TR_{DM}, in Figure 2.2 is

$$TR_{DM} = \frac{F_T}{F_1} = K_1 K_2 H_1(i\omega) H_2(i\omega) \qquad [2.1]$$

Assuming the two systems are each SDOF undamped, for simplicity purposes, mass-spring systems with external applied forces, equations for $H_{1,2}$ are:

$$H_1(i\omega) = \frac{x_1}{F_1} = \left|\frac{1}{-M_1\omega^2 + K_1}\right| \qquad H_2(i\omega) = \frac{x_2}{F_2} = \left|\frac{1}{-M_2\omega^2 + K_2}\right| \qquad [2.2],[2.3]$$

where $M_{1,2}$ are the masses of the two respective systems and

$$\omega_i = \sqrt{\frac{K_i}{M_i}} \; for \; i = 1,2 \qquad [2.4]$$

A diagram showing both the coupled system and the inidividual systems are shown in Figure 2.3.

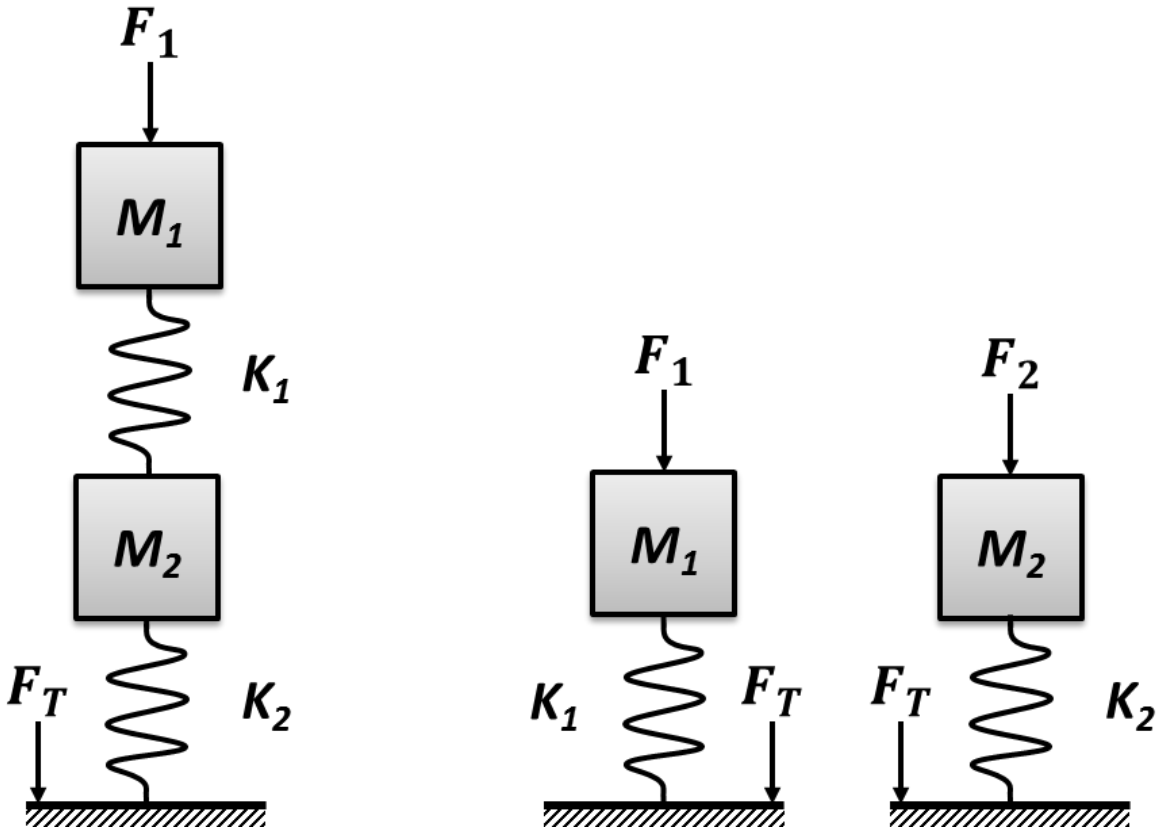

(A) **(B)**

Figure 2.3 – Diagram of (A) Coupled System and (B) Individual Systems 1 & 2

It should be noted that in equating Figure 2.3B to the block diagram shown in Figure 2.2, the force transmitted to the base of M_1, F_t is the force used to excite M_2 and therefore equal to F_2. Substituting Equation [2.2],[2.3] into Equation [2.1] gives

$$TR_{DM} = \frac{K_1 K_2}{(M_1 M_2)\omega^4 - (K_1 M_2 + K_2 M_1)\omega^2 + K_1 K_2} \qquad [2.5]$$

The roots of the denominator polynomial of the system force transmissibility in Equation [2.5], $\omega^2_{DM_{1,2}}$ are the natural frequencies of the *Darby Method* combined system.

$$\omega_{DM_{1,2}}^2 = \frac{1}{2}\left[\left(\frac{K_1}{M_1}\right)+\left(\frac{K_2}{M_2}\right) \pm \sqrt{\left[\left(\frac{K_1}{M_1}\right)+\left(\frac{K_2}{M_2}\right)\right]^2 - 4\left(\frac{K_1}{M_1}\right)\left(\frac{K_2}{M_2}\right)}\right]$$
$$= \frac{1}{2}\left[\left(\frac{K_1}{M_1}\right)+\left(\frac{K_2}{M_2}\right) \pm \left[\left(\frac{K_1}{M_1}\right)-\left(\frac{K_2}{M_2}\right)\right]\right] = \omega_{1,2}^2 \qquad [2.6]$$

The two solutions to Equation [2.6] can be shown to be

$$\omega_{DM_1}^2 = \frac{K_1}{M_1} = \omega_1^2 \qquad \omega_{DM_2}^2 = \frac{K_2}{M_2} = \omega_2^2 \qquad [2.7],[2.8]$$

Equation [2.7],[2.8] show that the natural frequencies of the TPA approximation, $\omega_{DM_{1,2}}^2$ and the natural frequencies of the independent mass-spring oscillators, $\omega_{1,2}^2$ are equal. This equation proves that the natural frequencies of the *Darby Method* are equal to the natural frequencies of the individual mass-spring oscillators and not the natural frequencies of the coupled system which are shown subsequently to be different. This observation is an indication that the *Darby Method* may not capture the system level dynamics sufficiently at low frequencies and warrants closer examination.

2.3.2 Limitations of the Darby Method

While current industry methods, i.e., the *Darby Method*, for testing mechanical equipment using sequential procedures are quite effective and accurate, there are certain conditions where the dynamic interaction between the equipment and the support structure need to be fully accounted for in the physical testing. The main assumption in the *Darby Method* is that the two systems are assumed to be isolated from interacting with each other and affecting each other's dynamics. It is difficult to quantify the exact frequency at which effective isolation occurs and this assumption is valid. The natural frequency of the system can easily be calculated and previous research derived equations for transmissibility (or the inverse which is referred to effectiveness), but the frequency where these two systems are completely independent of each other is difficult to calculate because there is a certain amount of energy transmitted at all frequencies (Sykes, 1956). However, the *Darby Method* is valid in a certain frequency range where

the energy transmitted between the two systems could be described as in-phase and is effectively attenuated and therefore the amount of energy transmitted is considered negligible.

The *Darby Method* approximates the dynamics of the combined system by multiplying the frequency response function magnitudes of the two independent systems. This method preserves the resonances of either the independent systems into the dynamics of the coupled system which can be inaccurate and overly conservative. By multiplying the magnitudes, it is assumed to be an in-phase relationship between the two systems. This assumption results in the magnitude being greater than the actual dynamics of the coupled system. In actuality the system switches between in-phase and out-of-phase before and after the resonances of the system, respectively. Figure 2.4 shows the phase relationship between a two stage isolation system as an example. The dotted line shows the resonance of the first system and the solid line shows the resonance of the second system. The *Darby Method* is accurate when the two systems are in-phase, i.e. low frequencies and high frequencies. The frequency range around where the two systems are out-of-phase, is the frequency range where the coupling of the two systems is important to include in the predictions of the full system transmitted vibration.

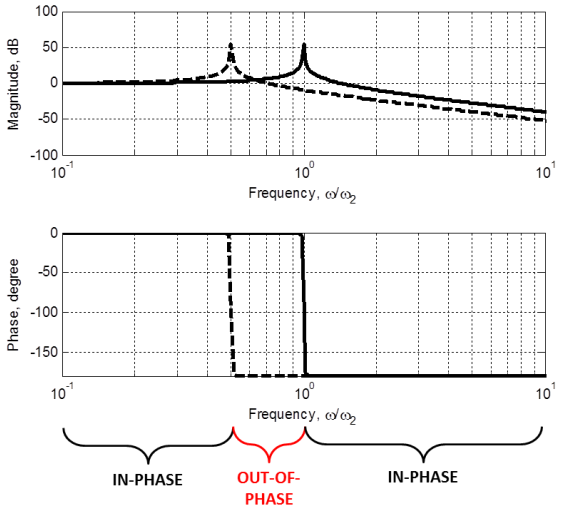

Figure 2.4 – Phase Relationship between Two Isolation Systems

Comparing the equation for transmissibility derived using the *Darby Method* to the coupled system transmissibility it can be determined at which frequency the *Darby Method* is an accurate representation of the system. Figure 2.5 shows the system diagram of the coupled system.

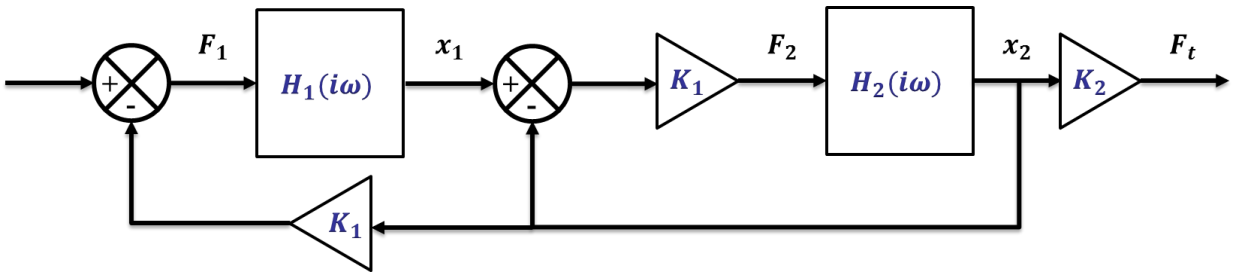

Figure 2.5 – System Diagram of the Coupled System

The system diagram of the coupled system includes the feedback loop that is ignored by the *Darby Method* as can be seen by comparing Figure 2.2 and Figure 2.5. This loop represents the reactant forces of the interaction between the two systems. Using the same derivation as used in Section 2, the force transmissibility equation of the coupled system, TR_{CPL} is:

$$TR_{CPL} = \frac{F_T}{F_1} = \frac{K_1 K_2 H_1(i\omega) H_2(i\omega)}{1 + K_1 H_2(i\omega) - K_1^2 H_1(i\omega) H_2(i\omega)} \quad [2.9]$$

Substituting Equation [2.2],[2.3] into Equation [2.9] results in:

$$TR_{CPL} = \frac{K_1 K_2}{(M_1 M_2)\omega^4 - (K_1 M_2 + K_2 M_1 + K_1 M_1)\omega^2 + K_1 K_2} \quad [2.10]$$

Solving for the roots of of the denominator of Equation [2.10] gives:

$$\omega^2_{CPL_{1,2}} = \frac{1}{2}\left[\left(\frac{K}{M}\right)_1 + \left(\frac{K}{M}\right)_2 + \frac{M_1}{M_2} \pm \sqrt{\left[\left(\frac{K}{M}\right)_1 + \left(\frac{K}{M}\right)_2 + \frac{M_1}{M_2}\right]^2 - 4\left(\frac{K}{M}\right)_1 \left(\frac{K}{M}\right)_2}\right] \quad [2.11]$$

where $\omega^2_{CPL_{1,2}}$ are the roots of the coupled system transmissibility denominator. The differences of these two solutions, can be observed by normalizing TR_{CPL}, Equation [2.10], by TR_{DM}, Equation [2.5].

$$\frac{TR_{CPL}}{TR_{DM}} = \frac{\omega^4 - \left(\frac{K_1}{M_1} + \frac{K_2}{M_2}\right)\omega^2 + \frac{K_1 K_2}{M_1 M_2}}{\omega^4 - \left(\frac{K_1}{M_1} + \frac{K_2}{M_2} + \frac{K_1}{M_2}\right)\omega^2 + \frac{K_1 K_2}{M_1 M_2}} \quad [2.12]$$

This ratio can be calculated for different stiffness and mass ratios. Equation [2.12] is set equal to the magnitude value at which the frequency response functions are approximated as sufficiently accurate. For this study the magnitude value, Δ that was used was 1dB or 12.2%. Equation [2.12] then can be rearranged by setting the transmissibility ratio equal to Δ, multiplying both sides by the denominator, and combining like terms into the polynomial expression shown below:

$$(\Delta - 1)\left[\omega_E^4 + \left(\frac{K_1}{M_1} + \frac{K_2}{M_2}\right)\omega_E^2 + \frac{K_1 K_2}{M_1 M_2}\right] + \Delta\frac{K_1}{M_2}\omega_E^2 = 0 \quad [2.13]$$

where ω_E is the solution to this polynomial. This ω_E value is the frequency at which the *Darby Method* becomes sufficiently accurate. The values for ω_E are calculated by rearranging Equation [2.13] in the following equation.

$$\omega_E^4 + \left(\frac{K_1}{M_1} + \frac{K_2}{M_2} + \left(\frac{\Delta}{\Delta - 1}\right)\frac{K_1}{M_2}\right)\omega_E^2 + \frac{K_1 K_2}{M_1 M_2} = 0 \quad [2.14]$$

Solving for the roots of Equation [2.16] gives

$$\omega_E^2 = \frac{1}{2}\left[-\left(\frac{K_1}{M_1} + \frac{K_2}{M_2} + \left(\frac{\Delta}{\Delta - 1}\right)\frac{K_1}{M_2}\right) \pm \sqrt{\left(\frac{K_1}{M_1} + \frac{K_2}{M_2} + \left(\frac{\Delta}{\Delta - 1}\right)\frac{K_1}{M_2}\right)^2 - 4\frac{K_1 K_2}{M_1 M_2}}\right] \quad [2.15]$$

Figure 2.6 shows these $\omega_E$values for various mass and stiffness ratios of the two independent systems. For this example, K_2 and M_2 are fixed to unity (therefore ω_2 equals one) and K_1 and M_1 were varied to achieve different mass and stiffness ratios. Because ω_2 was kept equal to one, the results shown in Figure 2.6 are effectively normalized by the resonate frequency of the second system, ω_2. The equation for these results is given by

$$\frac{\omega_E}{\omega_2} = \frac{1}{\sqrt{2}}\left[-\left(\frac{K_1}{K_2}\frac{M_2}{M_1} + 1 + \left(\frac{\Delta}{\Delta - 1}\right)\frac{K_1}{K_2}\right) \pm \sqrt{\left(\frac{K_1}{K_2}\frac{M_2}{M_1} + 1 + \left(\frac{\Delta}{\Delta - 1}\right)\frac{K_1}{K_2}\right)^2 - 4\frac{K_1}{M_1}}\right]^{1/2} \quad [2.16]$$

Equation [2.16] can also be shown in terms of the natural frequencies of the two substructures, ω_1 and ω_2, respectively. Using Equation [2.7],[2.8] to substitute for the natural frequencies of the two substructures, Equation [2.16] gives

$$\frac{\omega_E}{\omega_2} = \frac{1}{\sqrt{2}}\left[-\left(\frac{\omega_1^2}{\omega_2^2} + 1 + \left(\frac{\Delta}{\Delta - 1}\right)\frac{K_1}{K_2}\right) \pm \sqrt{\left(\frac{\omega_1^2}{\omega_2^2} + 1 + \left(\frac{\Delta}{\Delta - 1}\right)\frac{K_1}{K_2}\right)^2 - 4\omega_1^2}\right]^{1/2} \quad [2.17]$$

Since Equation [2.14] is a second order polynomial, there are two roots of the polynomial. Equation [2.15], [2.16] and [2.17] give both roots of the polynomial. This is due to the fact that the *Darby Method* solution and the exact coupled solution do approach each other at higher frequencies as previously discussed but also at low frequencies below the resonant frequencies of the system as they approach 0Hz. This analysis is concerned with the largest solution to the polynomial.

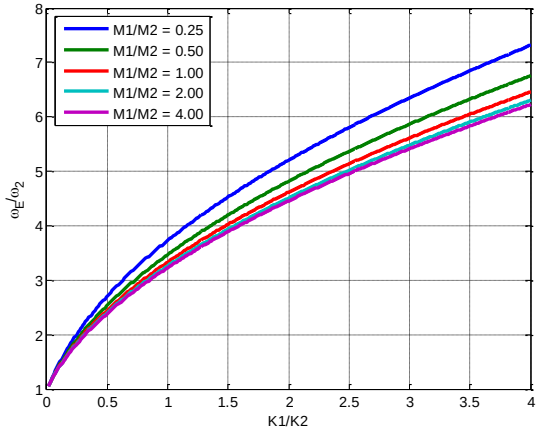

Figure 2.6 – ω_E Values for Various Values of Mass and Stiffness Ratios

Figure 2.7 shows an example of this analysis on a simple numerical model of a two degree of freedom system. The natural frequency of the first system is 5Hz and the natural frequency of the second system is 10Hz. For simplicity, M_1 and M_2 were kept equal, therefore the ratio of K_1 to K_2 is 0.25. Solving Equation [2.16] using these mass and stiffness ratios, we get a $\frac{\omega_E}{\omega_2}$ ratio of 1.86. Since ω_2 is 10Hz, ω_E is

determined to be 18.65Hz. As mentioned before, Equation [2.16] is a second order polynomial. Therefore, there are two solutions to the equation. Both of the solutions are marked with a black vertical dashed line on Figure 2.7A and Figure 2.7B. Because the lesser solution is relatively close to zero, this analysis is not interested in this solution and only focuses on the greater of the two solutions. Figure 2.7B shows the difference between the *Darby Method* solution and the coupled system exact solution. These results support the solution to Equation [2.16] by showing that 18.65Hz is the point where the difference between the *Darby Method* and the coupled solution is equal to 1dB and at frequencies greater than this value, the difference is less than 1dB.

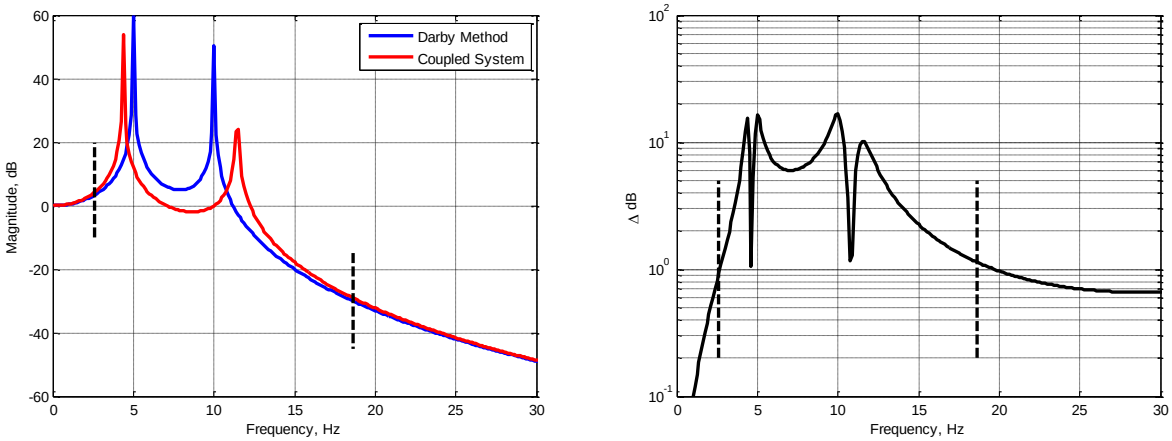

(A) **(B)**

Figure 2.7 – (A) Comparison of Darby Method and Coupled Solution to Numerical Example (B) Difference between the Two Solutions

This analysis was done ignoring damping (0% damping). In order to see what effect damping coefficients would have on this solution, various values were tried. Since this paper is interested in lightly damped structures, values from 0% - 5% were tried because these values are what is generally considered lightly damped. The results ranged from 18.65Hz for 0% damping (as shown above) to 19.75 for 5% damping. Within the damping coefficient range of interest, ω_E varies about 1Hz. This value is considered a negligible variation for this analysis. This analysis shows the *Darby Method* can accurately represent the system dynamics at frequencies higher than the natural frequencies of the system. However, at frequencies around the natural frequencies of the system, the *Darby Method* is not an accurate

assumption. Near the natural frequencies of the system, it is important to represent the dynamics of the coupled system. RTHS is a potential solution to how the coupled system can be quantified prior to when a fully experimental system tests are possible.

2.4 RTHS Methodology for Vibration Testing of Mechanical Equipment

Real-time hybrid substructuring (RTHS) is a relatively new test method and is proposed here as a method to perform system level vibration testing of a mechanical system. RTHS can represent the dynamics of the coupled system as well as provide insight into the design of mechanical systems using system level mechanical vibration. RTHS provides the capability to isolate and physically test the critical complex components of a mechanical system while including the dynamic interaction with a numerical representation of the remainder of the linear portions of the system. Generally, most work in the RTHS field done to date was exclusively in the field of Earthquake Engineering. RTHS studies done related to this field are typically experiments where the input is exactly known and therefore is simulated as a part of the numerical portion of the RTHS loop. Also, in a normal earthquake engineering instance of RTHS the displacements required to be transmitted to the physical substructure by way of the transfer system are large displacements (analogous to the large displacements of the earthquake excitation). These large displacements cause the, typically hydraulic, transfer system to be fairly linear and easier to compensate. Also, typically these earthquake engineering experiments of RTHS have substructures with larger amounts of damping which allows for lenient requirements for the resulting time delay of the transfer system, i.e. it is satisfactory for the transfer system to have a significant amount of time delay and still have a stable RTHS control loop.

RTHS of mechanical equipment is a unique application due to the distinct characteristics of the dynamics of a typical mechanical system. First, the excitation of the system may not be quantifiable and therefore cannot be simulated. If this is the case, the physical substructure will contain the system excitation and the numeric substructure will be the reactant substructure which is the opposite of the typical earthquake engineering RTHS experiment done to date. Second, the displacements required of the transfer system are

significantly less than earthquake displacements. This presents a potential challenge because the required displacement of the hydraulic transfer system may be difficult to transmit because the displacements may not be within the linear displacement ranges of the hydraulic actuators that make up the transfer system as well as there is a "noise floor" of the control hardware to contend with. The last significant difference between mechanical equipment RTHS and earthquake RTHS is that mechanical equipment is typically lightly damped which reduces the amount of time delay that the transfer system can have while still having a stable control loop. This creates more strict requirements for the compensation of the dynamics of the transfer system.

Recent work (Botelho R. , 2015) presented a systematic method for designing and conducting a RTHS experiment. This process is:

1. Substructure Partitioning and Boundary Condition Consideration
2. Transfer System Compensation
3. Stability and Performance Analysis
4. Real Time Hybrid Substructuring Experiment

This paper follows this method for preparation of this RTHS experiment.

2.4.1Partitioning and Boundary Conditions

A RTHS test involves partitioning the whole system into physical and numerical substructures in a feedback loop than can have stability issues. It has been shown in previous studies that the proportions of mass and stiffness along with the amount of damping, of the RTHS substructures are critical to the stability of the closed loop system so it is critical to intelligently divide the mechanical system into effective physical and numerical substructures (Botelho, Christenson, & Franco, 2013).

A typical mechanical system consists of multiple levels of lumped masses and isolation systems. Typically, the mechanical equipment would be designed with its own isolation system and the support structure would be design with its own isolation system similar to was is shown in previous sections' simplified numerical examples. It would then be advantageous to have the complex mechanical

equipment as the physical substructure and the assumed linear behaving support structure as the numerical substructure. The mechanical system for this experiment was designed with this idea in mind. In this experiment a similar approach was taken and the two systems were substructured so each system includes the structure and their respective isolation system. Figure 2.8 shows the general substructured layout of the RTHS approach to a mechanical system.

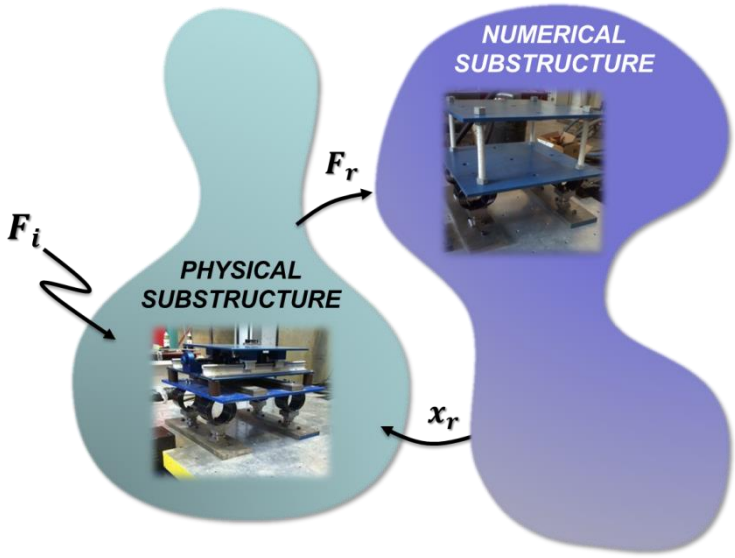

Figure 2.8 – General Diagram for RTHS Approach

The block diagram shown in Figure 2.5 is an accurate representation of the coupled system but it does not lend itself to the RTHS approach. This block diagram can be used to derive a more advantageous block diagram for this RTHS experiment. First, it is advantageous to simplify the dual-feedback loops into a single feedback loop. Figure 2.10 and shows an equivalent control diagram of the coupled system as Figure 2.5 but with a single feedback loop. Next, in Figure 2.10, the K_1 term that is in the through path of the feedback loop can be moved outside of the loop in order to combine like system terms, i.e., K_1's with $H_1(s)$'s.

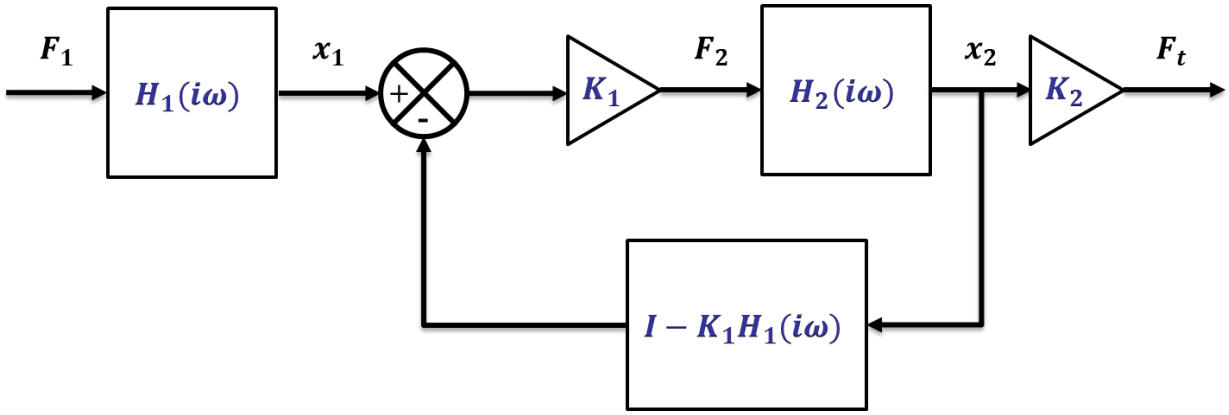

Figure 2.9 – Single Feedback Loop System Diagram of the Coupled System

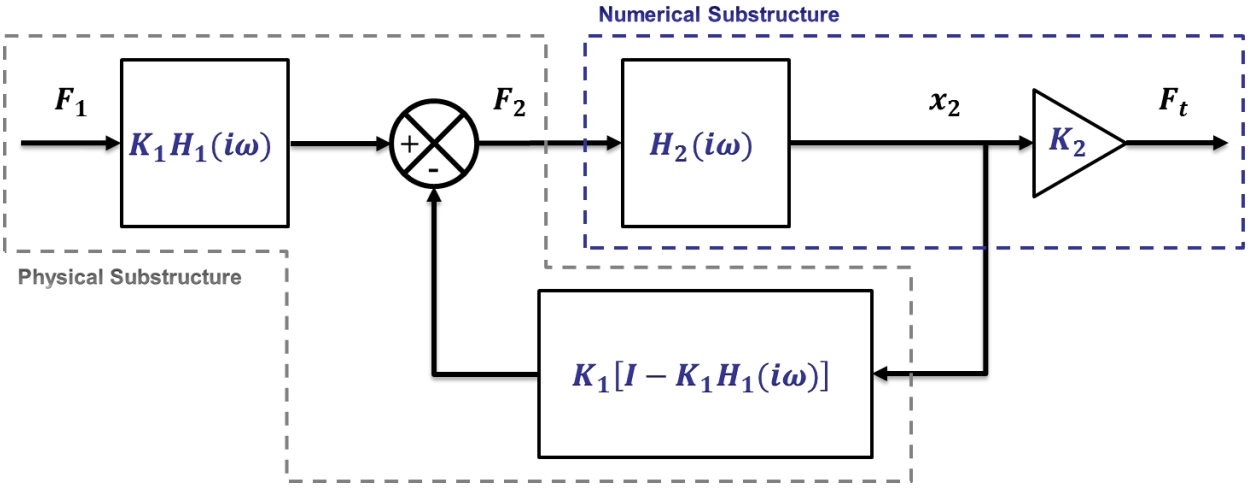

Figure 2.10 –Simplified System Diagram of the Coupled System

This diagram more clearly shows the contribution of the feedback term of the coupled system control diagram opposed to the *Darby Method* control diagram with consists of just the through path. The $K_1H_1(i\omega)$ term represents the force transmissibility of the first system to the second system. The $K_1[I - K_1H_1(i\omega)]$ term represents the reactant force due to the motion of the second system onto the first system (dynamic stiffness) in order to enforce equilibrium and the difference of these two force terms is the true excitation force onto the second system. Finally, by multiplying the motion of the second system by its stiffness, it calculates the transmitted force to the base of the system. The resulting diagram also lends itself very well to the RTHS approach. Figure 2.10 shows how this coupled system is divided into the physical and numerical substructures using the RTHS approach.

As in any substructuring method, it is important to couple the necessary degrees of freedom of the substructures in order to accurately represent the desired dynamics. Four tri-axial force sensors placed underneath the isolation system of the physical substructure at the four bottom corners are used to measure and transmit the reactant forces to the numerical substructure.

In this preliminary experiment, whose purpose is to validate the approach of using RTHS for quantification of mechanical equipment, the interest is only the lowest frequency dominant modes of the system. Each of these substructures is a multi-degree of freedom system with multiple directional and cross-coupled modes however, the target of this study are only the low frequency in-phase and out-of-phase uni-directional lateral modes. Since this experiment is only interested in the lateral modes of the system, an uni-axial servo-hydraulic actuator system is sufficient to achieve the interface between the physical and numerical substructures of the RTHS.

The TPA and coupled system comparison analysis described in the previous section was used to determine the frequency range in which uni-axial RTHS would be beneficial. A stiffness ratio, K_1/K_2 and a mass ratio, M_1/M_2 both equal to one were used to calculate the necessary bandwidth. Solving Equation [2.16] using these mass and stiffness ratios, we get a $\frac{\omega_E}{\omega_2}$ ratio of 3.33. Since ω_2 is 4Hz, ω_E is determined to be 13.2Hz. Therefore a substructuring bandwidth of 0-13Hz would be sufficient to mimic the desired low frequency dynamics of the experimental system. However, because this study is only interested in the lateral motion of the system which occurs below 8Hz, a bandwidth of 0-8Hz was used during the RTHS.

2.4.2 Transfer System Compensation

The servo-hydraulic control system used to connect the physical and numerical substructures typically referred to as the transfer system, has frequency dependent dynamics that need to be compensated for in order to provide accurate tracking of desired displacements. The frequency response function between the commanded input and the measured output with the physical substructure present on the shake table gives

a measurement of the frequency dependent dynamics of the actuator. These dynamics are potentially detrimental to the stability of the real time hybrid feedback loop and need to be compensated.

The feedforward compensator is designed to cancel the modeled dynamics of the servo hydraulic system, which would ideally be the inverse of the model fit of the servo hydraulic dynamics. Let $A(i\omega)$ be the frequency domain transfer function of the servo hydraulic dynamics and let $C(i\omega)$ be the feedforward compensator transfer function.

$$A(i\omega) = \frac{\prod_{i=1}^{n}(i\omega - z_i)}{\prod_{i=1}^{n}(i\omega - p_i)} \quad [2.18]$$

$$C(i\omega) = A(i\omega)^{-1} \quad [2.19]$$

If the transfer function model fit has equal number of poles, p_i and zeroes, z_i then an exact inverse can be taken. However, in most cases, the model has few zeroes. Therefore, when the model is inverted is not a proper transfer function, i.e. more zeros than poles. The low pass inverse compensator design methodology described in (Carrion & Spencer, 2007), uses a linear scaling factor, α to duplicate the existing poles of the SISO transfer function as additional poles at higher frequencies. These additional poles balance the inverted transfer function and make it so an inversion is stable. Instead of using an arbitrary α to multiply the existing poles, this α was designed to scale the actuator poles so they are placed as close to the Nyquist frequency as possible. The theory being that if the additional poles are as large as possible, they will have a minimal effect on the desired dynamics at low frequencies. To determine our value of α, first we assume that the delay that we want to compensate for is a pure time delay whose frequency domain transfer function, $A(i\omega)$ takes the form:

$$A(i\omega) = \frac{1}{i\omega\tau + 1} \quad [2.20]$$

where τ is the assumed time delay of the system. Solving for the pole of this transfer function, p_o gives

$$p_o = -\frac{1}{\tau} \quad [2.21]$$

If we then say that we want to place the new pole, p' at the Nyquist frequency, $\omega_{nyquist}$ there exist a linear scaling factor, α that would duplicate the existing pole of $A(i\omega)$ and force it as close to the Nyquist frequency as possible. Substituting $\omega_{nyquist}$ for p' and the known value of $p_o$into the equation for α gives

$$\alpha = \frac{p'}{p_o} = \frac{-\omega_{nyquist}}{-1/\tau} = \omega_{nyquist}\tau \quad [2.22],[2.23]$$

This α is used in the design of the low pass filter, $L(i\omega)$ using the equation below where n is the number of poles of the actuator transfer function curve fit.

$$L(i\omega) = \frac{\prod_{i=1}^{n} \alpha_i p_i}{\prod_{i=1}^{n}(i\omega - \alpha_i p_i)} \quad [2.24]$$

$$C(i\omega) = A(i\omega)^{-1} L(i\omega) \quad [2.25]$$

2.4.3Stability and Performance Analysis

Presence of apparent time delay and magnitude attenuation in the real time hybrid substructuring feedback loop due to servo hydraulic actuator dynamics can lead to unwanted instability and loss of accuracy during RTHS testing. There are basically two causes for instability: inherent instability and feedback instability. Inherent instability is when the system is naturally unstable meaning even an open loop representation would be unstable. The second cause for instability is feedback. This source of instability works like a viscous circle, where the feedback signal causes the numerical substructure to command increasingly higher and higher displacements to the servo hydraulic transfer system. In the design of mechanical systems, any system design that has inherent instabilities would not be an adequate design and therefore the instability concerns with real time hybrid substructuring are those of feedback stability.

Real time hybrid substructuring is a control problem of reference tracking opposed to disturbance rejection. The numerical substructure calculates a displacement to be commanded to the servo hydraulic transfer system and then to the physical substructure. It is critical that this commanded displacement is communicated with accurate magnitude and phase.

The robust stability analysis methodology (Botelho R. , 2015), is used to provide insight on acceptable time delay for stable closed-loop testing by casting stability analysis as an uncertainty problem. Since stability is only dependent on the dynamics of the control loop, the control blocks outside the control loop in Figure 2.10 are ignored which leaves the physical substructure is given as

$$P(i\omega) = K_1[I - K_1 H_1(i\omega)] \quad [2.26]$$

And the numeric substructure is given as

$$N(i\omega) = H_2(i\omega) \quad [2.27]$$

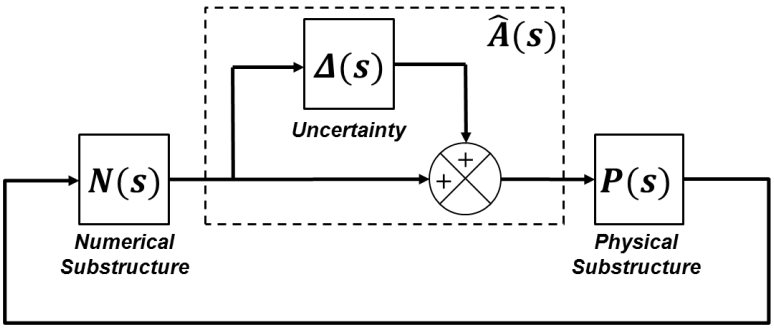

Figure 2.11 – Schematic of Robust Stability Analysis Feedback Loop

Figure 2.11 shows how the robust stability analysis methodology sets up the RTHS feedback loop in order determine whether the loop will be stable or not. The robust stability analysis methodology says the sufficient condition for robust stability is

$$\|\Delta(i\omega)T_0(i\omega)\|_\infty < 1 \quad [2.28]$$

where

$$T_0(i\omega) = [I + P(i\omega)N(i\omega)]^{-1}P(i\omega)N(i\omega) \quad [2.29]$$

$$\Delta(i\omega) = \hat{A}(i\omega) - I = [I - A(i\omega)K(i\omega)]^{-1}\{A(i\omega)C(i\omega) - I\} \quad [2.30]$$

where $\hat{A}(i\omega)$ is the compensated dynamics of the transfer system which usually consists of $A(i\omega)$, the uncompensated dynamics of the transfer system, $K(i\omega)$, the feedback gain of the transfer system and $C(i\omega)$ the feed-forward compensator of the transfer system.

2.5 Notional Mechanical Equipment Real-Time Hybrid Substructuring Test

A notational mechanical system consisting of mechanical equipment and a support structure is used here to demonstrate real time hybrid substructuring for use in predicting system level vibration performance of mechanical equipment. The RTHS test is conducted in the Structures Research Laboratory at the University of Connecticut on the uniaxial shake table. A Quanser Shake Table II, serves as the mechanical equipment, is mounted on four linear coil springs spaced 18 inches horizontally and 11 inches laterally. The support structure was placed on similar four linear coil springs spaced 18 inches horizontally and 11 inches laterally. The support structure is two 24.0 by 24.0 x 0.5 inches horizontal steel plates connected with nine 1 inch diameter threaded rods. The plates are 12 inches apart, vertically. Figure 2.12 shows each of these systems as well as these two systems assembled into the mechanical system.

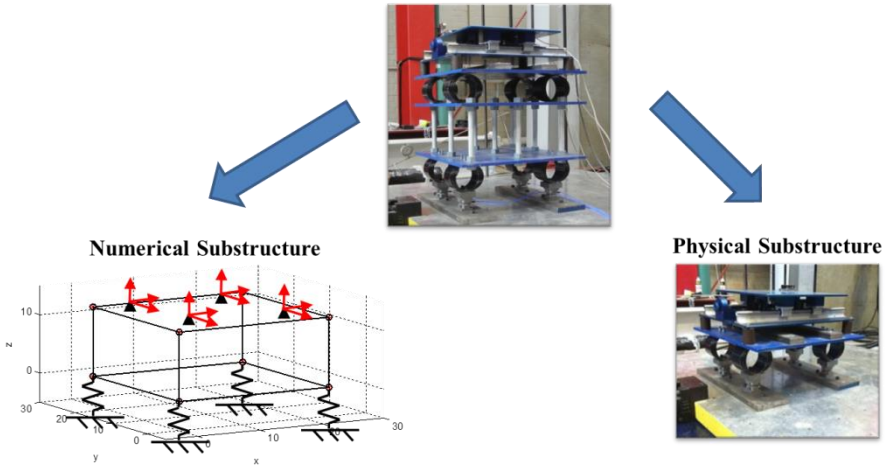

Figure 2.12 – Experimental Substructuring Approach

The complete notational mechanical system (shown in Figure 2.12) was constructed and the vibration force transmitted through the system to the base was measured below the four corner isolation points using four PCB Piezoelectric tri-axial force sensors Model #261A02. The Quanser shake table was commanded a band limited white noise (BLWN) with a roll off at higher frequencies. The roll off at higher frequencies is achieved with an 8th order Butterworth filter with a cutoff frequency of 20Hz. This ensures that low frequency resonances are sufficiently excited but also excites higher frequencies with lower energy so to avoid pushing the Quanser Shake Table II towards its mechanical limits. Auto power spectral densities (PSDs) of the measured force under the bottom layer of the four coil springs were recorded using a Data Physics dynamic signal analyzer. Figure 2.13 shows the force transmitted to the force sensors at the base of the full system. These results represent the force transmitted through the full system and will later be used to validate the RTHS results.

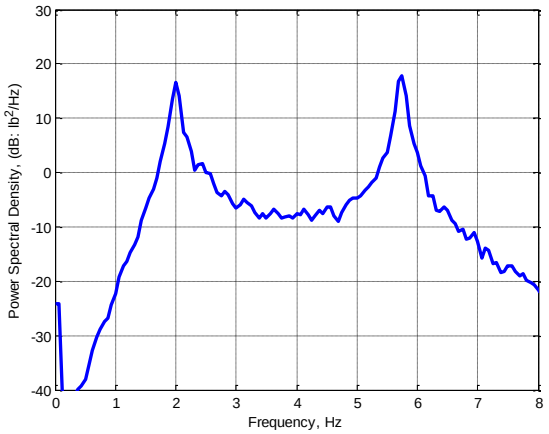

Figure 2.13 – PSD of the Total Force Transmitted to the Base of the Full System in the Horizontal Direction

The mechanical equipment, i.e. the Quanser Shake Table II, assembly was then attached to the same four PCB Piezoelectric tri-axial force sensors. The Quanser Shake Table II was commanded with the same band limited white noise (BLWN) as in the full system test. Auto power spectral densities (PSDs) of the measured force under the four coil springs were recorded using a Data Physics dynamic signal analyzer. These results represent the response of the first mass-spring oscillator which will later be the physical substructure of the real time hybrid simulation. Since this experiment is being used to verify a single

degree of freedom real time hybrid simulation, only the horizontal degree of freedom of interest and is shown in Figure 2.14.

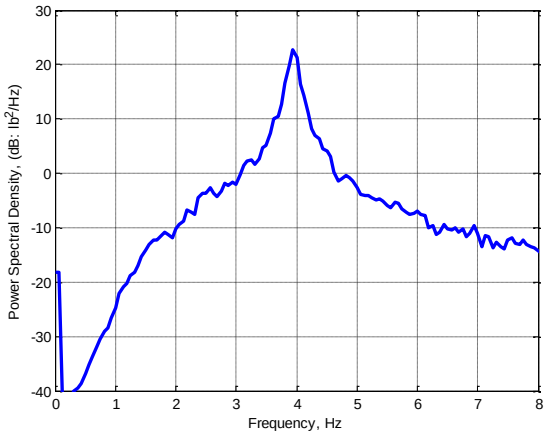

Figure 2.14 – PSD of the Total Force Transmitted to the Base of the Mechanical Equipment in the Horizontal Direction

The support structure is assumed linear and an accurate numerical model of this structure is developed. This portion of the system will later be the numerical substructure of the real time hybrid simulation. The numerical model constructed was a six degree of freedom (DOF) state space model with 12 states. A frequency response function of horizontal displacements due to horizontal forces was calculated as is shown in Figure 2.15.

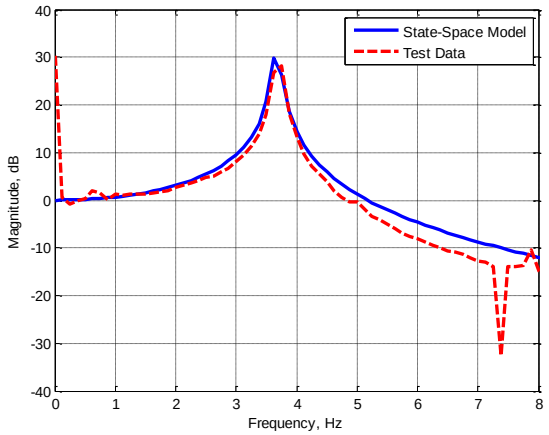

Figure 2.15 – Frequency Response Function of Horizontal Displacement Due to Horizontal Force Excitation.

2.5.1 Transfer System Compensation

System identification was performed to quantify the servo-hydraulic control system frequency dependent dynamics. The servo hydraulic actuator is given a commanded displacement BLWN with a range of RMS values from .02 to .04 and then the actual displacement of the actuator is measured. The frequency response function between the commanded input and the measured output gives a measurement of the frequency dependent dynamics of the actuator. Figure 2.16 shows the magnitude and phase measurement of the frequency response function between the commanded and measured actuator displacement.

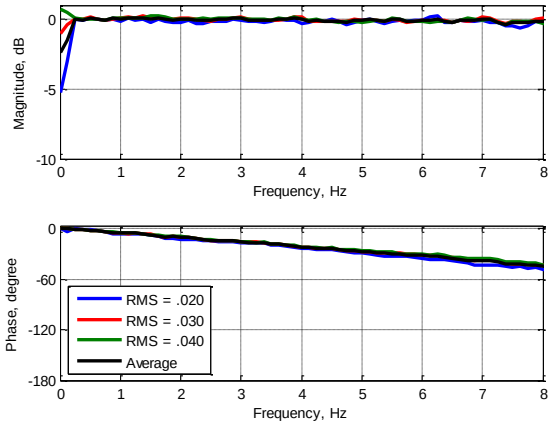

Figure 2.16 – Frequency Response Function of Servo Hydraulic Actuator Dynamics

A low pass inverse compensator was designed using this frequency response function data. The MATLAB function *invfreqs* was used to curve fit the data up to 8Hz. A third order denominator with a constant numerator was used to fit the data.

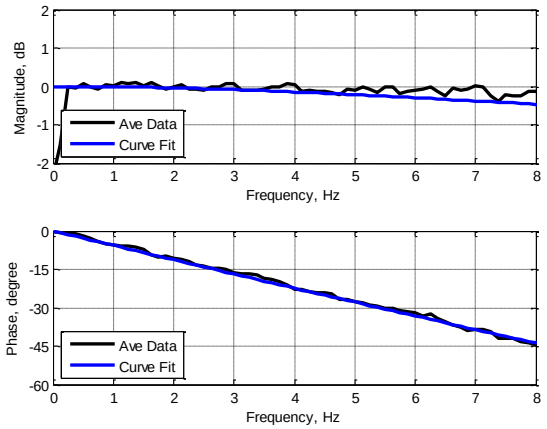

Figure 2.17 – Curve Fit of the Servo Hydraulic Actuator Frequency Response Function

The frequency response function from the curve fit was used to design a low pass inverse compensator for the feed-forward portion of the control system. Various values of the feedback gain, *K*, were tried during system identification of the hydraulic system with feed forward compensators. The LPIC mentioned above seemed to be independent of the feedback gain that was used. Since the system became more aggressive as more feedback was added, K = 0.3 was determined to be an adequate feedback gain for the RTHS.

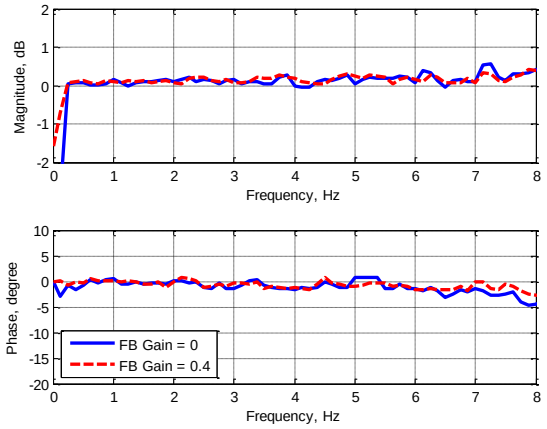

Figure 2.18 – Frequency Response Function of LPIC with Various Values of FB Gain

2.5.2 Stability and Performance Analysis

The robust stability analysis methodology was used to provide insight on acceptable time delay for the RTHS test of the notional mechanical equipment. Figure 2.19 shows the results of this analysis for the uncompensated transfer system, the compensated transfer system using just the feedforward compensator and then the compensated transfer system using both feedforward and feedback compensation.

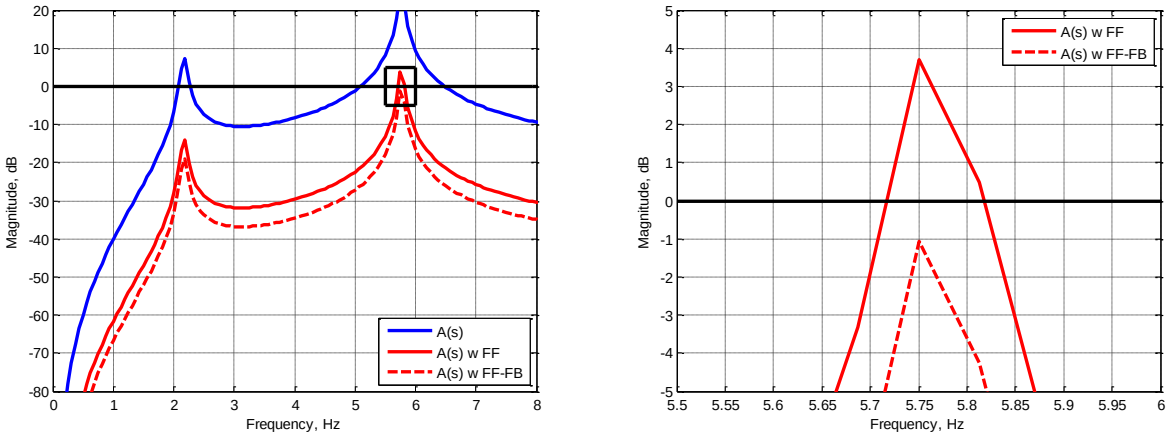

Figure 2.19 – Robust Stability Analysis for the Uncompensated and Compensated Transfer System.

These results show that the RTHS feedback loop is marginally stable with the feedback compensator. The feedback gain that was used helps reduce the stability curve slightly greater which bring the curve below the 0dB line.

2.5.3 Real Time Hybrid Simulation Results

The RTHS is conducted in the Structures Research Laboratory at the University of Connecticut. The mechanical equipment was placed on the linear springs mounted to the tri-axial force sensors. This setup was placed on the single degree of freedom servo hydraulic actuator shake table. The state space multi degree of freedom numerical model of the support structure was used in the real time hybrid simulation. A dSpace DS1103 digital controller was used to communicate between the computer simulation and the hydraulic actuator.

The Quanser Shake Table II was driven with the same band limited white noise as in the previous mechanical equipment tests. The forces from the tri-axial sensors are sent through the dSPACE controller into the numerical model. These forces drove the numerical model of the support structure. The displacement response of the support structure is calculated by the state space numerical representation and then communicated to the hydraulic actuator which displaces the base of the component. This same numerical displacement response is then used to calculate the transmitted force at the base of the support structure numerical model. The output of the state space numerical model is the reaction displacement at

the CG of the support structure. Then through a rigid body transformation, equivalent displacements at the four isolators were calculated and then multiplied by the stiffness of the isolators to calculate equivalent transmitted forces. This calculated transmitted force was then compared to the test of the component assembly mounted to the top of the support structure.

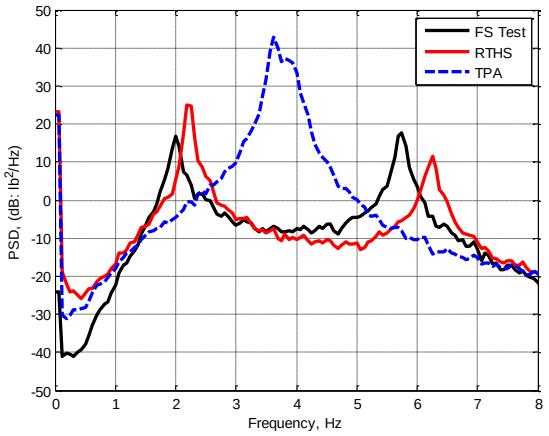

Figure 2.20 – Comparison of RTHS vs. Experimental Test Results

The results from the RTHS experiment show favorable coherence to the full system experiment results. Comparing these results to the *Darby Method* proves that RTHS can be a significantly more accurate and less conservative representation of the phase relationship of the coupled system than current methods. However, there still exist subtle inaccuracies in the RTHS experiment when compared to full system experimental results. There are two potential reasons for these inaccuracies.

The transfer system enforces only lateral compatibility between the numerical substructure and the physical substructure. However, even the low frequency resonant frequencies that were thought of as lateral modes aren't purely lateral and do consist of other directional coupling. Data from the full system test was used to plot the displacement of the numerical substructure at 2Hz and 5.75Hz assuming a rigid body. These experimentally obtained "mode shapes" are shown in Figure 2.21.

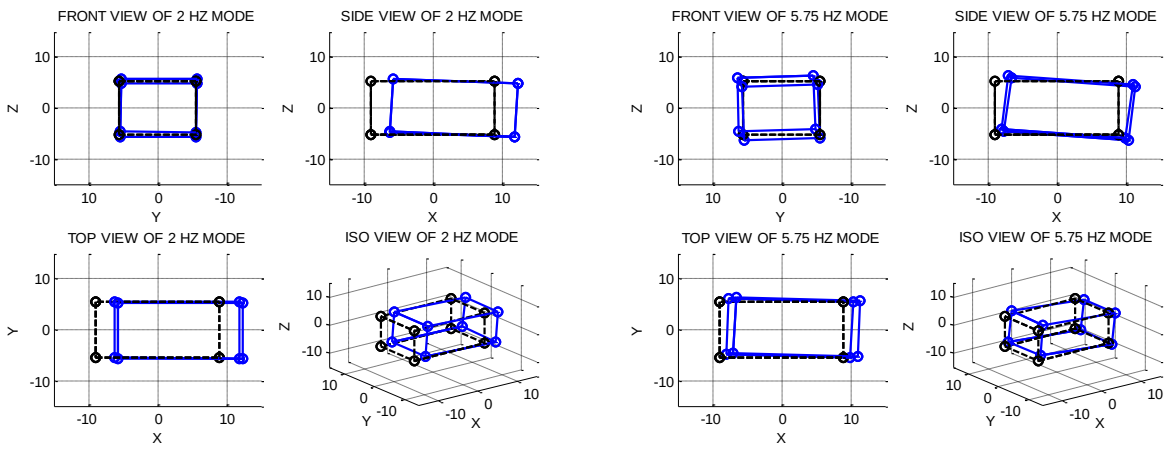

Figure 2.21 – Experimental Mode Shapes of the Numerical Substructure

These results show that the resonance frequencies of 2 and 5.75Hz do not consist of only lateral motion but contain slight vertical and/or rotational motion. These results may explain the remaining inconsistencies between the full system test resonant frequencies and the RTHS resonant frequencies. By not connecting the other DOF between the numerical and physical substructures the interaction between these two substructures is essentially constrained and therefore not accurate.

To verify this theory, fully numerical simulations of the RTHS experiment were done by simulating both complete 6 DOF coupling between the substructures and 1 DOF coupling which represents the RTHS experiment performed in this paper. These simulations were performed by using the physical substructure data shown in Figure 2.14 and then combining it numerically with the numeric substructure shown in Figure 2.15 and then either coupling them in all 6DOF or restricting the coupling to only the lateral DOF. The results of both of these simulations are shown in Figure 2.22.

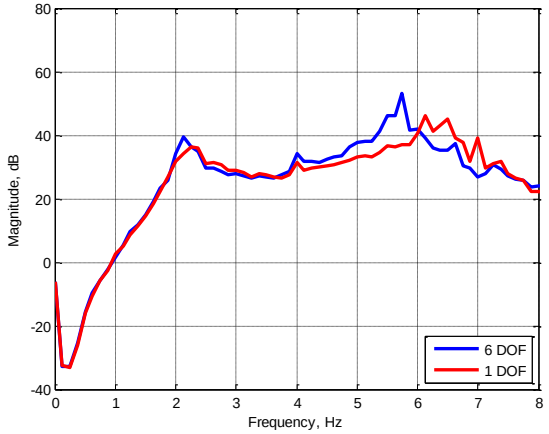

Figure 2.22 – Comparison of 6DOF and 1DOF RTHS Simulations.

These results show consistent results with the results shown in Figure 2.20 of the RTHS experiment. This supports the assumption that the discrepancies in the RTHS experiment results are due to the limit connectivity between the physical and numeric substructures. This is improved upon by coupling all 6DOF between the two substructures in future research.

Another potential reason for the discrepancies is the marginal stability of the RTHS control loop. Previous work with the robust stability method shows that marginal stability, however still stable, can result in performance inaccuracies, (Botelho R. , 2015). This work also states that robust performance is when

$$\|\Delta(s)T_0(s)\|_\infty \ll 1 \qquad [2.31]$$

which is interpreted as the maximum singular value being an order of magnitude less than one, in decibel scale is -20. As shown in Figure 2.19, the RTHS control loop has frequency ranges of robust stability but not robust performance i.e., less than zero dB but greater than -20 dB, which could lead to inaccurate results. These frequency range's non-robust performance coincide with the frequency ranges of inaccuracy of the RTHS results shown in Figure 2.20. What appears to be a frequency shift, between the full system test and the RTHS results is also potentially explained by (Botelho R. , 2015). This research describes critical frequencies at which a system will oscillate when marginally stable. These critical frequencies, in lightly damped systems are typically relatively close to the natural frequencies of the

system. The system oscillations, due to marginal stability will correspond to these critical frequencies instead of the natural frequencies of the system. Since, these critical frequencies are typically very close to the natural frequencies of the system, the results can misleadingly show what seems to be a frequency shift in resonance when compared to system dynamics without time delay i.e., the full system test shown in Figure 2.20. Further research is necessary to prove this theory.

2.6 Conclusion

This chapter describes the development and implementation of RTHS for quantification of system level vibration of mechanical equipment systems using the example of a simplified multi stage mechanical system. RTHS was used to interface a physical substructure, notional mechanical equipment, to a notional support structure, which was represented numerically, forming a multi stage system. This experiment was accomplished by closed-loop RTHS testing using a model-based feedforward-feedback actuator tracking controller with a low pass inverse compensation (LPIC). The consistent results of the RTHS with the full system experimental test proves that RTHS can accurately represent the dynamics of the coupled system as well as provide insight into the design of mechanical systems using system level mechanical vibration.

2.7 References

Akey, J G. (1963). Transfer-Matrix Method and Computer Program for the Vibration Analysis of Series Plane-Frame Structures Having Material Damping and Complex Terminations. *Defense Technical Information Center*.

Botelho, R. (2015). *Real-Time Hybrid Substructuring for Marine Application of Vibration Control and Structural Acoustics.* University of Connecticut.

Botelho, R. B., Christenson, R., & Franco, J. (2013). Exact Stability Analysis for Uniaxial Real Time Hybrid Simulation of 1-DOF and 2-DOF Structural Systems. *Engineering Mechanics Institute Conference.*

Carmeli, M. S., Castelli-Dezzaa, F., Mauri, M., & Marchegiani, G. (2013). Novel Mechanical Hardware in the Loop Platform for Distributed Generation Systems. *Distributed Generation and Alternative Energy Journal, 28*(3), 7-27.

Carrion, J. E., & Spencer, B. (2007). Model Based Strategies for Real Time Hybrid Testing. *NSEL Report No NSEL-006*.

Christenson, R., & Lin, Y. Z. (2008). Real Time Hybrid Simulation of a Siesmically Excited Structure With Large Scale Magneto Rheological Fluid Dampers. In *Hybrid Simulation Theory, Implementation and Applications.*

Darby, A. P., Blakeborough, A., & Williams, M. S. (1999). Real Time Substructure Test Using Hydraulic Actuator. *Journal of Engineering Mechanics, 125*(10), 1133-1139.

Darby, R. A. (1964). A Practical Method for Predicting Acoustic Radiation or Shock Excursions of Navy Machinery. *The Shock and Vibration Bulletin, 3*.

de Klerk, D., Rixen, D. J., & Voormeeren, S. N. (2008). General Framework for Dynamic Substructuring: History, Review and Classification of Techniques. *AIAA Journal, 46*(5), 1169-1181.

de Klerk, D., Rixen, D., & de Jong, J. (2006). The Frequency Based Substructuring Method Reformulation According to the Dual Domain Decomposition Method. *Proceedings of the Fifteenth International Modal Analysis Conference.* St. Louis, MO.

Dimig, J., Shield, C., French, C., Bailey, F., & Clark, A. (1999). Effective Force Testing: A Method of Siesmic Simulation for Structural Testing. *Journal of Structural Engineering, 125*(9), 1028-1037.

Fathy, H. K., Ahlawat, R., & Stein, J. L. (2005). Proper powertrain modeling for engine-in-the-loop simulation. *ASME 2005 International Mechanical Engineering Congress and Exposition*, 1195-1201.

Filipi, Z., & Kim, Y. J. (2010). Hydraulic hybrid propulsion for heavy vehicles: Combining the simulation and engine-in-the-loop techniques to maximize the fuel economy and emission benefits. *il & Gas Science and Technology–Revue de l'Institut Francais du Petrole, 65*(1), 155-178.

Filipi, Z., Fathy, H., Hagena, J., Knafl, A., Ahlawat, R., Liu, J., . . . Stein, J. (2006). Engine-in-the-loop testing for evaluating hybrid propulsion concepts and transient emissions-HMMWV case study. *AE Technical Paper*.

Gao, X., Castaneda, N., & Dyke, S. J. (2013). Experimental validation of a generalized procedure for MDOF real-time hybrid simulatio. *Journal of Engineering Mechanics, 140*(4).

Gordis, J., Bielawa, R., & Flannelly, W. (1991). A Generalized Theory for Frequency Domain Structural Synthesis. *Journal of Sound & Vibration, 150*, 139-158.

Hanselmann, H. (1993). *Hardware-in-the loop simulation as a standard approach for development, customization, and production test of ECU's.* SAE Technical Paper.

Horiuchi, T., Inoue, M., Konno, T., & Namita, Y. (1999). Real Time Hybrid Experimental System With Actuator Delay Compensation and It's Applications to a Piping System With Energy Absorber. *Earthquaker Engineering and Structural Dynamics, 28*(10), 1121-1141.

Isermann, R., Schaffnit, J., & Sinsel, S. (1999). Hardware-in-the-loop simulation for the design and testing of engine-control systems. *Control Engineering Practice, 7*(5), 643-655.

Jetmundsen, B., Bielawa, R. L., & Flannelly, W. G. (1988). Generalized frequency domain substructure synthesis. *Journal of the American Helicopter Society, 33*(1), 55-64.

Jiang, Z., Kim, S. J., Plude, S., & Christenson, R. (2013). Real Time Hybrid Simulation of a Complex Bridge Model with MR Dampers Using the Convolution Integral Method. *Journal of Smart Materials and Structures, 22*(10).

Nakashima, M., & Masaoka, N. (1999). Real Time On-Line Test for MDOF Systems. *Earthquake Engineering and Structural Dynamics, 28*, 393-420.

Phillips, B. M., & Spencer Jr., B. F. (2012). Model-based multiactuator control for real-time hybrid simulation. *Journal of Engineering Mechanics, 139*(2), 219-228.

Sykes, A. O. (1956). The Evaluation of Mounts Isolating Nonrigid Machines From Nonrigid Foundations. *ASME Applied Machanics Division Conference.*

Wright, D. V. (1958). Impedance Analysis of Distributed Mechanical Systems. *Colloquim on Mechanical Impedance Methods fro Mechanical Vibrations.* ASME.

3 TRANSFER PATH HYBRID SUBSTRUCTURING FOR EXPERIMENTAL-NUMERICAL DYNAMIC TESTING OF MECHANICAL EQUIPMENT

3.1 Abstract

In the design of mechanical systems, there are constraints imposed on the vibration of mechanical equipment to limit the vibration transmission into its support structure. To accurately predict the coupled system response, it is important to capture the coupled interaction of the two portions, i.e., the mechanical equipment and the support structure, of the mechanical system. Typically during a design, the analysis of the full mechanical system is not possible because a large part of the system may be non-existent. Existing methods known as Transfer Path Analysis and Frequency Based Substructuring are techniques for predicting the coupled response of vibrating mechanical systems. In this paper, a feedback based hybrid substructuring approach to Transfer Path Analysis is proposed. By recognizing the similarities between feedback control and dynamic substructuring, this paper demonstrates that this approach can accurately predict the coupled dynamic system response of multiple substructured systems including operating mechanical equipment with a complex vibration source. The main advantage of this method is that it uses blocked force measurements in the form of a power spectral density matrix measured uncoupled from the rest of the system. This substructuring method is demonstrated using a simplified case study comprised of a two-stage vibration isolation system and excited by operating mechanical equipment.

3.2 Introduction

Vibration of mechanical equipment can result in fatigue, detection, and/or environmental concerns for a support structure. A critical aspect of the design of systems, that include mechanical equipment, is quantifying the level of transmitted vibration energy from the mechanical equipment and through the supporting structure. The system design typically consists of strict constraints imposed on the vibration transmission of the mechanical equipment through the support structure. During the design phase of a

system, the mechanical equipment is pre-existing either from previous designs or they are commercially available components purchased from a vendor. The support structure is typically non-existent and is designed and optimized using Computer Aided Design (CAD) software. This makes testing of the full mechanical system, impossible. For these reasons, the analysis of the mechanical system normally requires the combination of multiple quantifications of dynamics of various substructures of the mechanical system. Dynamic Substructuring takes advantage of the theories of finite element analysis (FEA) to accurately combine the dynamics of multiple substructures. One of the earliest methods for dynamic substructuring was degree of freedom condensation method proposed by (Guyan, 1965). This method reduced the mass and stiffness matrices of numerical models of structural substructures in order to reduce complexity and ease computation of the coupled dynamics of a support structure. However, there are many assumptions and conditions necessary to take advantage of these methods. First and foremost, Dynamics Substructuring is used for the coupling of multiple theoretical numerical (nowadays, typically FEA) models which are inherently linear stationary approximations of various substructures of a system. These methods also generally require square sets of linear equations, i.e., the number of response locations is equal to the number of locations of excitation for a given substructure representation, so that an inverse can be calculated.

Existing methods, in the field of substructuring, known as Transfer Path Analysis (TPA) are frequency response functions (FRF) based techniques that describe the dynamics of the mechanical system by the multiplication of the FRFs of the system substructures. This method can also be used to combine theoretical (FEM) models and experimental measurements of system substructures and were developed by (Plunt, 1998) and (Plunt, 2004) for the automotive industry and (Darby R. A., 1964) for the marine industry. However, the disadvantage of these TPA methods is that they do not always consider the dynamic coupling between the receiving and exciting substructures. This limitation becomes critical at low frequencies due to the interaction between the modes of the individual substructures.

Variations of TPA methods are known as Frequency Based Substructuring (FBS) methods which allow for the calculation of the entire mechanical system dynamic response based on the FRFs of the system substructures using various methods. Primary developments of FBS methods are (Crowley, Klosterman, Rocklin, & Vold, 1984), (Jetmundsen, Bielawa, & Flannelly, 1998), (Imregun, Robb, & Ewins, 1987) and later on (Gordis, Bielawa, & Flannelly, 1991) and (de Klerk, Rixen, & de Jong, 2006). Generally, this work demonstrated a wide variety of methods to couple substructures based on either numerically computed or experimentally measured FRFs. There are many other variations of FBS methods including (Su & Juang, 1994)and later on (Sjovall & Abrahamsson, 2007)which developed state-space based methods to couple structural substructures together, as well as recently (Rixen & van derValk, 2013) who developed a time-domain based substructuring technique which is analogous to the aforementioned frequency-domain techniques. This method takes advantage of either numerically or experimentally measured impulse response functions (IRF). All of these methods allow the coupling of system substructures, as long as they can be linearized in a stationary operation condition, have constant parameters and have nodal connection points. If the excitation is known, one can also calculate the dynamic responses of the total mechanical system. One large advantage of these methods is that they are a hybrid approach, which means that both measured and numerically obtained components can be combined. In this way, the strengths of both numerical and experimental analyses can be capitalized upon; nonlinearities and complexities of the experimental system substructures can be coupled to the numerical FEA models in order to accurately predict the coupled dynamics of the entire mechanical system. However, a large drawback of these methods is that they generally require that the vibratory excitation be known and be able to be quantified; (de Klerk, Rixen, & Coomeeren, 2008) did significant work to develop methods to identify and quantify these excitation sources. However, this can be fairly difficult and labor intensive in a real life experimental environment.

Real-time hybrid substructuring (RTHS) is a relatively new test method, recently made more practical because of advances in computer power, digital signal processing hardware/software, and hydraulic

control hardware that is used for vibration testing for calculating the dynamic performance of a mechanical system by partitioning a mechanical system into physical and numerical substructures and then interfacing them together in real-time similar to hardware-in-the-loop testing. Early developments of RTHS include (Horiuchi, Inoue, Konno, & Namita, 1999), (Nakashima & Masaoka, 1999), and (Darby, Blakeborough, & Williams, 1999). As with FBS methods, RTHS is a hybrid method, which takes advantage of both experimental methods along with numerical computational methods of system substructures. This method allows the dynamic excitation of the system to be unknown since it is represented in the physical substructure. Since RTHS runs in real time, this test method also allows the dynamic testing of time-variant systems. Also, because the rest of the rest of the mechanical system is represented by a numeric substructure, virtual sensors are used to calculate various metrics which can be recorded in real time which allows the use of advanced signal processing for non-linear behavior or other time-variant dependencies. However, this system is highly dependent on the performance of the actuator system that is used to transmit the displacement feedback from the numerical substructure to the physical substructure. For low frequencies, this is typically a servo-hydraulic system which can be difficult to get accurate reference tracking performance.

In this paper, a practical control based hybrid experimental-numerical approach to substructuring, referred to Transfer Path Hybrid Substructuring (TPHS) is proposed. This approach was developed out of recognition of the similarities of techniques in both the feedback control, i.e. RTHS, and the dynamic substructuring fields. (Botelho & Christenson, 2015) provides a comparison of the mathematically similar formulations for both feedback control theory and dynamic substructuring. By identifying these similarities, it allows the leveraging of elementary feedback control theory, to the Transfer Path Analysis and Frequency Based Substructuring fields. This paper leverages these similarities in order to demonstrate that this new TPHS method can be used to accurately predict the coupled dynamics of multiple substructures of a mechanical system. This method is also a hybrid approach which allows for each of the system substructures to be represented by either experimentally obtained or numerically computed FRFs.

This paper will demonstrate in a simplified case study how a power spectral density (PSD) matrix can be used as input to the substructuring procedure.

3.3 Experimental-Numerical Substructuring Incorporating Dynamics Interaction

Often it is desirable to physically test a component in the substructuring framework. Real Time Hybrid Substructuring (RTHS) is a test method that provides the capability to isolate and physically test the more advanced critical mechanical equipment of a mechanical system at the design phase of the system while including the dynamic interaction with a numerical representation of the remainder of the support structure. This is advantageous over more traditional substructuring techniques because the portion of the system that makes up the physical substructure is not required to be dynamically quantified. A typical RTHS test is made up of the numerical substructure, the physical substructure as well as the actuator system required to command calculated displacements from the numeric substructure to the physical substructure. Figure 3.1 shows this typical RTHS test layout displayed as a control based block diagram.

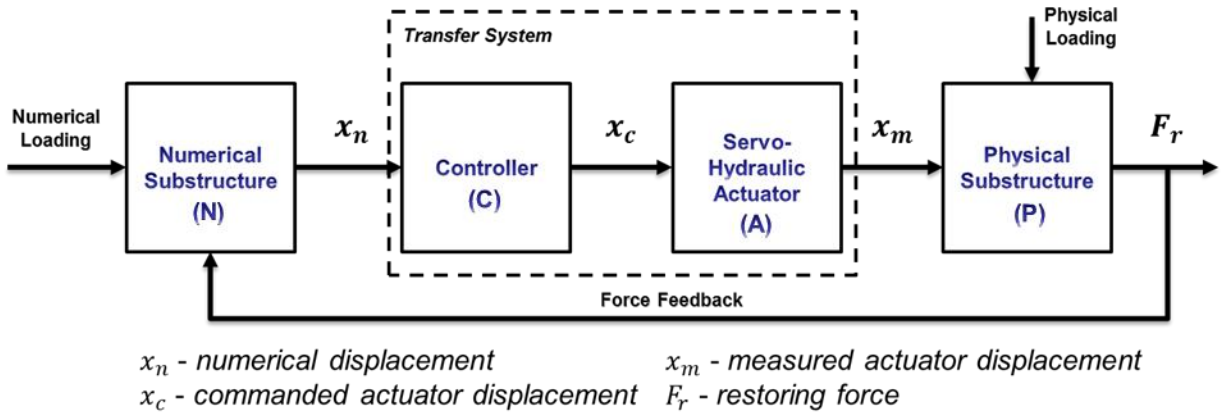

Figure 3.1 – Control Block Diagram of a Typical RTHS Test

The main challenge of RTHS is the dependence on this transfer system's dynamics. At low frequencies, where dynamic coupling of system substructures is necessary, this transfer system is typically a servo-hydraulic actuator system. Servo-hydraulic actuator systems tend to have significant frequency dependent

magnitude attenuation and time delay. A large portion of the research done concerning RTHS is compensating and controlling these frequency dependent dynamics.

The mechanical system of interest in this paper is that which consists of mechanical equipment, which is the vibration source, and its support structure. The mechanical portion of the system lends itself well to the physical substructure portion of the RTHS layout. This mechanical equipment typically has complex dynamics and acoustic excitations which are difficult to model with classic numerical methods also possibility because of non-linarites and time-variant properties. The support structure, on the other hand, lends itself well to the numerical substructure of the RTHS layout shown in Figure 3.1. This paper's interest is the system excitation source's that come from the mechanical component, i.e., the physical substructure and is not interested in vibratory excitations that come from the support structure, i.e., the numerical substructure. Therefore, the numerical loading shown in Figure 3.1 will be ignored for this paper.

The physical loading shown in Figure 3.1 is analogous to what is known in the controls field as a system disturbance. In this case, the disturbance is the excitation of the physical substructure and it is the interest of this paper to quantify how that excitation affects the system dynamics as well as how the excitation is transmitted through the system. Spite the difference in the desired outcome of the analysis, feedback control analysis methods and tools can be leveraged to analyze the system.

3.4 Feedback-Based Approach to Transfer Path Hybrid Substructuring

This paper attempts to use the RTHS control diagram shown in Figure 3.1 and simple feedback diagram analysis to develop a new approach to substructuring referred to Transfer Path Hybrid Substructuring (TPHS). From the block diagram shown in Figure 3.1 (not including the numerical loading), the equation for the closed loop feedback diagram is given by

$$F_r = -P\hat{A}NF_r + P_iF_i \qquad [3.1]$$

where P is the physical substructure, N is the numeric substructure, $\hat{A}$ is the compensated transfer system, and P_i is the excitation load on the system, referred to here as the physical loading. Rearranging Equation [3.1] for the reactant force, F_r due to an input force, F_i gives the fundamental equation of TPHS shown below

$$\left\{\frac{F_r}{F_i}\right\} = \left[\frac{1}{1 + P\hat{A}N}\right] P_i \qquad [3.2]$$

This equation solves the coupled reactant force of the numerical and physical substructures at the interaction points between the two substructures.

One portion of the control diagram shown in Figure 3.1 that is not necessary with this method is the actuator dynamics frequency domain transfer function, $\hat{A}$. Specifically, when the physical substructure, P is tested, the input signals to the FRF calculations are the measured random input displacements, x_m. Since x_m is used as the physical substructure input signal, then the measured FRF does not include the actuator dynamics and the measured performance of the physical substructure, P is calculated in terms of a normalized input. Perfect actuator tracking, x_m is equal to the commanded displacement, x_c, can be assumed and the $\hat{A}$ transfer function then becomes identity and therefore is removed from Equation [3.2].

This is a significant advantage of this method over RTHS. A large portion of the complication of RTHS is compensating for the frequency dependent actuator dynamics which can be substantial. TPHS bypasses this complication by assuming ideal actuator reference tracking. This simplifies the governing equation of TPHS even further to

$$\left\{\frac{F_r}{F_i}\right\} = [I + PN]^{-1} P_i \qquad [3.3]$$

Equation [3.3] calculates the coupled reactant forces at the interaction points between the two substructures; however, this is not the metric of interest. To calculate the force at the base of the full system, the reactant force is then multiplied by a force transmissibility frequency domain transfer function

which is equal to the numeric substructure multiplied by the base isolator stiffness, $K_b N$. The TPHS equation for the base forces of the full system is

$$\left\{\frac{F_b}{F_i}\right\} = K_b N[I + PN]^{-1} P_i \qquad [3.4]$$

where F_b is the force at the base of the full system. Figure 3.2 shows Equation [3.4] as a simple feedback control diagram.

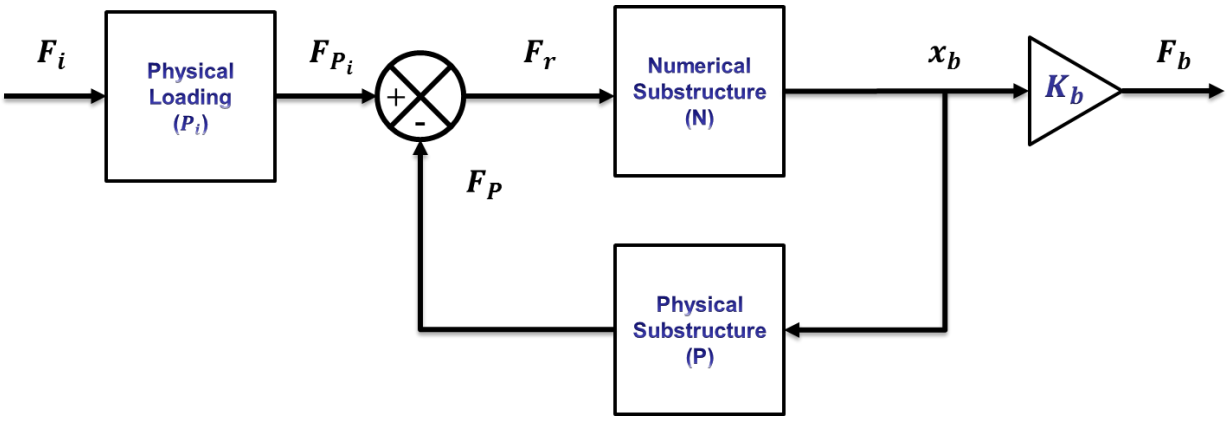

Figure 3.2 – Control Diagram Representing the TPHS Method

Figure 3.2 shows that the critical part of this analysis method is the feedback loop. Without it, the open-loop solutions is given by

$$\left\{\frac{F_b}{F_i}\right\} = K_b N P_i \qquad [3.5]$$

and by comparing this to Equation [3.4], it is shown that this critical feedback loop is represented by the $[I + PN]^{-1}$ term. The difference between the closed-loop and open-loop analysis will be demonstrated later on.

3.4.1Physical Loading Using Auto Power Spectral Densities

In most cases, mechanical systems have many complex excitations and it may be very difficult to quantify them. Therefore, mechanical equipment vibration is typically quantified in power spectral densities (PSD). This is a main disadvantage of most transfer path and frequency base substructuring methods; the

source of the dynamics is needed in order to experimentally measure FRFs of the physical substructure used in these hybrid methods.

This is the main advantage of Transfer Path Hybrid Substructuring. The controls based approach allows the physical excitation of the system to be in the form of a PSD (or a PSD matrix for the MDOF case). In the case of MDOF, the power spectral density matrix consists of auto power spectral densities along the diagonal of the matrix and cross power spectral densities in the off-diagonal terms between the two respective signals. The form of this PSD matrix is given below

$$G_{\mathrm{F}_i\mathrm{F}_i} = \begin{bmatrix} G_{11} & G_{12} & \cdots & G_{1n} \\ G_{21} & G_{22} & \cdots & G_{2n} \\ \vdots & \vdots & \ddots & \vdots \\ G_{n1} & G_{n2} & \cdots & G_{nn} \end{bmatrix} \quad [3.6]$$

where $G_{\mathrm{F}_i\mathrm{F}_i}$ is the PSD matrix of the force input to the system from the physical loading and n is the number of signal locations. The diagonal terms, G_{11}, G_{22}, … G_{nn} are the auto power spectral densities while all other off diagonal terms, G_{12}, G_{21}, … terms are the cross power spectral densities. Using this as the input to Equation [3.4] gives

$$\{G_{\mathrm{F}_b\mathrm{F}_b}\} = K_b N[I + PN]^{-1}\{G_{\mathrm{F}_i\mathrm{F}_i}\} \quad [3.7]$$

where $G_{\mathrm{F}_b\mathrm{F}_b}$ is the PSD matrix of the reactant base forces. In this case study, the excitation forces quantified in the PSD matrix is F_{P_i}shown in Figure 3.2.

3.5 Numeric Example

In order to demonstrate this method numerically, each of the substructures, as well as the physical loading, must be quantified. One complication of quantifying each of these quantities is that they are frequency dependent. The simplest solution to this issue is to use s-domain (Laplace domain) transfer functions to represent the frequency dependent response of the substructures. The following is a simplified example of this approach.

3.5.1Dynamic Substructuring

In order to verify that TPHS is an accurate method, it was compared to the traditional dynamic substructuring approach to solve a simple uni-axial two DOF system. Figure 3.3 shows a diagram of this example two DOF uni-axial system.

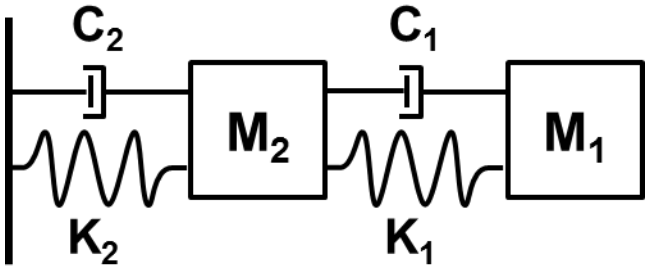

Figure 3.3 – Diagram of Example Two DOF Uni-axial System

For this example the displacement excitation is applied to M_1 and both the TPHS and traditional dynamic substructuring is used to solve for the reactant force at the connection between the two substructures similar to what is shown in Figure 3.2. The equations of motion of this system are given by the following system of equations.

$$\begin{Bmatrix} F_1 \\ F_2 \end{Bmatrix} = [\mathbb{M}s^2 + \mathbb{C}s + \mathbb{K}] \begin{Bmatrix} x_1 \\ x_2 \end{Bmatrix} \quad [3.8]$$

where

$$\mathbb{M} = \begin{bmatrix} M_1 & 0 \\ 0 & M_2 \end{bmatrix} \quad [3.9]$$

$$\mathbb{C} = \begin{bmatrix} C_1 & -C_1 \\ -C_1 & C_1 + C_2 \end{bmatrix} \quad [3.10]$$

$$\mathbb{K} = \begin{bmatrix} K_1 & -K_1 \\ -K_1 & K_1 + K_2 \end{bmatrix} \quad [3.11]$$

The same equation for reactant force due to input displacement shown in Equation [3.23] can be applied here but replacing the SDOF scalars with MDOF matrices.

$$\frac{\{F\}}{\{x\}} = (\mathbb{C}s + \mathbb{K}) \cdot \mathbb{M}s^2[\mathbb{M}s^2 + \mathbb{C}s + \mathbb{K}]^{-1} \quad [3.12]$$

The transfer functions for each of the blocks shown in Figure 3.2 are derived and then combined using Equation [3.4].

3.5.2 Transfer Path Hybrid Substructuring

The numeric substructure, as shown in Figure 3.2, has a transfer function with a force input and a displacement output. The equation for this system transfer function is derived starting with the equation of motion

$$[Ms^2 + Cs + K]\{x_r\} = \{F_i\} \quad [3.13]$$

where M, C and K are the substructures' mass, damping and stiffness properties, F_i is the input force, x_r is the reactant displacement and s is the Laplace constant. This transfer function is derived using a rigid body diagram shown in Figure 3.4.

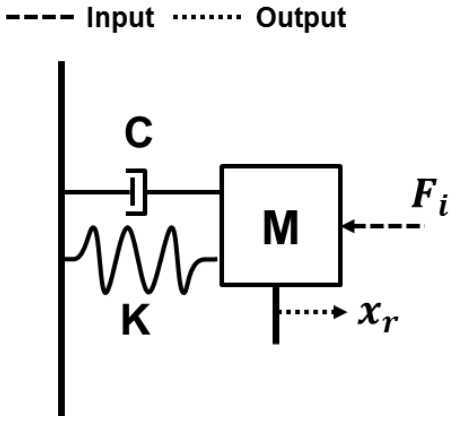

Figure 3.4 - Rigid Body Diagram of the Numerical Substructure

The transfer function equation of the numerical substructure, in the s-domain, is then derived by rearranging Equation [3.13] into

$$N = \left\{\frac{x_r}{F_i}\right\} = \frac{1}{Ms^2 + Cs + K} \quad [3.14]$$

The physical substructure, as shown in Figure 3.2 has an input base displacement and a resultant base force. This transfer function is derived using the following rigid body diagram shown in Figure 3.5.

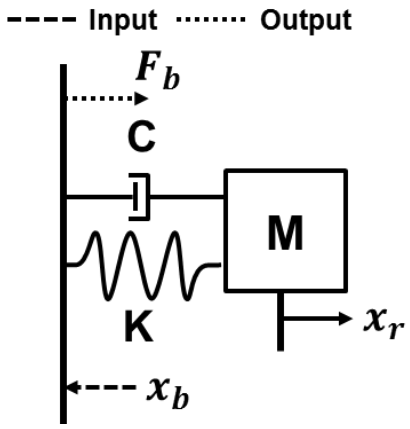

Figure 3.5 – Rigid Body Diagram of the Physical Substructure

where F_b is the reactant force at the base due to the input base displacement, x_b.The characteristic equation of motion of this system is Equation [3.13] where the input force is calculated by

$$F_i = [Cs + K]x_b \quad [3.15]$$

Therefore, the equation of motion becomes

$$[Cs + K]x_b = [Ms^2 + Cs + K]x_r \quad [3.16]$$

Rearranging this equation to solve for the reactant displacement due to base input displacement gives

$$\frac{x_r}{x_b} = \frac{Cs + K}{Ms^2 + Cs + K} \quad [3.17]$$

Using Equation [3.17] in the equation for the reactant force of the spring-damper shown below

$$F_b = [Cs + K](x_b - x_r) \quad [3.18]$$

gives the s-domain transfer function for the physical substructure

$$P = \left\{\frac{F_b}{x_b}\right\} = [Cs + K]\left(1 - \frac{Cs + K}{Ms^2 + Cs + K}\right) \quad [3.19]$$

This is the equation for the reactant base force due to a base displacement excitation, also sometimes known as dynamics stiffness.

Lastly, the physical loading needs to be realized using s-domain transfer functions. For this simple example it is assumed that the physical loading has a commanded displacement excitation. The transfer

function of the physical loading is reactant force due to an input displacement excitation. This transfer function is derived using a rigid body diagram shown in Figure 3.6.

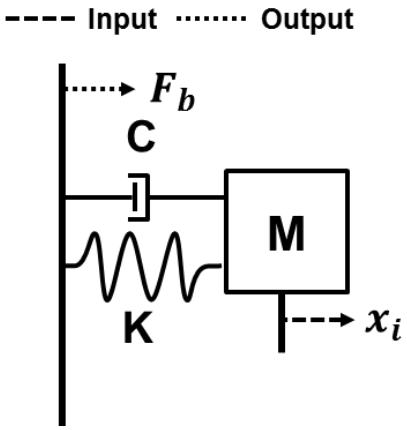

Figure 3.6 - Rigid Body Diagram of the Physical Loading

where x_i is the input displacement.The characteristic equation of motion of this system is Equation [3.13] where the input force is calculated by

$$F_i = Ms^2 x_i \qquad [3.20]$$

Therefore, the equation of motion becomes

$$[Ms^2 + Cs + K]\{x_r\} = Ms^2 x_i \qquad [3.21]$$

Rearranging this equation to solve for the system displacement due to base input displacement gives

$$\frac{x_r}{x_i} = \frac{Ms^2}{Ms^2 + Cs + K} \qquad [3.22]$$

From this equation, to get the reactant forces, we multiply by the characteristic equation of the system's spring/damper shown in

$$P_i = \left\{\frac{F_b}{x_i}\right\} = (Cs + K)\frac{Ms^2}{Ms^2 + Cs + K} \qquad [3.23]$$

The results from Equation [3.12] and the results from the TPHS using Equation [3.7] are compared in Figure 3.7.

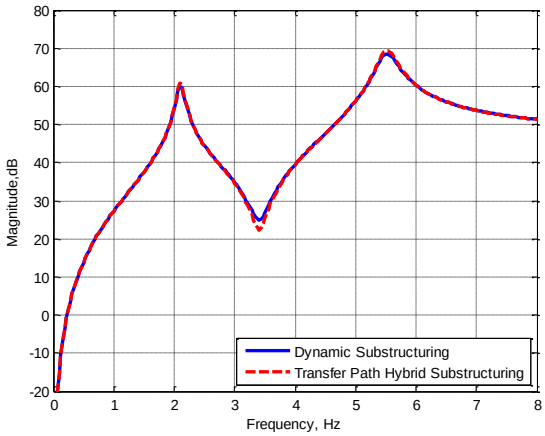

Figure 3.7 – Comparison of Dynamic Substructuring vs. Transfer Path Hybrid Substructuring

These results show that the TPHS method can accurately substructure two substructures together in the same manner as dynamic substructuring. This example shows that the fundamental theory of TPHS is equivalent to the more traditional method of dynamic substructuring.

3.6 Experimental Example

Because of the realization that the feedback closed loop equation, shown in Equation [3.4], can be solved discretely in the frequency domain, it is observed that TPHS leads itself well to similar Frequency Based Substructuring (FBS) methods. These methods allow the calculation of the entire mechanical system dynamic response based on the FRFs of the system substructures. FBS methods are usually a hybrid method, which means that they incorporate both experimentally measured system dynamics as well as numerically computed system dynamics. Using FBS techniques, experimental results can be used interchangeably with respective numerical results. Therefore, FBS methods allow the substructuring of numerical substructures with other numerical substructures, the substructuring of experimental substructures with numerical substructures, as well the substructuring of experimental substructures with other experimental substructures. The same multi degree of freedom (MDOF) notional mechanical system used in previous chapters was used to verify the TPHS method using a combination of both numerical and experiment substructures to accurately predict the dynamics of a mechanical system.

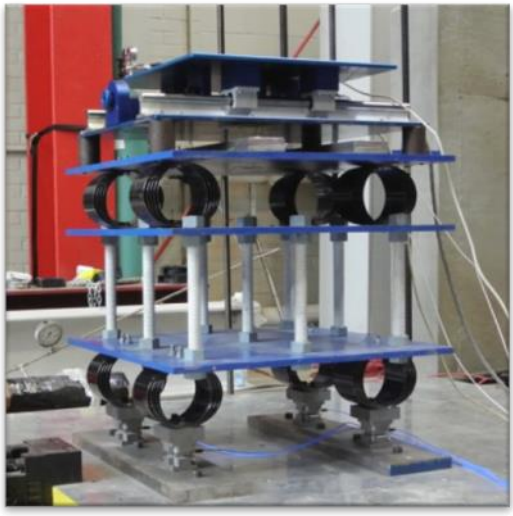

Figure 3.8 – MDOF Test Case Mechanical System

As in previous work, the complete notational mechanical system, shown in Figure 3.8, was constructed and the vibration force transmitted through the system to the base was measured below the four corner isolation points using four PCB Piezoelectric tri-axial force sensors Model #261A02 that can be seen in Figure 3.8. The Quanser shake table was commanded a band limited white noise (BLWN) with a roll off at higher frequencies. The roll off at higher frequencies is achieved with an 8th order Butterworth filter with a cutoff frequency of 20Hz. This ensures that low frequency resonances are sufficiently excited but also excites higher frequencies with lower energy so to avoid pushing the Quanser Shake Table II towards its mechanical limits. Auto power spectral densities (PSDs) of the measured force under the bottom layer of the four coil springs were recorded using a Data Physics dynamic signal analyzer. Figure 3.9 shows the force transmitted to the force sensors at the base of the full system. These results represent the force transmitted through the full system and will later be used to validate the TPHS results.

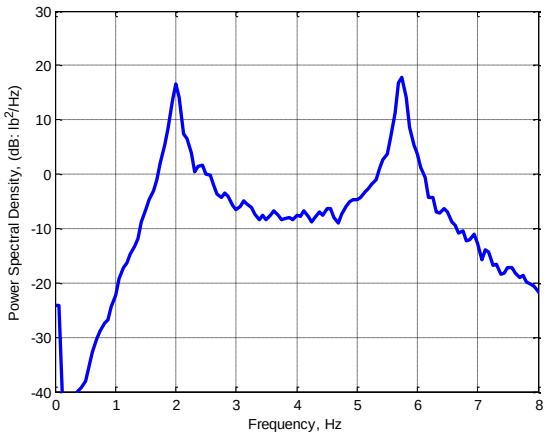

Figure 3.9 – PSD of the Total Force Transmitted to the Base of the Full System in the Horizontal Direction

The mechanical equipment assembly was then attached to the same four PCB Piezoelectric tri-axial force sensors. The Quanser Shake Table II was commanded with the same band limited white noise (BLWN) as in the full system test. Auto power spectral densities (PSDs) of the measured force under the four coil springs were recorded using a Data Physics dynamic signal analyzer. These results represent the response of the first mass-spring oscillator which is the physical substructure of the TPHS. Since this experiment is being used to verify a single degree of freedom real time hybrid simulation, only the horizontal degree of freedom of interest and is shown in Figure 3.10.

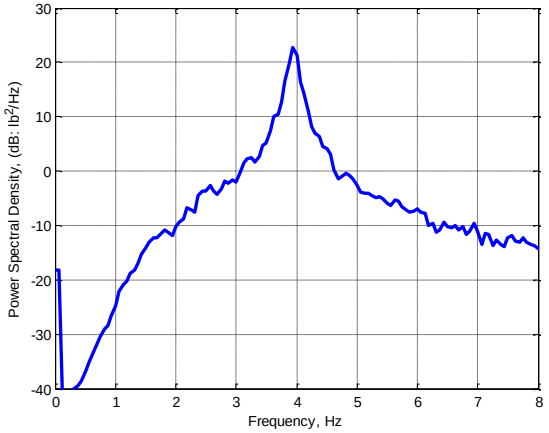

Figure 3.10 – PSD of the Total Force Transmitted to the Base of the Mechanical Equipment in the Horizontal Direction

The support structure is assumed linear and an accurate numerical model of this structure is developed. This portion of the system is the numerical substructure of the TPHS. The numerical model constructed

was a six degree of freedom (DOF) state space model with 12 states. A frequency response function of horizontal displacements due to horizontal forces was calculated as is shown in Figure 3.11.

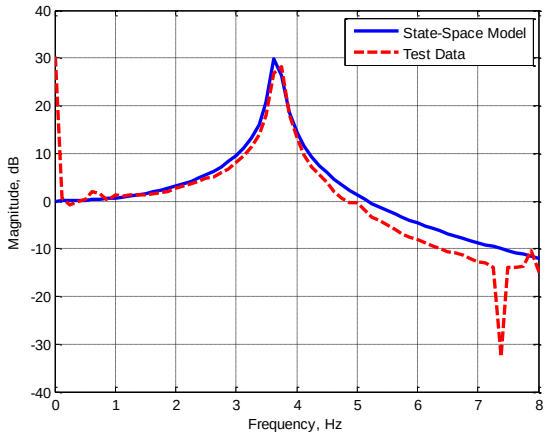

Figure 3.11 – Frequency Response Function of Horizontal Displacement Due to Horizontal Force Excitation.

Figure 3.12 shows both these physical and numerical substructures.

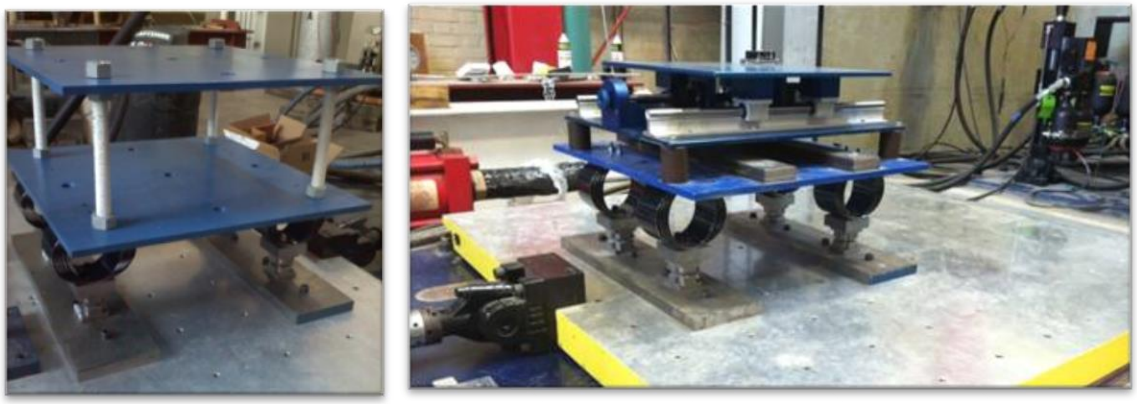

(A) **(B)**

Figure 3.12 – (A) Numerical Substructure (B) Physical Substructure

Lastly, the physical substructure was experimentally tested. In the TPHS arrangement, this is a reactant force due to a base displacement excitation. To experimentally measure this relationship, a six degree of freedom (6DOF) Shore Western Shake Table, shown in Figure 3.13, was used. Figure 3.13 also shows the physical substructure placed on the 6DOF shake table.

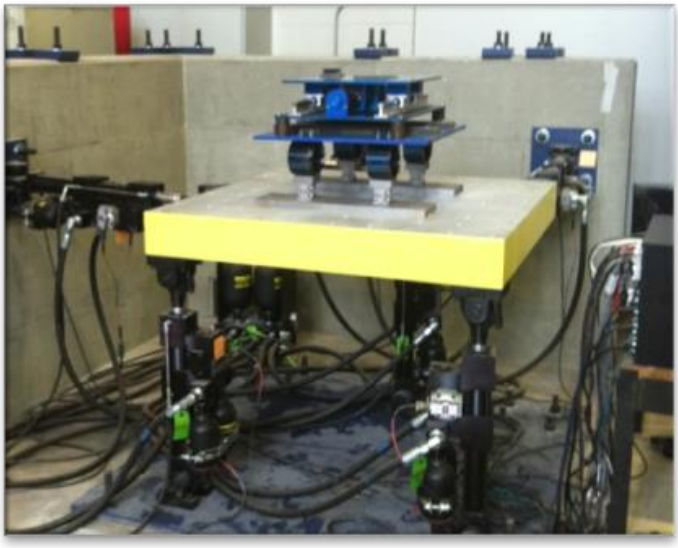

Figure 3.13 – Six Degree of Freedom Shore Western Shake Table

This table is able to apply a base displacement excitation in all six Cartesian coordinates, i.e., three translations and three rotations through the use of six actuators. The orientation of the six actuators (X1, X2, Y1, Z1, Z2, and Z3) are shown in Figure 3.14.

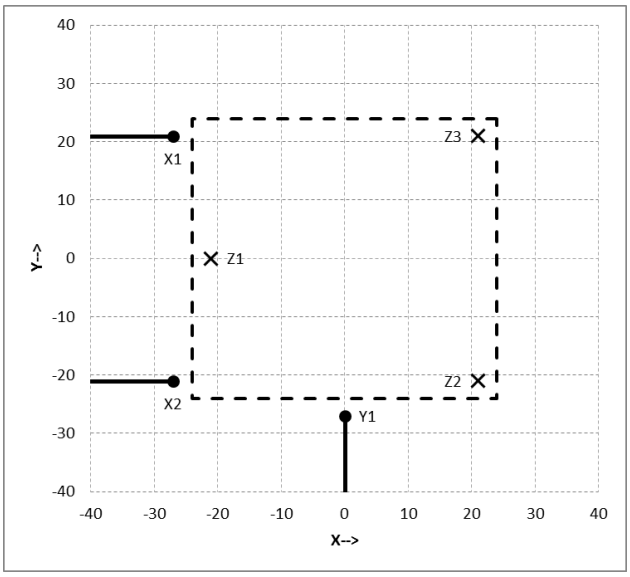

Figure 3.14 – Diagram of Actuator Orientation

The physical substructure was excited with a band-limited white noise (BLWN) displacement from 0 to 20 Hz in all six Cartesian directions. Similar to when the physical loading was recorded, the physical substructure had tri-axial force sensors below its isolators at the base to record the reactant force. This arrangement allowed for the direct measurement of the desired substructure transfer function. One issue

with this is that the inputs to this transfer function, i.e., the Cartesian base displacement excitations, are not in consistent DOF as with the numerical substructure and the physical loading. The numerical model, along with the physical loading, is quantified at the twelve interaction points between the two substructures, i.e., four tri-axial force sensors. The six shake table Cartesian coordinates can the transformed into the twelve interaction directions using a rigid body transform. Figure 3.15 shows a diagram of the necessary transformation from the six shake table Cartesian coordinates to the twelve interaction directions.

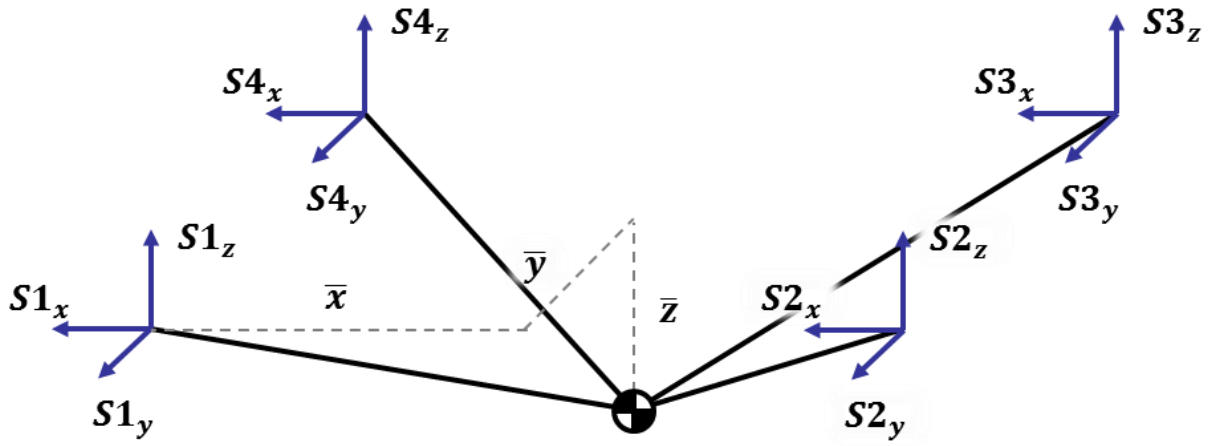

Figure 3.15 – Rigid Body Transformation From 6 Shake Table Cartesian Coordinates to 12 Interaction Directions

S1, S2, S3 and S4 indicate the four sensor locations while $\bar{x}$, $\bar{y}$, and $\bar{z}$ indicate the orthogonal distances between the shake table center of gravity and each respective sensor location. A simple linear transformation can be calculated by assuming a rigid body, i.e., there are no additional translations or rotations produced by the flexibility of the shake table, as well as assuming small angle theorem, which is defined below

$$sin\theta \cong \theta \quad cos\theta \cong 1 \tag{3.24}$$

The transformation is calculated using the following formula

$$T = \{[\boldsymbol{i} + \boldsymbol{j} + \boldsymbol{k}] \quad [x_i\boldsymbol{i} + y_i\boldsymbol{j} + z_i\boldsymbol{k}] \times [\boldsymbol{i} + \boldsymbol{j} + \boldsymbol{k}]\} \tag{3.25}$$

Where T is the transformation vector for each DOF, $[\boldsymbol{i}+\boldsymbol{j}+\boldsymbol{k}]$ is the unit directional vector of each DOF, and $[x_i\boldsymbol{i}+y_i\boldsymbol{j}+z_i\boldsymbol{k}]$ is the distance vector for each DOF location from the shake table CG. For example, the first DOF is the first sensor in the x direction, $S1_x$. Its direction vector is $[1.0\boldsymbol{i}+0.0\boldsymbol{j}+0.0\boldsymbol{k}]$ and its distance vector is $[\bar{x}\boldsymbol{i}+\bar{y}\boldsymbol{j}+\bar{z}\boldsymbol{k}]$. Therefore the transformation vector for the first DOF is $T=[1.0 \quad 0.0 \quad 0.0 \quad 0.0 \quad \bar{z} \quad -\bar{y}]$. Performing this calculation for all degrees of freedom gives a 12x6 matrix which transforms CG displacements translations and rotations to equivalent translations at the four corner interaction points shown below

$$T=\begin{bmatrix}1&0&0&0&\bar{z}&-\bar{y}\\0&1&0&-\bar{z}&0&\bar{x}\\0&0&1&\bar{y}&-\bar{x}&0\\1&0&0&0&\bar{z}&-\bar{y}\\0&1&0&-\bar{z}&0&-\bar{x}\\0&0&1&\bar{y}&\bar{x}&0\\1&0&0&0&\bar{z}&\bar{y}\\0&1&0&-\bar{z}&0&-\bar{x}\\0&0&1&-\bar{y}&\bar{x}&0\\1&0&0&0&\bar{z}&\bar{y}\\0&1&0&-\bar{z}&0&\bar{x}\\0&0&1&-\bar{y}&-\bar{x}&0\end{bmatrix} \quad [3.26]$$

The physical substructure was excited with a band-limited white noise (BLWN) displacement from 0 to 20 Hz in all six Cartesian directions. The BLWN was the same as was used to record the physical loading.

To experimentally verify the TPHS calculation using a PSD matrix as the physical loading, the numerical substructure model and the physical substructure experimental test were coupled together using Equation [3.4] and then compared to the experimental full system which was constructed and tested. Figure 3.16 shows the comparison of the TPHS method vs. the experimental measurement of the mechanical systems base force PSDs as well as the open-loop calculation of the system dynamics.

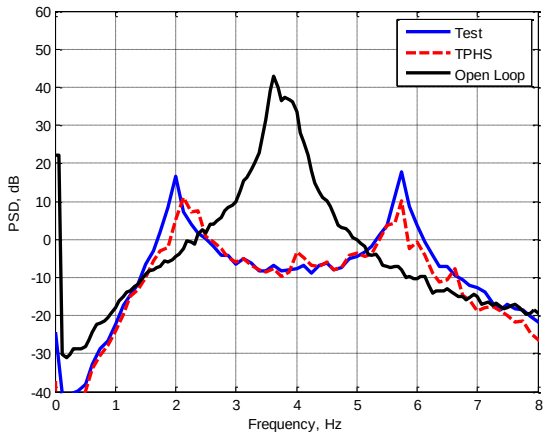

Figure 3.16 – Comparison of TPHS vs Full System Test PSDs

This comparison shows that TPHS is a viable substructuring method that can use PSDs of mechanical system excitation to calculate the coupled dynamics of the mechanical system. This is the major advantage of this method. The results also show the significant contribution of the feedback loop. The open loop does not include this feedback loop and is therefore essentially just a convolution of the dynamics of the two substructures. This does not accurately predict the resonant frequencies of the coupled system.

3.7 Conclusion

This chapter demonstrated a new frequency based substructuring method referred to as Transfer Path Hybrid Substructuring. It was demonstrated that this method is mathematically equivalent to traditional dynamic substructuring. In addition, it was shown that this method can be used to accurately couple physical loading with unknown vibration excitation, with the dynamics of a numerically modeled support structure. This is the main advantage of this method over other substructuring methods since typically it is very difficult to quantify the exact source of the system excitation.

This method does have required conditions. The physical loading should be measured with the physical substructure having a perfectly rigid interface to the test base in the frequency range of interest. This method also requires that the physical substructure transfer function (reactant force due to an applied base motion excitation) can be measured using linear signal processing techniques. This obviously assumes

that this substructure is a stationary, ergodic system. In the case study presented in this paper, this was true and the physical substructure transfer function was able to be measured because of the availability of a 6DOF shake table which could be used to apply a base motion and record the reactant forces of the physical substructure. This will typically be cost and time prohibitive so other methods to achieve this transfer function could be a subject of further research.

3.8 References

Botelho, R. (2015). *Real-Time Hybrid Substructuring for Marine Application of Vibration Control and Structural Acoustics.* University of Connecticut.

Crowley, J., Klosterman, A., Rocklin, G., & Vold, H. (1984). Direct Structural Modification using Frequency Response Functions. *Proceedings of the Second International Modal Analysis Conference.* Orlando, FL.

Darby, A. P., Blakeborough, A., & Williams, M. S. (1999). Real Time Substructure Test Using Hydraulic Actuator. *Journal of Engineering Mechanics, 125*(10), 1133-1139.

Darby, R. A. (1964). A Practical Method for Predicting Acoustic Radiation or Shock Excursions of Navy Machinery. *The Shock and Vibration Bulletin, 3*.

de Klerk, D., Rixen, D. J., & Voormeeren, S. N. (2008). General Framework for Dynamic Substructuring: History, Review and Classification of Techniques. *AIAA Journal, 46*(5), 1169-1181.

de Klerk, D., Rixen, D., & de Jong, J. (2006). The frequency based substructuring (FBS) method reformulated according to the dual domain decomposition method. *24th international modal analysis conference. Vol. 36.* New York.

Gordis, J., Bielawa, R., & Flannelly, W. (1991). A Generalized Theory for Frequency Domain Structural Synthesis. *Journal of Sound & Vibration, 150*, 139-158.

Guyan, R. (1965). Reduction of Stiffness and Mass Matrices. *AIAA Journal*, 380-380.

Horiuchi, T., Inoue, M., Konno, T., & Namita, Y. (1999). Real Time Hybrid Experimental System With Actuator Delay Compensation and It's Applications to a Piping System With Energy Absorber. *Earthquaker Engineering and Structural Dynamics, 28*(10), 1121-1141.

Imregun, M., Robb, D., & Ewins, D. (1987). Structural Modifications and Coupling Dynamic Analysis Using Measured FRF Data. *Proceedings of the Fifth International Modal Analysis Conference.* London, UK.

Jetmundsen, B., Bielawa, R. L., & Flannelly, W. G. (1988). Generalized frequency domain substructure synthesis. *Journal of the American Helicopter Society, 33*(1), 55-64.

Nakashima, M., & Masaoka, N. (1999). Real Time On-Line Test for MDOF Systems. *Earthquake Engineering and Structural Dynamics, 28*, 393-420.

Plunt, J. (1998). Strategy for Transfer Path Analysis applied to Vibro-Acoustic Systems at Medium and High Frequencies. *Proceddings of the Twentythird Internationsl Conference on Noise & Vibration Engineering.* Leuven, BE.

Plunt, J. (2004). Examples of using Transfer Path Analysis together with CAE-models to Diagnose and find Solutions for NVH Problems late in the Vehicle Development Process. *SAE*, 2005-01-2508.

Rixen, D. J., & van derValk, P. L. (2013). An Impulse Base Substructuring Approach for Impact Analysis and Load Case Simulation. *Journal of Sound and Vibration*, 7174-7190.

Sjovall, P., & Abrahamsson, T. (2007). State Space Model Identification for Component Synthesis. *Porcedding of the 25th International Modal Analysis Conference.* Society for Experimental Mechanics.

Su, T. J., & Juang, J. N. (1994). Substructure System Identification and Synthesis. *Journal of Guidance, Control and Dynamics*, 1087-1095.

4 TRIALS AND TRIBULATIONS OF EFFECTIVE CONTROL OF A SIX DEGREE OF FREEDOM SHAKE TABLE WITH THE INTENDED USE OF REAL TIME HYBRID SUBSTRUCTURING

4.1 Abstract

Real-Time Hybrid Substructuring (RTHS) is a relatively new method of vibration testing that can be used to effectively characterize the system level performance of mechanical equipment. RTHS allows mechanical equipment to be physically tested while coupled through what is referred to as a transfer system to a real-time numerical simulation of the support structure. The challenge in applying RTHS to test mechanical equipment is twofold: the equipment itself can have little inherent damping which, coupled with the inherent dynamics in the transfer system, can result in unstable RTHS tests; and the interface at the attachment points can be complex with multi-directional and rotational motion which adds significant complexity to the RTHS transfer system. To insure stability and accurate representation of the complex interface between the physical and numerical substructures, a high fidelity multiple-input-multiple-output (MIMO) servo-hydraulic actuator system is needed for the RTHS transfer system. This paper presents a methodology to achieve effective control of a six degree-of-freedom (6DOF) shake table and describes the corresponding MIMO system identification and model-based feedforward feedback compensation to facilitate both stable and accurate RTHS testing of lightly damped mechanical systems. Results show that the proposed compensation method can improve the magnitude and phase tracking of a 6DOF shake table located at the University of Connecticut.

4.2 Introduction

Real-time hybrid substructuring (RTHS) provides the capability to isolate and physically test the critical components of a mechanical system early on in the design phase of a system. This capability is accomplished by including the dynamic interaction at the time of the component testing using a numerical representation of the remaining support structure. Figure 1 shows a general diagram of a RTHS closed loop test which illustrates the closed loop nature of this type of testing. RTHS is a relatively new method

of vibration testing, made more practical due to advances in computer power, digital signal processing hardware/software, and hydraulic control of critical transfer systems. RTHS can provide system level insight into the design of mechanical systems during the component level testing. In doing so, RTHS can potentially remove unnecessary conservatism from the design of the mechanical system. Critical in conducting stable and accurate RTHS tests is the ability to enforce the numerically calculated displacements onto the physical substructure through an effective transfer system.

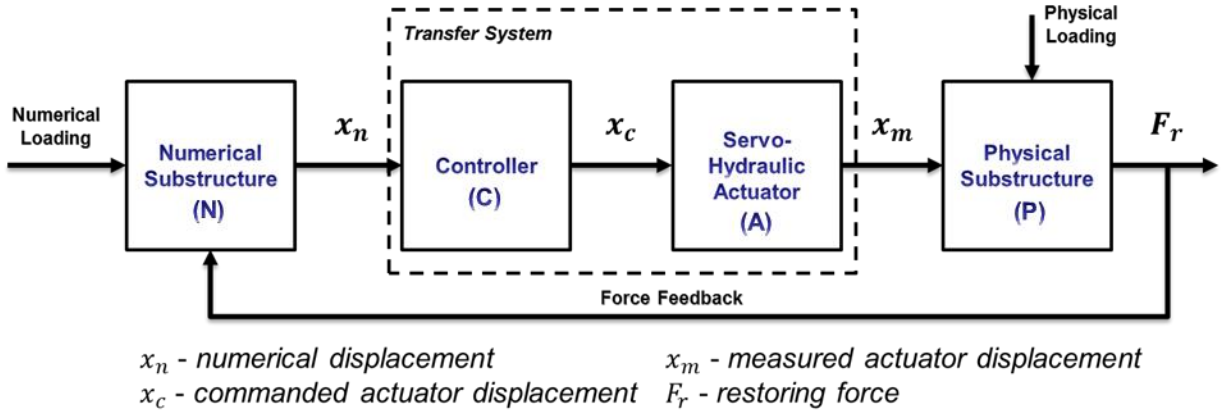

Figure 4.1 – General Block Diagram for RTHS Closed-Loop Testing

Early research in RTHS focused on earthquake engineering and structural engineering (Nakashima & Masaoka, 1999), (Darby, Blakeborough, & Williams, 1999), (Dimig, Shield, French, Bailey, & Clark, 1999), and (Horiuchi, Inoue, Konno, & Namita, 1999). RTHS was a significant element of the Network for Earthquake Engineering Simulation (NEES) with a comprehensive list of projects and publications posted at https://nees.org/wiki/RTHSwiki. A major focus of past RTHS research is on the transfer system and the development of actuator control methods for effective displacement tracking of the servo-hydraulic transfer system. (Horiuchi, Inoue, Konno, & Namita, 1999) used a frequency independent time-delay model to approximate the servo-hydraulic actuator dynamics, and then a polynomial prediction to compensate for the servo-hydraulic actuator dynamics. (Jung & Shing, 2006) and (Chen & Ricles, 2010) used similar compensation methods based on a control signal error-compensation methods. These methods rely on a simplified time domain representation of stationary servo-hydraulic actuator dynamics with relatively small time delays. (Carrion & Spencer, 2007) and (Phillips & Spencer, 2011) proposed

compensation techniques that involve higher order model-based strategies including a feedforward compensator. These model-based controllers create an approximate inverse of the actuator model to compensate for the servo-hydraulic actuator dynamics in the transfer system. (Phillips & Spencer, 2012) and (Gao, Castaneda, & Dyke, 2013) applied this approximate inverse method to multi degree of freedom (MDOF) servo-hydraulic actuator systems for actuators providing collinear displacements on a steel building frame. It is important to note that the prior tests in earthquake engineering have involved testing frames or dampers (not mechanical equipment) with larger amplitudes, higher levels of inherent damping, and transfer systems mostly limited to uni-axial motion.

A similar test method to RTHS is hardware-in-the-loop (HWIL). HWIL testing is typically used in mechanical applications to test control systems. In HWIL testing, the physical substructure is often an electrical component and the interface between the numerical and physical substructures is achieved through the direct transfer of electrical signals. HWIL testing has been conducted on mechanical equipment including HWIL research done in the design of electro-mechanical systems (Hanselmann, 1993), (Isermann, Schaffnit, & Sinsel, 1999), (Bouscayrol, 2008) and (Carmeli, Castelli-Dezzaa, Mauri, & Marchegiani, 2013) who have used HWIL to predict the electrical performance of electric motors and distributed electric generators, respectively. Similar research topics used a mechanical automotive engine as the physical substructure, referred to as engine-in-the-loop, has been reported in the literature (Fathy, Ahlawat, & Stein, 2005), (Filipi, et al., 2006), and (Filipi & Kim, 2010). All of these examples of HWIL testing have no physical transfer system.

When the interface between the physical and numerical components requires a physical transfer system, RTHS, as shown in Figure 4.1, is employed. This figure illustrates the closed loop nature of RTHS. The interface forces at the physical substructure connection points are measured by sensors, converted to digital signals and transmitted to the numerical substructure. The numerical substructure uses the measured interface forces along with any numerical loading to calculate the displacements at the same substructure connection points. These numerical displacements are then imposed upon the physical

substructure through a transfer system, typically a servo-hydraulic actuator transfer system. RTHS for mechanical components has a number of unique transfer system characteristics including low amplitudes, broad bandwidth, multi-axle motion, and high precision tracking.

Since RTHS involves a feedback loop it is critical, for test stability and accuracy, that all the forces and displacements are transmitted between the two substructures, accurately and timely, to insure compatibility of the substructures and stability of the system. Accuracy and delay in a RTHS test can be a result of the sensors, the analog to digital and digital to analog converters, and/or the computation time. However, it is typically dominated by the inherent dynamics, i.e. apparent time delay and magnitude distortion, of the transfer system. This effect can be compounded when considering multiple actuators tuned to work synchronously with one another as well as physical and numerical components that both have low inherent damping.

This paper presents a methodology to achieve effective control of a six degree-of-freedom (6DOF) shake table specifically for use in RTHS of mechanical equipment. A multiple input multiple output (MIMO) system identification is conducted for the 6DOF shake table and model-based feedforward feedback compensation is implemented, in an iterative fashion, to facilitate both stable and accurate RTHS testing of lightly damped mechanical systems. This approach compensates the actuator dynamics of the six individual actuators of the shake table to provide effective displacement tracking of the six Cartesian degrees-of-freedom (i.e., translations and rotations) of the shake table. Due to the small displacements required in this case study, the nonlinear transformation (Nakata, Spencer, & Elnashai, 2007) is linearized for use with feedforward inverse compensation without a loss of fidelity. Results show that the proposed compensation method can improve the magnitude and phase tracking of the Cartesian DOF of the 6DOF shake table located at the University of Connecticut to levels and bandwidth needed to conduct RTHS of mechanical equipment.

4.3 Six Degree of Freedom Real-Time Hybrid Substructuring

Real-Time Hybrid Simulation (RTHS) involves the combination of a physical substructure with a numerical substructure. This combination is performed by the use of sensors that transmit reactant forces from the physical substructure to the numerical substructure and servo-hydraulic actuators that transmit displacements, calculated by the numerical substructure, to the physical substructure. Figure 4.2 shows the general layout of a MIMO RTHS test of mechanical equipment at the University of Connecticut using a 6-DOF servo-hydraulic shake table. The real time digital signal processor (DSP) is a dSPACE DS1103 PPC controller board (DS1103). The numerical substructure, along with any compensation algorithms are developed in MATLAB Simulink and downloaded to the DS1103 through dSPACE's real time interface (RTI). The DS1103 has eight digital to analog (D/A) channels and twenty analog to digital (A/D) channels. The DSP controller sends commanded actuator displacements to the ShoreWestern SC6000 servo valve controller which has an internal analog PID reference tracking controller. This controller by itself is not sufficient for the level of reference tracking required for RTHS testing. Each actuator has an LVDT which measures the actuator displacement. This measured displacement is fed back into the internal PID control loop and the outer RTHS compensation control loop as well as being measured by the DataPhysics SignalCalc Mobilizer dynamic signal analyzer along with the desired displacement and any other measurements of interest.

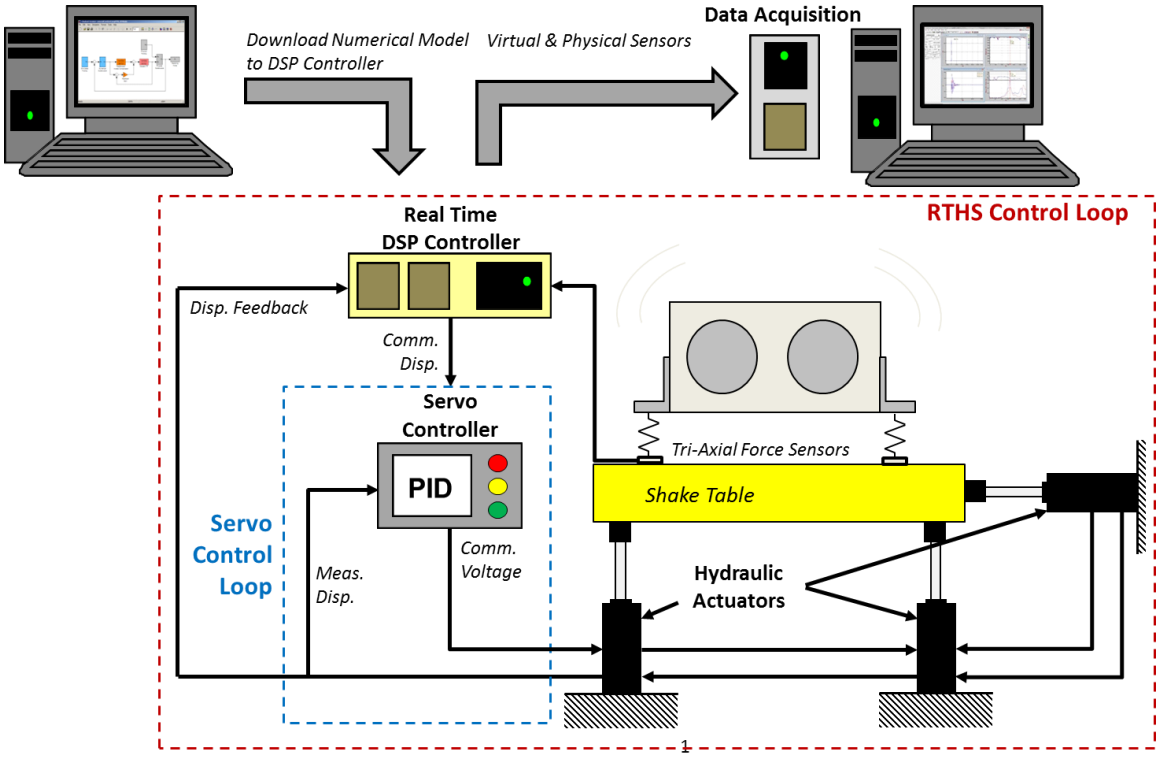

Figure 4.2 – System Diagram of 6-DOF RTHS Substructuring of Mechanical Equipment

A picture of the 6DOF shake table is shown in Figure 4.3.

Figure 4.3 – 6 Degree of Freedom Shake Table

The orientation of the six actuators (X1, X2, Y1, Z1, Z2, and Z3) are shown in Figure 4.4.

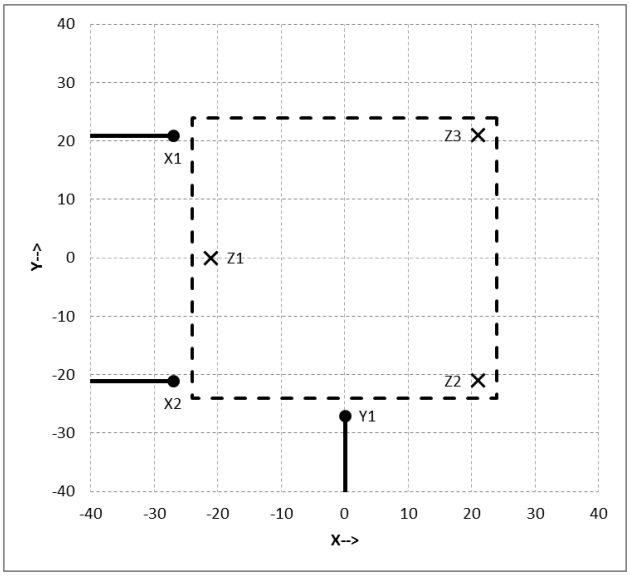

Figure 4.4 – Diagram of Actuator Orientation

The servo-hydraulic actuators have frequency dependent dynamics that can cause instability in the RTHS feedback loop. These frequency dependent dynamics need to be compensated to provide closed-loop stability and performance. The internal PID is present to provide open-loop stability and performance. However, this controller is typically not aggressive enough for stable closed-loop RTHS experiments. Typically, in previous earthquake engineering applications of RTHS, the frequency bandwidth of concern was concentrated on extremely low frequencies, i.e. below 10 Hz. In this application, the focus is a larger range of frequencies (0-30Hz). Also, in previous applications, the physical substructure possessed a significant amount of damping which helps relax the reference tracking requirements of the transfer system, i.e. time delay. In this application, the physical substructure is lightly damped which makes the reference tracking requirements of the transfer system more strict. Therefore, a fairly aggressive compensator is necessary for this RTHS application.

4.4 Cartesian To Actuator Transformation

The 6-DOF shake table uses external command inputs to drive each of the six individual actuators. The output of the numerical substructure during the RTHS test will be in six Cartesian directions (three translation and three rotations). The original nonlinear transformation matrix developed by (Nakata, Spencer, & Elnashai, 2007) takes an initial pin location p_i in 3D space and, by using translation and yaw-

pitch-roll matrixes, locates a new pin location. The Euclidean normal from the base point coordinates q_i to the new pin location is calculated and then the length of the initial actuator is subtracted which determines the necessary displacement of the actuator δl_i. The displacement calculation is done for each actuator in the control system given a set of input translations and rotations, $t_{x,y,z}$ and $\theta_{x,y,z}$ respectively.

The linear actuator displacements necessary to achieve Cartesian displacements of the shake table causes various issues when combined with linearized feedforward inverse compensation techniques. To achieve certain Cartesian displacements, certain actuators are sent signals with sharp discontinuities. These discontinuities cause high frequency content which causes unstable behavior in the simulation.

The nonlinear transformation can be linearized by assuming linear small angle theorem. This simplifies the terms of the transformation matrix by eliminating nonlinear trigonometric functions, which also eliminates the normal direction movement because of rotations. Using the small angle theorem,

$$sin\theta \approx \theta \quad cos\theta \approx 1$$

The linear transformation matrix becomes

$$\Psi(t_x, t_y, t_z, \theta_x, \theta_y, \theta_z) = \begin{bmatrix} 1 & -\theta_z & \theta_y & t_x \\ \theta_z + \theta_x\theta_y & 1 - \theta_x\theta_y\theta_z & -\theta_x & t_y \\ \theta_x\theta_z - \theta_y & \theta_x + \theta_y\theta_z & 1 & t_z \\ 0 & 0 & 0 & 1 \end{bmatrix} \quad [4.1]$$

The next step to simplify the transformation is to ignore any displacement that is not in the normal direction of the actuator. This is done by inspection of the transformation terms of each of the actuators. This simplification of the transformation matrix converts it from a 3D transformation into a 1D normal only transformation. The last step is to simplify the transformation by assuming that the horizontal actuators are vertically aligned with the CG of the table. This eliminates negligible vertical moment arms that require small actuator extensions. The final linear transformation matrix is then

$$\begin{Bmatrix} \delta l_1 \\ \delta l_2 \\ \delta l_3 \\ \delta l_4 \\ \delta l_5 \\ \delta l_6 \end{Bmatrix} = \begin{bmatrix} 1 & 0 & 0 & 0 & 0 & -p_{1y} \\ 1 & 0 & 0 & 0 & 0 & -p_{2y} \\ 0 & 1 & 0 & 0 & 0 & p_{3x} \\ 0 & 0 & 1 & p_{4y} & -p_{4x} & 0 \\ 0 & 0 & 1 & p_{5y} & -p_{5x} & 0 \\ 0 & 0 & 1 & p_{6y} & -p_{6x} & 0 \end{bmatrix} \begin{Bmatrix} t_x \\ t_y \\ t_z \\ \theta_x \\ \theta_y \\ \theta_z \end{Bmatrix} \quad [4.2]$$

where p_{ij} is the pin location of the i^{th} actuator in the j^{th} direction. Table 4.1 shows the pin location coordinates for each of the six actuators

ACT	X	Y	Z
X1	-27	21	-2.9375
X2	-27	-21	-2.9375
Y1	0	-27	-2.9375
Z1	-21	0	-8.8750
Z2	21	-21	-8.8750
Z3	21	21	-8.8750

Table 4.1 – Actuator Pin Locations

The linearized transformation, shown in Equation [4.2], can be easily used to determine the required actuator displacements to create the Cartesian displacements and rotations desired. In addition, a simple inverse of this transformation matrix can be used to calculate the shake table displacements and rotations from the measured actuator displacements which is an advantage of the linearized transformation over the non-linear version of the transformation.

A comparison of static shake table Cartesian displacements was calculated using the non-linear transformation and the linearized transformation derived above for static displacements of 0 to 10 inches. Figure 4.5 shows this comparison, where the six columns are the six Cartesian static displacements inputs to the shake table and the six rows are the actuator displacements necessary to achieve these static inputs. The blue lines are the non-linear transformation calculated displacements and the red lines are the linearized transformation calculated displacements. The vertical black lines are the physical limits of the six actuators that make up the shake table which are three inches for the horizontal actuators (X1, X2 and Y1) and two and a half inches for the vertical actuators (Z1, Z2 and Z3). Within the physical limits of the shake table, there are negligible differences between the two transformations. For a typical RTHS test, the

shake table would be generally given commanded displacements less than an inch. Figure 4.6 shows the same comparison shown in Figure 4.5 but zoomed in to less than an inch which is the range of concern for typical RTHS tests. Figure 4.6 shows that within the limits of a RTHS, i.e. 1 inch, the differences between the non-linear transformation and the linearized transformation are negligible.

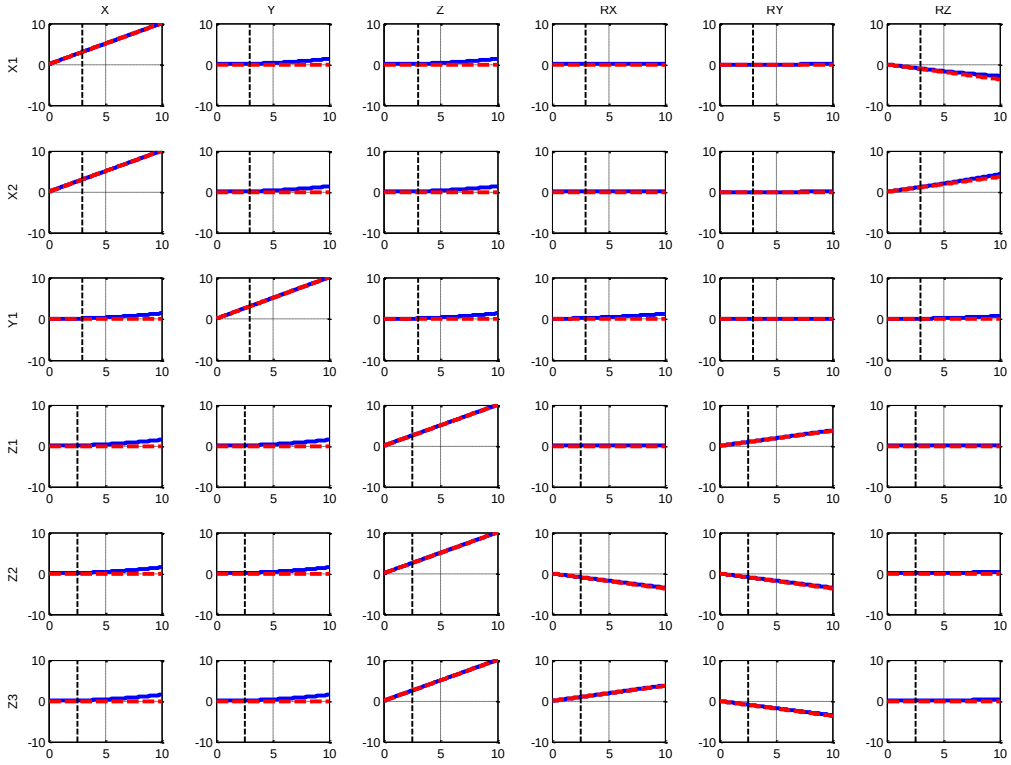

Figure 4.5 – Comparison of Non-Linear vs. Linearized Transformation: < 10in

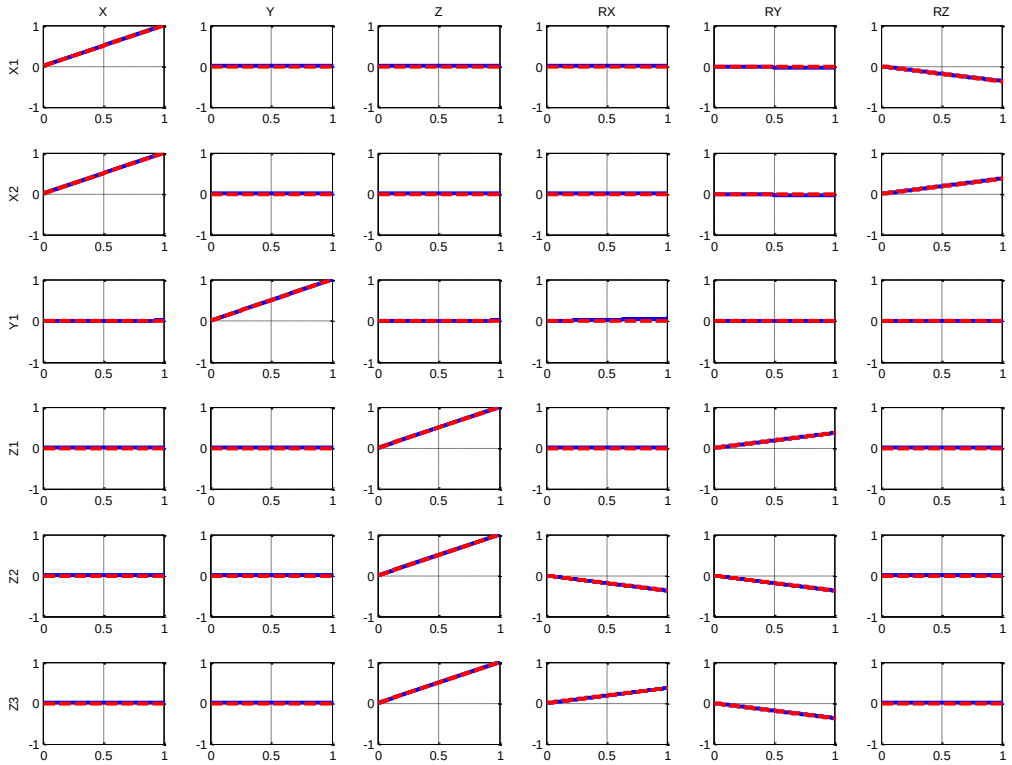

Figure 4.6 – Comparison of Non-Linear vs. Linearized Transformation: < 1in.

4.5 Actuator Dynamics System Identification

Initially the 6DOF shake table was studied without a payload present i.e. there is nothing attached to the shake table as shown in Figure 4.3. This was done initially to measure the unloaded dynamics of the shake table as well as a proof of principal study in order to show that the 6DOF shake table could be sufficiently compensated. Later, this paper will add a payload to the shake table.

The first step to derive a feedforward compensator is to experimentally obtain the frequency response function (FRF) of the actuator system. For a single actuator system, single input single output (SISO) system identification is required. For a multi-actuator system, multiple input, multiple output (MIMO) system identification can be conducted since the operation of each actuator can affect the dynamics of other actuators in the system due to cross-coupling from physical connections and hydraulic fluid.

A MIMO system identification test for a six actuator shake table requires six reference channels which are also the command channels and six measured channels. A compensated MIMO system identification test

for a six actuator shake table requires six reference channels, six command different command channels and six measured channels. Between the six reference channels and the six command channels, twelve output signals are needed. The dSPACE DS1103 PPC controller board, described above, has less D/A outputs than are required for a compensated MIMO system identification test. Because of this, six single input multiple output (SIMO) test are required. In this paper, it is verified that this multiple SIMO system identification technique is equivalent to a single MIMO system identification technique which is used to measure the frequency response of the multi-actuator system are described. The details of this verification are shown in APPENDIX A. The derivations of both SIMO and MIMO transfer functions are described in full detail in (Bendat & Piersol, 2011).

Using the theory of linear superposition, all of the actuators can be driven simultaneously with uncorrelated signals and the complete transfer function matrix can be calculated in one system identification test. As long as each actuator is driven with a signal that is uncorrelated with the other input signals, the correlation between each of the outputs and the inputs can also be calculated forming a coherence matrix of the MIMO system (Bendat & Piersol, 2011). To ensure each actuator is driven with an uncorrelated signal, six different band limited white noise (BLWN) signals were created using Simulink's BLWN generator function, each with the same properties but randomly generated separately which ensures the six signals are theoretically uncorrelated.

Figure 4.7, shows the coherence of the six actuators. These results indicate that each actuator acts independently with essentially no cross-talk. The coherence matrix shows unity coherence along the diagonal, which is the coherence of each of the actuators with itself. The off-diagonal terms of the coherence matrix are very low indicating negligible cross-coupling between the six actuators. Therefore when one actuator is excited, the response of the other five actuators is negligible. This allows each actuator to be treated essentially as its own SISO system.

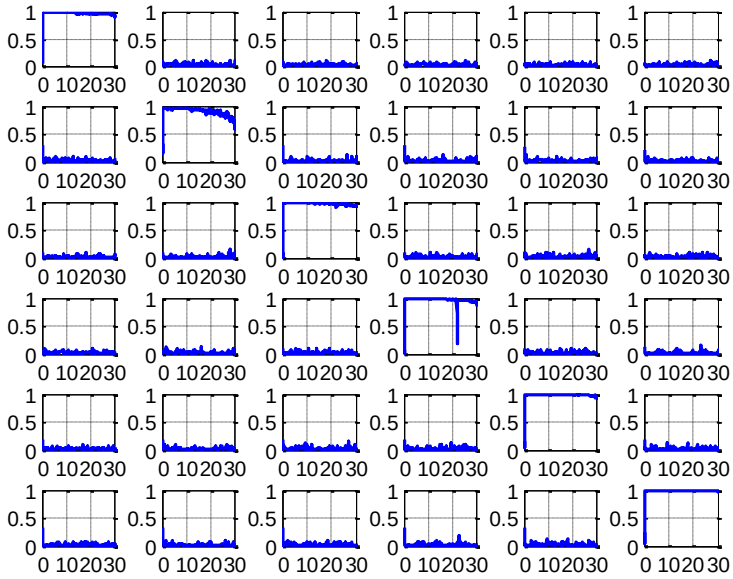

Figure 4.7– Coherence Matrix, γ_{yx}

Figure 4.8 shows the measured diagonal terms of the frequency response matrix of measured to commanded actuator displacement.

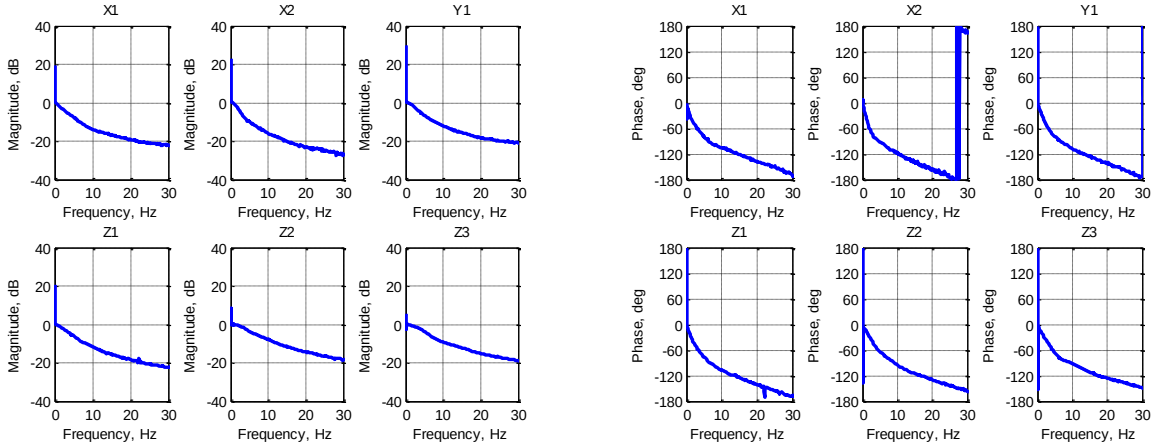

(A) **(B)**

Figure 4.8 - System Identification Frequency Response Function Magnitude (A) and Phase (B)

The results show that each of the actuators has its own unique dynamics but they are all somewhat similar. All the actuators show frequency-dependent magnitude attenuation that is approximately 20-25dB over the 30 Hz bandwidth. The actuators also have a frequency dependent effective time delay that is approximately 25-30ms.

4.6 Feedforward Inverse Compensation

The servo-hydraulic control system used to interface the physical and numerical substructures has frequency dependent dynamics that need to be compensated to provide accurate and timely tracking of desired displacements for stability and accuracy of a RTHS. Figure 4.9 illustrates the model-based feedforward-feedback control architecture from (Carrion & Spencer, 2007) used for compensating the actuator dynamics. The feedforward compensator is used to cancel the modeled actuator dynamics, while the feedback gain is tuned experimentally to provide robustness due to modeling errors and changes in physical substructure during the experiment.

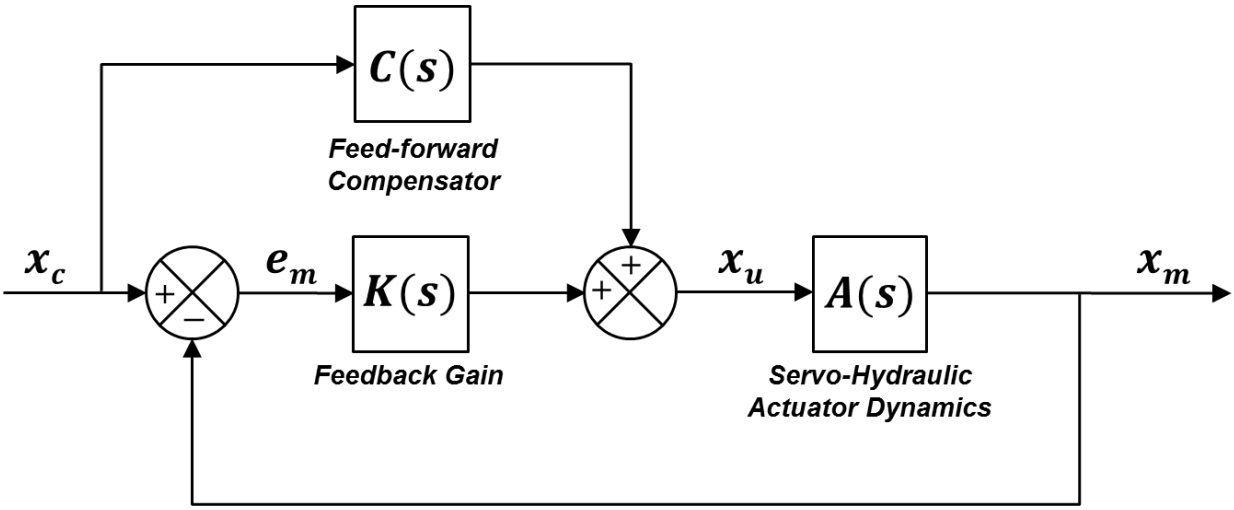

Figure 4.9 – Feedforward-Feedback Control for Actuator Dynamics Compensation

The feedforward inverse compensator is designed to cancel the modeled actuator dynamics of the servo-hydraulic system. Ideally, an exact inverse of the servo hydraulic transfer function would be the perfect compensator. The development of feedforward inverse compensator starts with deriving a s-domain (Laplace domain) transfer function model of the servo hydraulic dynamics from the m^{th} commanded to the n^{th} measured actuator displacement, which can be expressed as

$$A_{y_n x_m}(s) = \frac{\prod_{i=1}^{l}(s - z_{i,m,n})}{\prod_{i=1}^{k}(s - p_{i,m,n})} \quad [4.3]$$

where k is the number of poles and l is the number of zeros. If the transfer function model fit has equal number of poles, p_i and zeroes, z_i then an exact inverse can be used. However, in most cases, the model has less zeroes than poles making its inverse an improper transfer function, i.e. having more zeroes than poles. Low pass compensation, as discussed in previous chapters, can be used to address this issue.

4.6.1 Cascaded Feedforward Inverse Compensation

The dynamics of the actuators are displacement and load dependent and therefore non-linear over the bandwidth of interest. To accommodate for the inherent non-linearity of the actuator system and the very large frequency dependent dynamics, an approach referred to here as cascaded feedforward inverse compensation was implemented. In this approach, the system identification of the uncompensated system is used to develop an initial compensator. When this compensator is implemented, the commanded displacement can become a lot larger in at some frequencies to compensate for the frequency dependent attenuation in magnitude. Because the actuators are commanded a significantly larger displacement than the initial system identification, the dynamics of the system change. The initial compensator may no longer be sufficient to achieve the desired actuator dynamics and additional system identification is necessary. The dynamics of the actuator including the initial compensator is used to develop a second compensator using the same methodology of the initial compensator in order to compensate for the remaining time delay. These two compensators are then used in series as the feedforward compensator. Figure 6 illustrates the block diagram of the feedforward-feedback compensation with cascaded feedforward compensators.

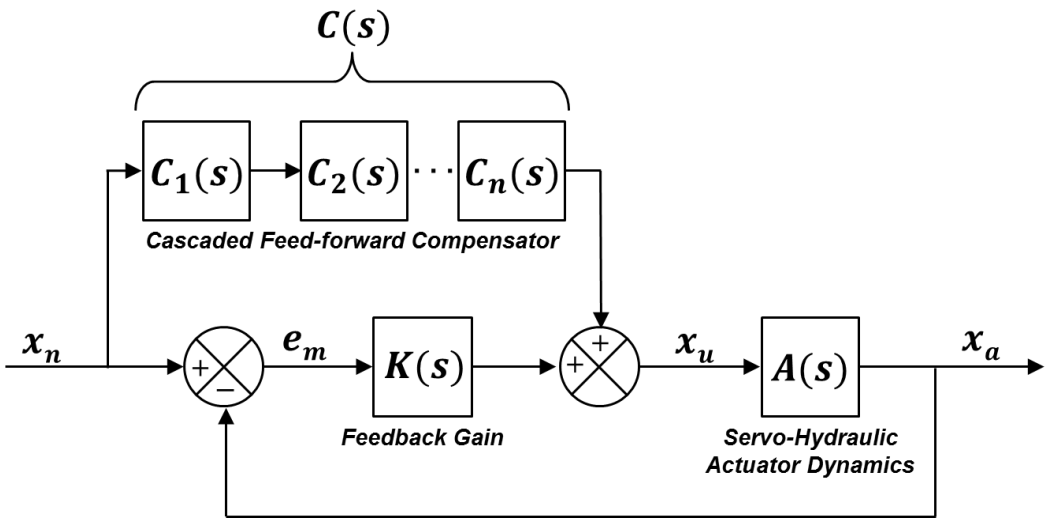

Figure 4.10 – Block Diagram of Cascaded Feedforward Inverse Compensation

4.6.2Low Pass Inverse Compensation

One approach to develop the feedforward compensators is to multiply the improper actuator inverse by a low pass transfer function to make a proper transfer function. As described in (Carrion & Spencer, 2007), this low pass inverse compensation (LPIC) technique involves an alpha scalar value to duplicate the poles of the actuator transfer function as additional poles at higher frequencies. These additional poles are used to create the low pass filter given by

$$L_{y_n x_m}(s) = \frac{\prod_{i=1}^{k} \alpha_i p_{i,m,n}}{\prod_{i=1}^{k} (s - \alpha_i p_{i,m,n})} \quad [4.4]$$

Multiplying the improper inverse of the actuator model by the low pass transfer functions yields the LPIC transfer function

$$C_{y_n x_m}(s) = A_{y_n x_m}(s)^{-1} L_{y_n x_m}(s) \quad [4.5]$$

Instead of using a α scalar to multiply the existing poles, the additional poles here are forced to be a specific frequency. This frequency should be high enough to minimize the effect on the low frequency dynamics over the control band but not too close to the sampling frequency so that accurate numerical integration is possible. The low pass transfer function is represented by

$$L_{y_n x_m}(s) = \frac{\prod_{j=1}^{k} \omega_j}{\prod_{j=1}^{k} (s - \omega_j)} \quad [4.6]$$

An independent inverse compensator was derived for each of the SISO actuator transfer functions. First, each of the input output pairs of the MIMO transfer function were curve fit using the *invfreqs* MATLAB function. A constant (zero order) numerator and a fourth order denominator was found to the best fit of the frequency response data. The form of the curve fit is shown as

$$A_j(s) = \frac{n_{0i}}{d_{4i}s^4 + d_{3i}s^3 + d_{2i}s^2 + d_{1i}s + d_{0i}} \quad [4.7]$$

These SISO transfer function were place in a MIMO transfer function matrix along the diagonal as

$$\mathbb{A} = \begin{bmatrix} A_1(s) & \cdots & 0 \\ \vdots & \ddots & \vdots \\ 0 & \cdots & A_j(s) \end{bmatrix} \quad [4.8]$$

Since this MIMO transfer function matrix is diagonal, each SISO transfer function along the diagonal can be independently inverted, which is the same as inverting the MIMO transfer function matrix. The LPIC transfer function matrix is then determined by

$$\mathbb{C} = \mathbb{A}^{-1}\mathbb{L} = \begin{bmatrix} C_1(s) & \cdots & 0 \\ \vdots & \ddots & \vdots \\ 0 & \cdots & C_j(s) \end{bmatrix} = \begin{bmatrix} A_1(s)^{-1}L_1(s) & \cdots & 0 \\ \vdots & \ddots & \vdots \\ 0 & \cdots & A_j(s)^{-1}L_j(s) \end{bmatrix} \quad [4.9]$$

System identification of the actuators was performed incorporating the low pass inverse feedforward compensator.

All the actuators show a significant decrease in the frequency-dependent magnitude attenuation that was approximately 20-25dB and was improved to approximately 0-2dB and the time delay that was approximately 25-30ms and was improved to approximately 2-3ms. Figure 4.11 shows uncompensated actuator frequency response functions versus the compensated actuator frequency response functions using the cascaded LPIC compensator approach using two iterations.

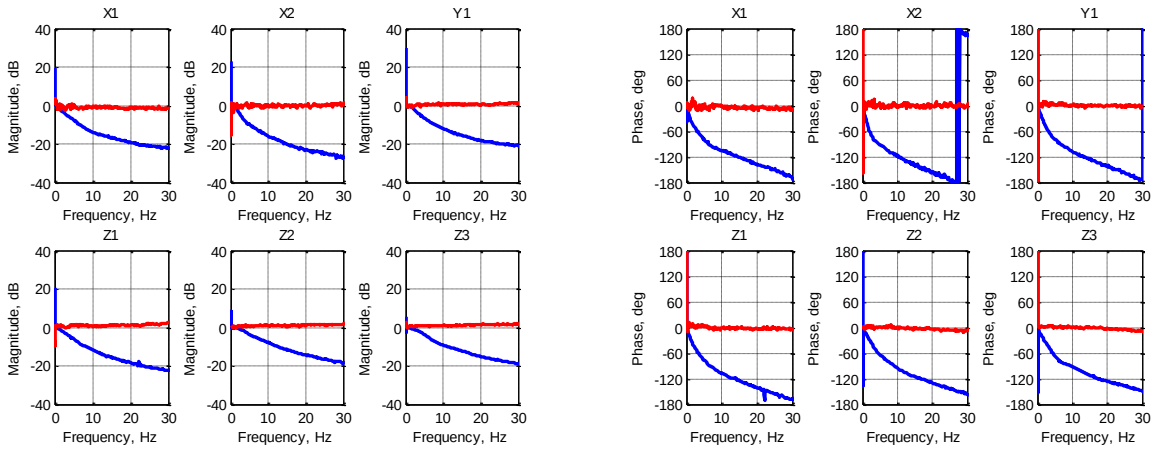

(A) **(B)**

Figure 4.11 – Frequency Response Function Magnitude (A) and Phase (B) of the Six Actuators Uncompensated and with Cascaded LPIC Compensator

The addition of the second LPIC compensator left the FRF magnitude mostly unchanged since that was not the goal of the additional compensation. The time delay that was approximately 2-3ms was improved to approximately 1ms. After two iterations of system identification, sufficient performance was seen from the actuators. This is proof that the shake table could be sufficiently compensated.

4.7 Payload System Identification

The next step in the compensation of the shake table for use in RTHS is to apply the payload. For the intended RTHS test, the payload is the physical substructure which is the same as the physical substructure described in previous chapters. The previous system identification and compensation methods used in previous sections were repeated once the payload was added to the shake table as shown in Figure 4.12.

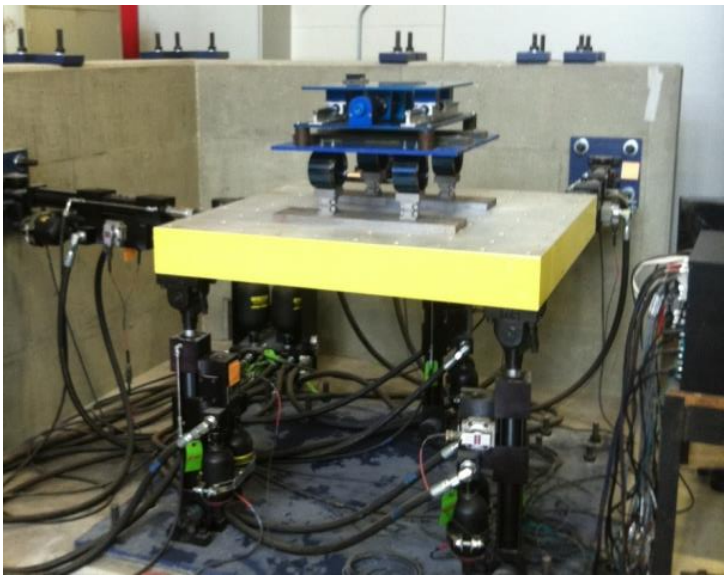

Figure 4.12 – Six Degree of Freedom Shake Table with Payload

The first step was to perform the system identification of the shake table with the payload present. Figure 4.13 shows the comparison of the shake table actuators uncompensated transfer functions with the payload not present in the blue and with the payload present in the red.

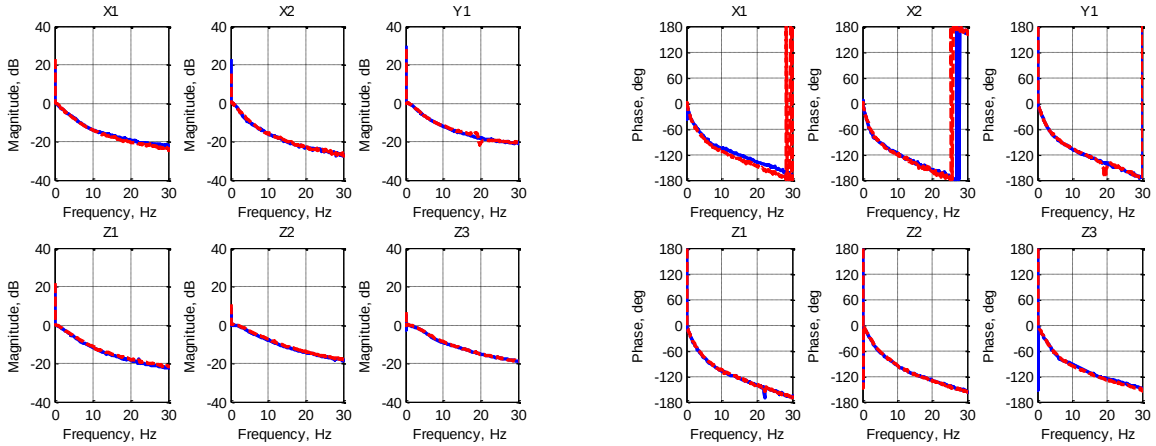

(A) **(B)**

Figure 4.13 - Frequency Response Function Magnitude (A) and Phase (B) of Six Actuators Uncompensated With and Without Payload

Generally, the dynamics seem to be unchanged however, the Y1 actuator shows a significant change in its dynamics due to the presence of the payload. The additional loading of the payload shifted the natural frequency of the Y1 actuator lower in frequency which brought it into the frequency range of interest. The natural frequency of each actuator results from the combination of the stiffness of the hydraulic fluid

column in the actuator and the mass load that the actuator has to excite. Prior to applying the payload, the natural frequency of the Y1 actuator was higher in frequency than of interest. When the payload was added to the shake table, the actuators were mass-loaded. This increases the mass term of the equation of natural frequency $\omega = \sqrt{K/M}$, which therefore decreases the natural frequency of the actuator. The Y-direction of the shake table has only one actuator, while the X-direction has two and the Z-direction has three. Since parallel stiffness terms summate, the X and Z directions' total stiffness terms are larger and therefore their natural frequencies are higher in frequency. Adding the additional mass of the payload still reduced the natural frequency in the X and the Z direction, however when it was reduced it was still higher than the frequency range of interest. Since the Y direction has only one actuator, its stiffness term is the least and since the mass term is the same in all directions, the Y direction has the lowest natural frequency. Therefore, when the additional mass of the payload was added, the natural frequency of the Y-direction was reduced into the frequency range of interest. This is a prime example of why the payload is necessary to be present on the shake table when system identification is performed.

An initial feedforward compensator was built using the same low pass inverse compensation and cascaded methods described previously. Because the initial feedforward compensator used in the cascaded feedforward compensation method is used to linearize the actuator dynamics, the resonant frequency of the Y1 actuator discussed above was ignored. Once the dynamics are linearized and a secondary compensator is built, this resonant frequency was compensated using the second feedforward compensator. Figure 4.14 shows the results of both iterations of compensation. These results are comparable to the performance achieved previously with the payload not present which is encouraging considering the extra dynamics present when the payload was added.

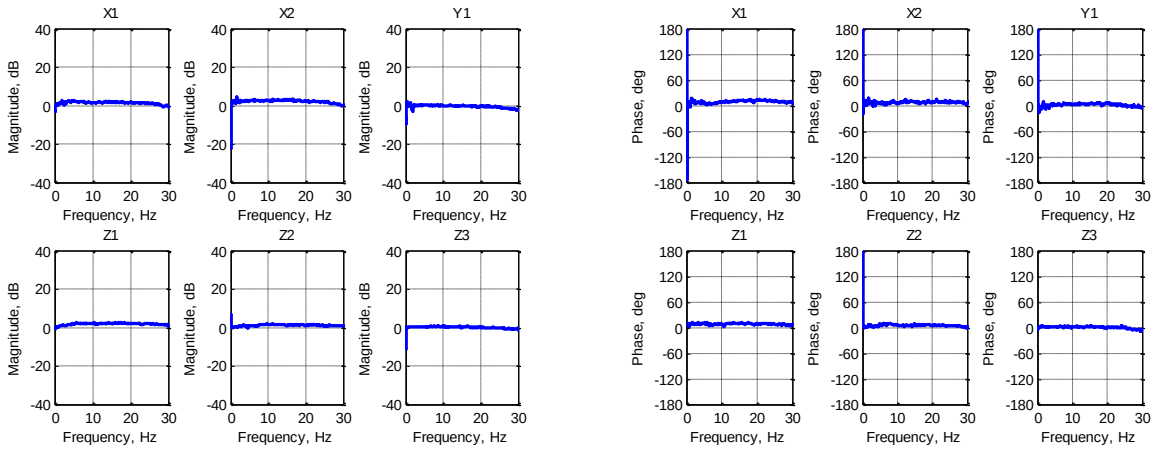

Figure 4.14 - Frequency Response Function Magnitude (A) and Phase (B) of Six Actuators Compensated with Payload Present

The system identification as well as feedforward compensation performed up to this point has been for a band limited white noise (BLWN) input to each of the actuators at a certain displacement level with a BLWN RMS level equal to 0.02 inches, i.e. the frequency spectrum of the input is essentially flat. This level of BLWN was chosen based on results shown in previous chapters, along with (Botelho R. , 2015), that show this displacement level was adequate for system identification of the transfer system. Realistically, RTHS displacement levels commanded to the transfer system do not resemble BLWN flat spectrums. The displacements typically commanded to a transfer system during a RTHS test are highly frequency dependent due to the resonant frequencies of the system and can significantly vary in magnitude. Because of this, it is important to test the transfer system at varying displacement magnitudes. This was done with the same feedforward compensator discussed previously. Figure 4.15 shows the system identification of the transfer system using the same feedforward compensator but at varying RMS levels from 0.10 inches to 0.30 inches in 0.05 increments.

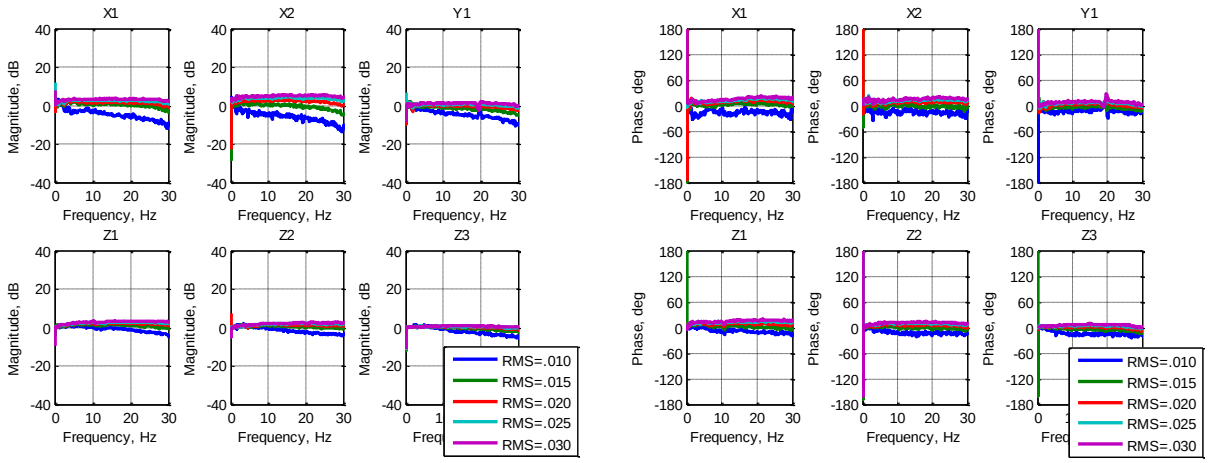

Figure 4.15 - Frequency Response Function Magnitude (A) and Phase (B) of Six Actuators Compensated at Varying RMS Input Levels

These results show a significant variation in performance depending on input displacement level. Previous research shown in the previous chapters, as well as (Botelho R. , 2015), shows transfer system dependence on displacement to be less significant A feedforward compensator was built using a moderate level of displacement and the performance of the transfer system was sufficient with this feedforward compensator regardless of varying input displacement levels. However, that research was performed using different transfer systems which were less dependent on displacement levels at this range. Because the commanded displacement levels of the transfer system vary significantly during a RTHS test, these results do not show that the transfer system compensation is adequate. Additional efforts were taken to improve this.

4.8 Proportional Gain Tuning

The ShoreWestern 6DOF shake table used in these studies was not initially intended to be used for real-time applications which explain why the uncompensated dynamics of the table are less than adequate. In addition, the ShoreWestern SC6000 servo valve controller has a proprietary internal digital adaptive control algorithm, in addition to its internal analog PID controller, which is used to improve reference tracking. However, this adaptive control algorithm is only used by the controller for internally generated inputs using the ShoreWestern signal generator and not used for external signals such as commanded

displacements used during RTHS to be commanded to the transfer system. In this case, the only controller used by the ShoreWestern servo valve controller is the internal analog PID controller which is only tuned to ensure stability, not necessarily desired reference tracking.

Because this internal PID controller was not initially tuned for the intent of reference tracking and just for stability, it was thought that it could be further tuned to improve the performance of the transfer system. However, tuning the internal analog PID controller involves an extensive manual procedure which could is difficult, time consuming, and potentially detrimental and irreversible. To avoid irretrievable damage to the controller, it was thought to digitally supplement the PID controller using the dSPACE DS1103 PPC controller board and the already existent control schematic. Figure 4.16 shows this control schematic which is similar to that which is shown in Figure 4.9 but specifically shows the PID controller internal to the ShoreWestern servo valve controller and the additional digitally supplemental PID gain.

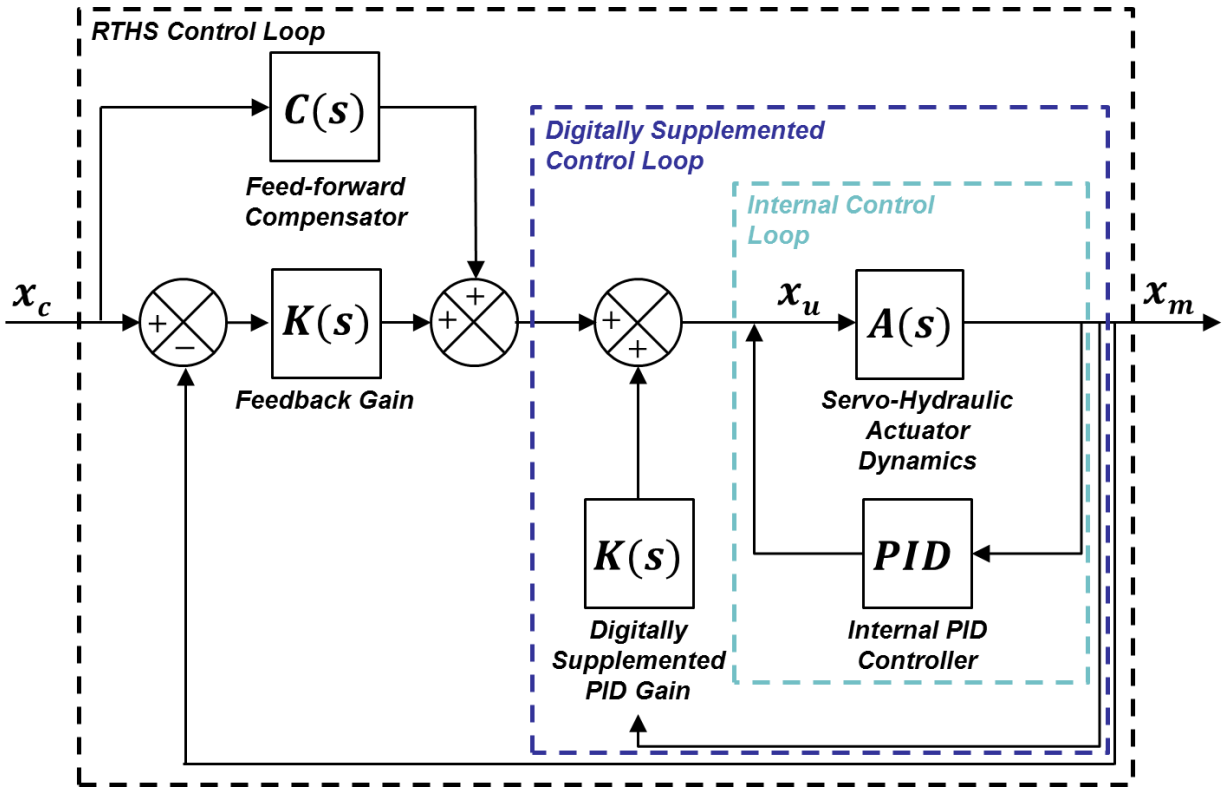

Figure 4.16 – Control Diagram with Additional Digitally Supplemented PID Gain

Through trial and error, the optimum values for the supplemental proportional gain for each actuator was determined to be were [6 6 5 5 4 4] for the X1, X2, Y1, Z1, Z2, and Z3 actuators, respectively. Using these gains and the control diagram shown in Figure 4.16, the transfer system was tested at various RMS levels similar to previous tests. The results of these new tests are shown in Figure 4.17.

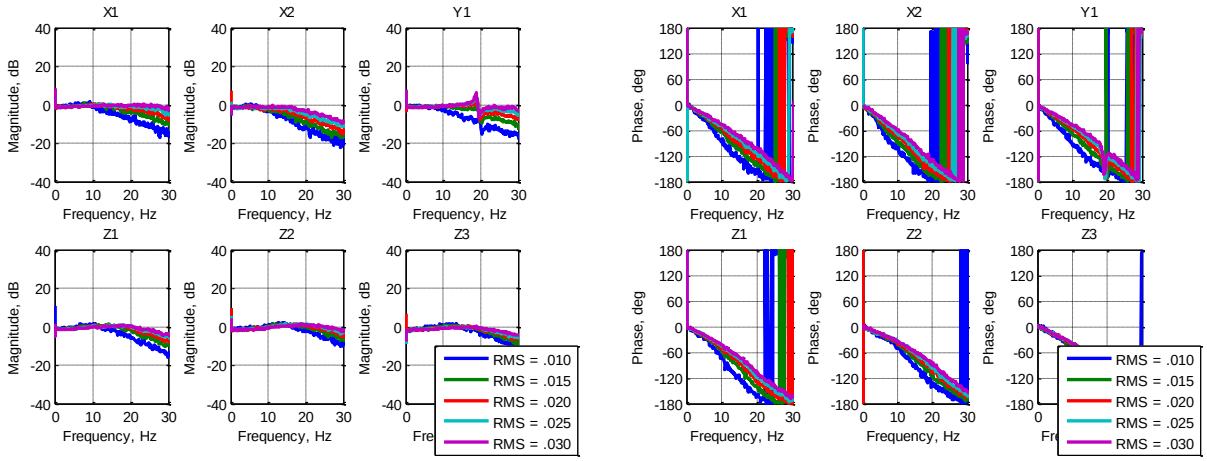

(A) **(B)**

Figure 4.17 - Frequency Response Function Magnitude (A) and Phase (B) of Six Actuators with Supplemental Proportional Gain at Varying RMS Input Levels

These results are interesting for multiple reasons. First, the supplemental proportional gain had a significant effect in the performance of the actuators' magnitude tracking when compared to the results shown in Figure 4.13. With the additional of the proportional gain, the magnitude, which was, previously, significantly attenuated, shows great improvements across the entire frequency range. At the worst frequencies, the attenuation was reduced and at the frequencies below approximately 10Hz, the actuators show almost exact magnitude tracking and independence of RMS excitation level which is a significant improvement over previous results. Another reason why these results are interesting is that the phase wasn't necessarily improve but it seems to have become somewhat more linearized, i.e. the frequency dependent phase resembles a straight line across the frequency range which indicates a frequency independent, constant time delay. The previous uncompensated system identification results, shown in Figure 4.8, Figure 4.11 and Figure 4.13, show frequency dependent time delay results. The results in Figure 4.17 show a more linearized relationship between frequency and phase (this of course varies with

the level of RMS level excitation; some are more linearized than others). This linear relationship is more desirable because a linear phase-frequency relationship means a frequency independent, constant time delay. A constant time delay is less difficult to predict, and therefore quantify, and therefore compensate for.

The same compensation process as described previously was used to compensate for these dynamics and the system was retested with the feedforward compensator present in addition to the supplemental PID proportional gain. The results of this retest are shown in Figure 4.18. For graphing simplification purposes, only .01, .02, and .03 RMS level excitation results are shown.

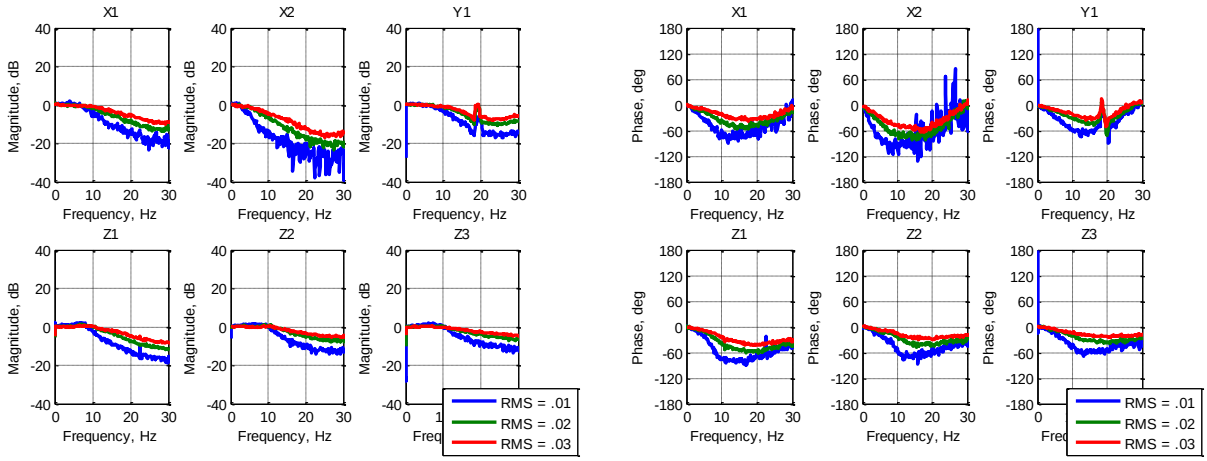

Figure 4.18 - Frequency Response Function Magnitude (A) and Phase (B) of Six Actuators with Supplemental Proportional Gain and Cascaded Feedforward Compensator at Varying RMS Input Levels

These results show a slight improvement over the results shown in Figure 4.17 but are unexpectedly detrimental when compared to the results shown in Figure 4.15. This led to the conclusion that the addition of the supplemental PID proportional gain was not the correct approach. With the additional of the supplemental gain, it is not a linear relationship between the actuator dynamics and the feedforward compensator, i.e. a more complicated calculation of the appropriate feedforward compensator is necessary. This paper was not interested in a compensation method that was more complicated than necessary so the idea of the addition of the supplemental PID proportional gain was abandoned.

4.9 Hybrid System Identification

The issue with the transfer system compensation so far is that an adequate feedforward compensator can only be constructed for a known input, however, the compensator is only valid for that exact input, i.e., if the input is changed, the compensator may no longer be adequate. Up until this point, flat spectrum RMS displacement excitation have been used for system identification for the actuator dynamics and the results show sufficient reference tracking for the given input, but insufficient tracking for any other levels of input. The concern is that with RTHS, the frequency dependent displacement levels can vary drastically and the non-robust compensators shown so far would not be adequate for the large variation in displacement commands.

However, if the frequency dependent displacement levels could be sufficiently predicted, a robust feedforward compensator could be built using the pre-described method. Based on research shown in previous chapters, frequency based substructuring techniques such as Transfer Path Hybrid Substructuring (TPHS) can be used to calculate a prediction of the displacement that will be commanded to the transfer system. This method used experimentally obtained system identification of the physical substructure and the numeric model of the numerical substructure to numerically couple the dynamics of the full system. This method can also be used to predict the displacement levels seen by the transfer system during the RTHS experiment. The governing equation of TPHS is

$$\left\{\frac{F_r}{F_i}\right\} = [I + PN]^{-1}P_i \qquad [4.10]$$

Where F_r is the reactant force between the physical substructure, P and the numerical substructure, N and the system excitation from the physical substructure is represented by P_i. The input force to the system is F_i. To use this approach to determine the displacements transmitted by the transfer system, x_n, Equation [5.5] is transformed into

$$\left\{\frac{x_n}{F_i}\right\} = N[I + PN]^{-1}P_i \qquad [4.11]$$

Figure 4.19 shows the results of this calculation for the previous RTHS test case described in previous chapters.

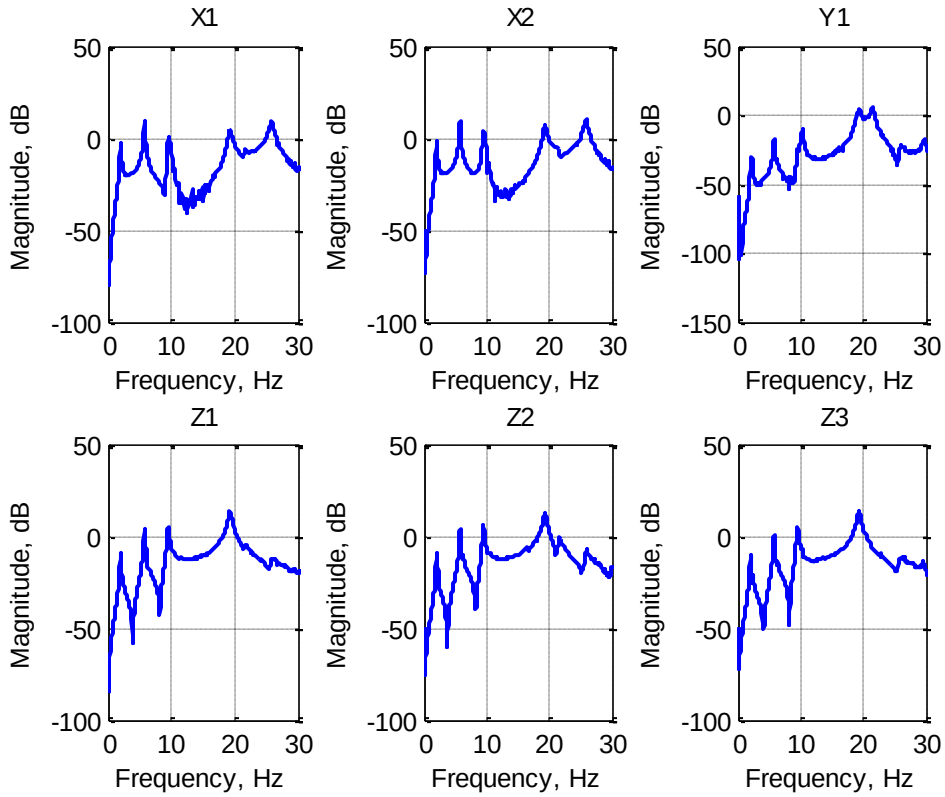

Figure 4.19 – Transfer Path Hybrid Substructuring Prediction of Actuator Commanded Displacements

For this case study, a MDOF state-space Laplace domain model was used to represent the transfer function based on the results shown in Figure 4.19. To determine the appropriate continuous Laplace domain function, the results shown in Figure 4.19 were manually curve fit.

4.9.1 Curve Fitting of Frequency Response Function

The first step of manually curve fitting the FRF data was to determine the correct closed form continuous function for a single resonance frequency. Based on previous research shown in previous chapters, it was determined that the correct transfer function is

$$TF(s) = (Cs + K)\left[1 - \frac{Cs + K}{Ms^2 + Cs + K}\right] \quad [4.12]$$

which can be rewritten as

$$TF(s) = \frac{Ms^2(Cs + K)}{Ms^2 + Cs + K} \quad [4.13]$$

and if it is given that

$$\omega_n = \sqrt{\frac{K}{M}} \quad \zeta = \frac{C}{2\sqrt{KM}} \quad [4.14], [4.15]$$

then Equation [4.13] becomes

$$TF(s) = \frac{Ms^2\left(2\zeta\omega_n s + \omega_n^2\right)}{s^2 + 2\zeta\omega_n s + \omega_n^2} \quad [4.16]$$

where ω_n is the natural frequency of the resonance frequency and ζ is the damping coefficient and M is the mass of the system. Since the mass of the system is known, the only unknowns are the natural frequency and the damping coefficient. The natural frequencies and damping coefficients can be estimated by examining the FRF data that is being curve fit and using linear superposition, the transfer functions of each individual pole (resonance) and zero (anti-resonance) of the system can be convolved together to give a continuous function that sufficiently approximates the data shown in Figure 4.19.

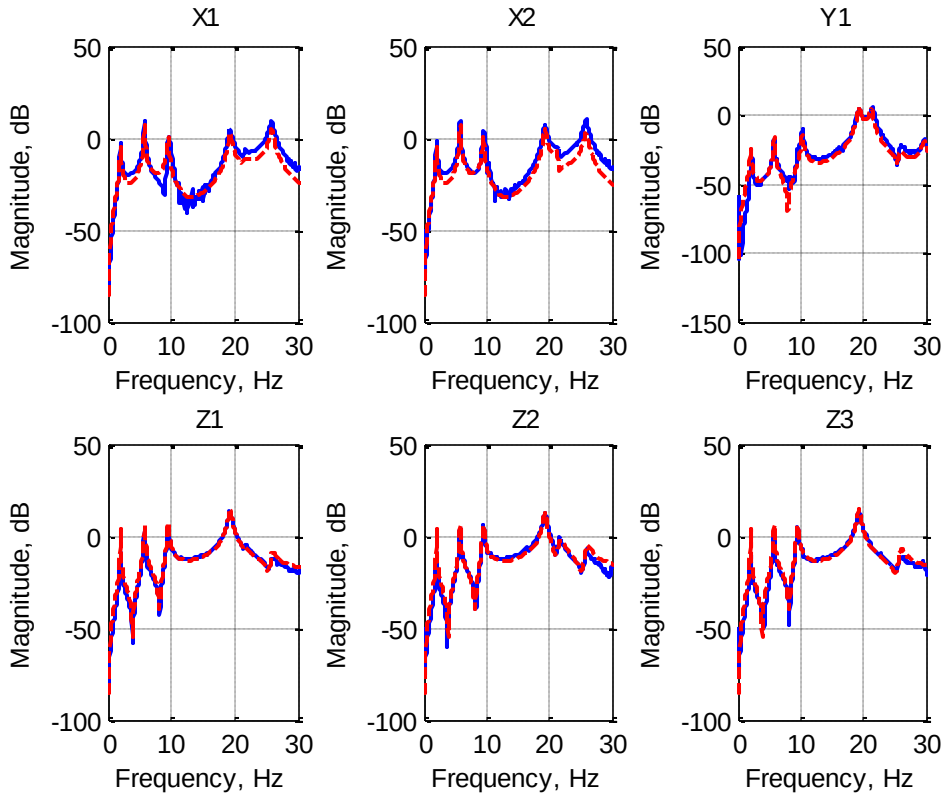

Figure 4.20 – Curve Fits of Actuator Commanded Displacements

Now that there are six Laplace domain transfer functions that represent the dynamics of each of the six actuators commanded displacements, these six functions can be converted into one six-input six-output state space model to be used in the system identification control system. The six Laplace domain transfer functions were assembled into a diagonal matrix and then this system matrix was converted to an equivalent state space model using the MATLAB function *tf2ss* which takes s-domain (Laplace domain) transfer functions and converts them to a state space model.

This state space was then used to recreate the same frequency dependent commanded displacement that the actuators will be commanded during the RTHS. The output of the state space is then commanded to the actuators and the transfer system is tested similar to before. Figure 4.21 shows the uncompensated results of the system identification where the blue lines are the measured frequency response functions and the grey lines are the coherence of the respective frequency response function.

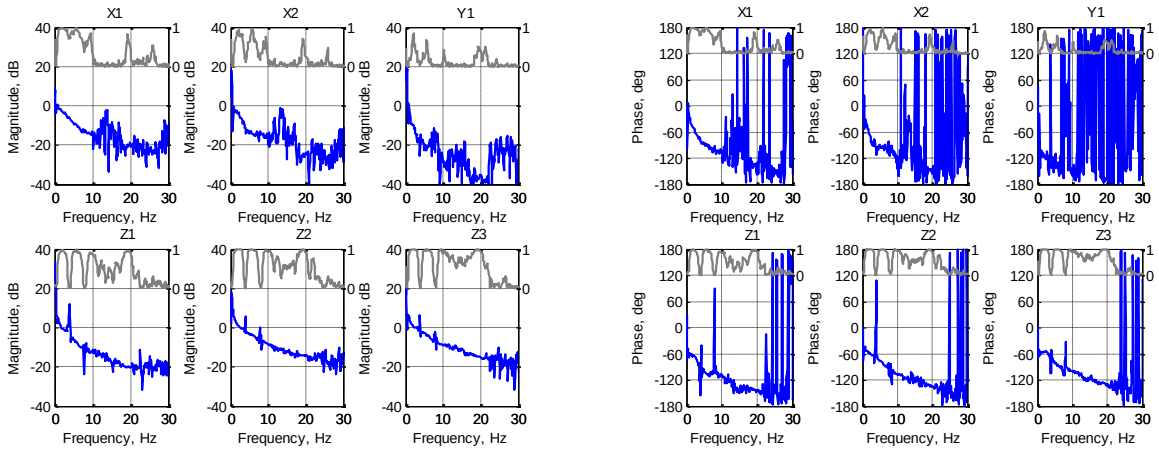

Figure 4.21 - Frequency Response Function Magnitude (A) and Phase (B) of Six Actuators Uncompensated Using the Hybrid System Identification Approach

These results show that there are frequency ranges of low coherence and therefore noisy frequency response function results. These low coherence frequency ranges are caused by lower levels of command displacement excitation which is due to the "valleys" of the commanded displacement frequency response functions shown in Figure 4.19 and Figure 4.20. The commanded displacement in these frequency ranges is so small, the reference tracking is not critical; therefore it isn't an issue that poor results are recorded in these ranges.

The same process as described previously was used to compensate for these dynamics except for one difference in the curve fitting process. Previously, all frequency results were used to calculate an approximate Laplace domain transfer function using the MATLAB function *invfreqs* which uses a least-mean square approximation algorithm to determine the optimum Laplace domain continuous transfer function to approximate the desired FRF. With these hybrid system identification results, the frequencies where there was low coherence and therefore poor quality results should not be included in the LMS algorithm. The MATLAB *invfreqs* has the functionality of a weight factor which is a value from zero to one for every frequency that allows the algorithm fit-errors to be weighted versus frequency, i.e., if the weight factor for a frequency is zero, that frequency data is essentially ignored. The recorded coherence of the frequency response function was an ideal weight factor array to be used in the *invfreqs* function

since it is data with values from zero to one which essentially represents the quality of the data. In summary, if the coherence data is used as a weight factor in the MATLAB *invfreqs* function, poor quality data is essentially ignored in the curve fitting algorithm and only the good quality data is curve fit. Figure 4.22 shows the results of the cascaded feedforward inverse compensation efforts using the hybrid system identification approach where the blue lines are the measured frequency response functions and the grey lines are the coherence of the respective frequency response function.

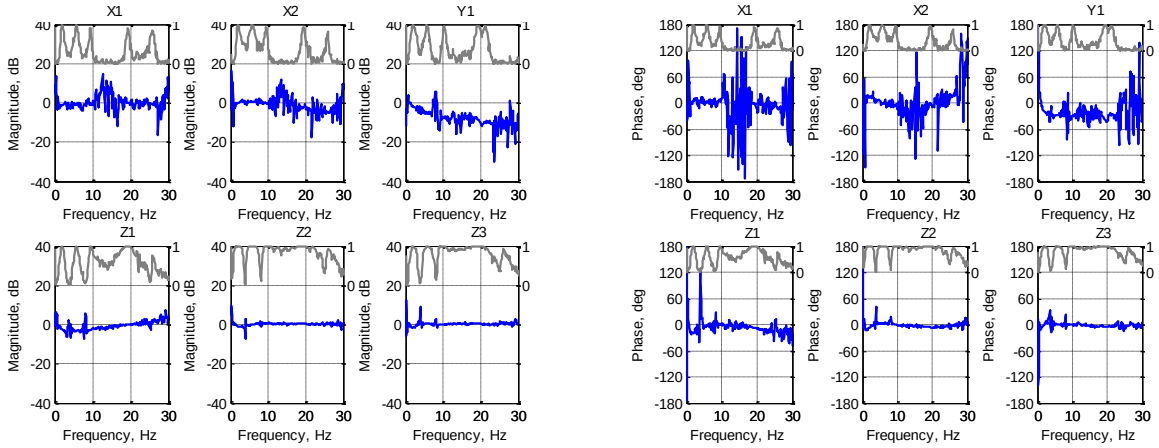

(A) **(B)**

Figure 4.22 - Frequency Response Function Magnitude (A) and Phase (B) of Six Actuators Compensated Using the Hybrid System Identification Approach

These results show sufficient reference tracking for all the actuators except the Y1 actuator. The Y1 actuator commanded displacement is significantly less than the rest of the actuators which results from the excitation of the system being predominantly in the X direction. The X direction excitation cross-couples to the Z direction because of rotation of the system but the X direction excitation doesn't couple to the Y direction, therefore the absolute levels of displacement are significantly less. This causes low coherence almost over the entire frequency range of interest. This makes the dynamics of the Y1 actuator very difficult to compensate for. But, since the displacement is almost negligible, its dynamics may not be of concern. Future research will be done to determine if the Y1 actuator is actually necessary during the RTHS. Other than the Y1 actuator, all the actuators show sufficient reference tracking, in frequency ranges of concern, i.e., good coherence, with generally less than ±1dB of amplification/attenuation and

generally less than one millisecond of time delay which is adequate for the planned RTHS testing of lightly damped structures.

4.10 Conclusion

This chapter described MIMO system identification and model-based feedforward feedback compensation of a six degree of freedom shake table for conducting stable RTHS testing of lightly damped mechanical systems. First, the nonlinear transformation matrix relating the Cartesian degrees of freedom of the shake table to the six individual actuators was linearized. This allowed compensation of the actuator dynamics of the six individual actuators of the shake table to provide effective displacement tracking of the six Cartesian degrees of freedom (i.e., x, y, z translations and rotations) of the shake table. This compensation was accomplished by calculating a MIMO transfer function quantifying the frequency dependent magnitude and time delay. Initial proof of principle test cases show once the actuator dynamics was quantified, a cascaded feedforward inverse compensation was successfully developed to linearize the actuator dynamics and reduce the inherent time delay.

However, these initial results still showed a significant dependence on commanded displacement levels. Digitally supplemental PID controller proportional gain was added to attempt to reduce this dependence without success. However, a new system identification method was introduced, which leverages displacement predictions using frequency based substructuring technique known as Transfer Path Hybrid Substructuring, to mimic the commanded input to the actuators, during the RTHS, during the system identification of the transfer system. This eliminates the concern of the displacement excitation level dependence. Using the same compensation methods used in preliminary test cases, the transfer system was linearized and reduced the inherent time delay. The cascaded feedforward inverse compensation and linearized transformation can be used to perform multiple degree of freedom RTHS testing of lightly damped mechanical systems using the six degree of freedom shake table as part of future research.

4.11 References

Bendat, J. S., & Piersol, A. G. (2011). *Random Data: Analysis and Measurement Procedures.* John Wiley & Sons.

Botelho, R. (2015). *Real-Time Hybrid Substructuring for Marine Application of Vibration Control and Structural Acoustics.* University of Connecticut.

Bouscayrol, A. (2008). Different types of hardware-in-the-loop simulation for electric drives. *Industrial Electronics*, pp. 2146-2151.

Carmeli, M. S., Castelli-Dezzaa, F., Mauri, M., & Marchegiani, G. (2013). Novel Mechanical Hardware in the Loop Platform for Distributed Generation Systems. *Distributed Generation and Alternative Energy Journal, 28*(3), 7-27.

Carrion, J. E., & Spencer, B. (2007). Model Based Strategies for Real Time Hybrid Testing. *NSEL Report No NSEL-006*.

Chen, C., & Ricles, J. M. (2010). Tracking Error Based Servohydraulic Actuator Adaptive Compensation For Real Time Hybrid Simulation. *Journal of Structural Engineering, 10*, 432-440.

Darby, A. P., Blakeborough, A., & Williams, M. S. (1999). Real Time Substructure Test Using Hydraulic Actuator. *Journal of Engineering Mechanics, 125*(10), 1133-1139.

Dimig, J., Shield, C., French, C., Bailey, F., & Clark, A. (1999). Effective Force Testing: A Method of Siesmic Simulation for Structural Testing. *Journal of Structural Engineering, 125*(9), 1028-1037.

Fathy, H. K., Ahlawat, R., & Stein, J. L. (2005). Proper powertrain modeling for engine-in-the-loop simulation. *ASME 2005 International Mechanical Engineering Congress and Exposition*, 1195-1201.

Filipi, Z., & Kim, Y. J. (2010). Hydraulic hybrid propulsion for heavy vehicles: Combining the simulation and engine-in-the-loop techniques to maximize the fuel economy and emission benefits. *il & Gas Science and Technology–Revue de l'Institut Francais du Petrole, 65*(1), 155-178.

Filipi, Z., Fathy, H., Hagena, J., Knafl, A., Ahlawat, R., Liu, J., . . . Stein, J. (2006). Engine-in-the-loop testing for evaluating hybrid propulsion concepts and transient emissions-HMMWV case study. *AE Technical Paper*.

Gao, X., Castaneda, N., & Dyke, S. J. (2013). Experimental validation of a generalized procedure for MDOF real-time hybrid simulatio. *Journal of Engineering Mechanics, 140*(4).

Hanselmann, H. (1993). *Hardware-in-the loop simulation as a standard approach for development, customization, and production test of ECU's.* SAE Technical Paper.

Horiuchi, T., Inoue, M., Konno, T., & Namita, Y. (1999). Real Time Hybrid Experimental System With Actuator Delay Compensation and It's Applications to a Piping System With Energy Absorber. *Earthquaker Engineering and Structural Dynamics, 28*(10), 1121-1141.

Isermann, R., Schaffnit, J., & Sinsel, S. (1999). Hardware-in-the-loop simulation for the design and testing of engine-control systems. *Control Engineering Practice, 7*(5), 643-655.

Jung, R. Y., & Shing, P. B. (2006). Performance Evaluation of a Real Time Pseudodynamic Test System. *Earthquake Engineering Structural Dynamics, 35*(7), 789-810.

Nakashima, M., & Masaoka, N. (1999). Real Time On-Line Test for MDOF Systems. *Earthquake Engineering and Structural Dynamics, 28*, 393-420.

Nakata, N., Spencer, B., & Elnashai, A. (2007). *Multi-dimensional Mixed-mode Hybrid Simulation Control and Applications.* Newmark Structural Engineering Laboratory. University of Illinois at Urbana-Champaign.

Phillips, B. M., & Spencer Jr., B. F. (2012). Model-based multiactuator control for real-time hybrid simulation. *Journal of Engineering Mechanics, 139*(2), 219-228.

Phillips, B. M., & Spencer, B. F. (2011). *Model Based Servo Hydraulic Control For Real Time Hybrid Simulation.* University of Illinois, Urbana-Champaign, IL: Newmark Structural Engineering Laboratory Report Number NSE-028.

5 MULTIPLE DEGREE OF FREEDOM SYSTEM LEVEL VIBRATION TESTING OF MECHANICAL EQUIPMENT USING REAL-TIME HYBRID SUBSTRUCTURING

5.1 Abstract

Real-Time Hybrid Substructuring (RTHS) is a relatively new method of vibration testing that can be used to effectively characterize the system level performance of mechanical equipment. RTHS allows mechanical equipment to be physically tested while coupled through what is called a transfer system to a real-time numerical simulation of the support structure. The challenge in applying RTHS to test mechanical equipment is two-fold: the equipment itself can have little inherent damping which, coupled with the inherent dynamics of the transfer system, can result in marginally stable or unstable RTHS tests; and the interface at the attachment points can be complex with multi-directional and rotational motion and reactions which adds significant complexity to the RTHS transfer system. To insure stability and accurately represent the complex interface between the physical and numerical substructures, a high fidelity multiple-input-multiple-output (MIMO) servo-hydraulic actuator system is used for the RTHS transfer system. This paper demonstrates effective control of a six degree-of-freedom (6DOF) shake table for RTHS applications and describes the corresponding model-based feedforward feedback compensation to facilitate both stable and accurate RTHS testing of lightly damped mechanical systems. The results show that the proposed compensation methods allow for successful multiple degree of freedom (MDOF) RTHS experiments that capture the coupled dynamics of the full system. Next, a RTHS case study is performed and is verified by the experimental testing of the mechanical system. It is shown that RTHS can provide an improved method for system-level vibration testing of mechanical equipment to accurately predict the vibration transmission of mechanical equipment into the support structure.

5.2 Introduction

Real-time hybrid substructuring (RTHS) provides the capability to isolate and physically test the critical components of a mechanical system early on in the design phase of a system. This capability is

accomplished by including the dynamic interaction at the time of the component testing by using a numerical representation of the remainder support structure not being physically tested. RTHS is a relatively new method of vibration testing, made more practical due to advances in computer power, digital signal processing hardware/software, and hydraulic control. RTHS has potential to accurately capture the dynamics of the coupled system at the lower frequencies as well as provide system level insight into the design of mechanical systems during the component level testing. In doing so, RTHS can potentially remove unnecessary conservatism from the design of the mechanical system. Figure 1 shows a general diagram of a RTHS test which illustrates the closed loop nature of this type of testing.

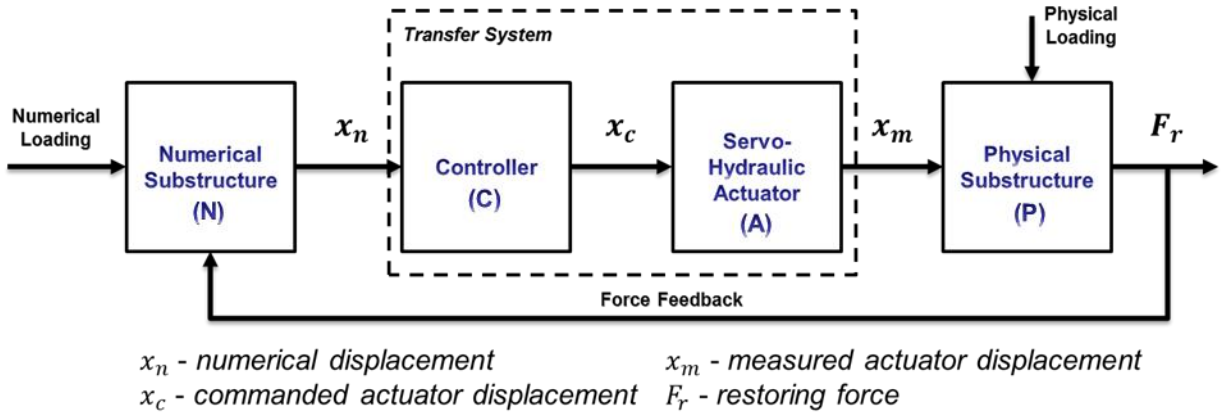

Figure 5.1 – General Block Diagram for RTHS Closed-Loop Testing

Early research in RTHS focused on earthquake engineering and structural engineering (Nakashima & Masaoka, 1999), (Darby, Blakeborough, & Williams, 1999), (Dimig, Shield, French, Bailey, & Clark, 1999), and (Horiuchi, Inoue, Konno, & Namita, 1999)). RTHS was a significant element of the Network for Earthquake Engineering Simulation (NEES) with a comprehensive list of projects and publications posted at https://nees.org/wiki/RTHSwiki. A major focus of past RTHS research is the development of actuator control methods for effective displacement tracking of the servo-hydraulic transfer system. (Horiuchi, Inoue, Konno, & Namita, 1999) used a frequency independent time-delay model to approximate the servo-hydraulic actuator dynamics, and then a polynomial prediction to compensate for the servo-hydraulic actuator dynamics. (Jung & Shing, 2006) and (Chen & Ricles, 2010) used similar compensation methods based on a control signal error-compensation methods. These methods rely on a

simplified time domain representation of stationary servo-hydraulic actuator dynamics with relatively small time delays. (Carrion & Spencer, 2007) and (Phillips & Spencer, 2011) proposed compensation techniques that involve higher order model-based strategies including a feedforward compensator, that creates an approximate inverse of the actuator model to compensate for the servo-hydraulic actuator dynamics in the transfer system. (Phillips & Spencer, 2012) and (Gao, Castaneda, & Dyke, 2013) applied this approximate inverse method to multi degree of freedom (MDOF) servo-hydraulic actuator systems for actuators providing collinear displacements on a steel building frame. These tests involved testing frames or dampers (not mechanical equipment) with higher levels of inherent damping and with transfer systems mostly limited to uni-axial motion.

A similar test method to RTHS is hardware-in-the-loop (HWIL). HWIL testing is typically used in mechanical applications to test various types of control systems. Earliest publications of what is considered HWIL are research related to flight simulations where the early goals were to simulate the instruments with a fixed cockpit (N.N., 1964) and (Marienfeld, 1965). In HWIL testing, the physical substructure is often an electrical component and the interface between the numerical and physical substructures is achieved through the direct transfer of electrical signals. As such, the system connecting the physical and numerical components, known as the transfer system in RTHS, does not require any servo-hydraulic control system for HWIL. HWIL testing has been conducted on mechanical equipment including HWIL research done in the design of electro-mechanical systems (Hanselmann, 1993) and (Isermann, Schaffnit, & Sinsel, 1999)) and (Bouscayrol, 2008) and (Carmeli, Castelli-Dezzaa, Mauri, & Marchegiani, 2013) who use HWIL to predict the electrical performance of electric motors and distributed electric generators, respectively. Similar research topics used a mechanical automotive engine as the physical substructure, referred to as engine-in-the-loop (Fathy, Ahlawat, & Stein, 2005), (Filipi, et al., 2006), and (Filipi & Kim, 2010). HWIL is typically characterized by having no physical transfer system.

RTHS allows for the combined testing of physical and numerical substructures as shown in Figure 5.1. This figure illustrates the closed loop nature of RTHS. The interface forces at the physical substructure connection points are measured by force sensors, converted to digital signals and transmitted to the numerical substructure. The numerical substructure uses the measured interface forces along with any numerical loading to calculate the displacements at the same substructure connection points. These numerical displacements are then imposed upon the physical substructure through a transfer system, typically a servo-hydraulic actuator transfer system. While the transfer systems of typical RTHS tests in civil earthquake engineering are usually single hydraulic actuators and uniaxial, the transfer system for the support of a piece of mechanical equipment can be more complex, involving not only multiple translations, but rotations as well.

Since RTHS involves a feedback loop, it is critical for test stability and accuracy that all the forces and displacements are transmitted between the two substructures accurately and timely, to insure compatibility of the substructures and stability of the system. Accuracy and delay in a RTHS test can be a result of the sensors, the analog to digital and digital to analog converters, and the computation time, however, it is typically dominated by the inherent dynamics (i.e. apparent time delay and magnitude distortion) of the transfer system. This effect can be compounded when considering multiple actuators tuned to work synchronously with one another.

RTHS can accurately represent the dynamics of the coupled system as well as provide insight into the design of mechanical systems using system level mechanical vibration. RTHS provides the capability to isolate and physically test the critical complex components of a mechanical system while including the dynamic interaction with a numerical representation of the remainder of the linear portions of the system.

Different application of RTHS can be sufficiently unique to require full analysis and examination of the assumptions, equipment and resulting stability and accuracy prior to conducting any testing. This paper proposes a systematic approach to analyze the feasibility of RTHS for the system level vibration testing of mechanical equipment. First, the mechanical system should be logically portioned into its physical and

numerical substructures. The general logic is that the portion of the system that is relatively complex and difficult to quantify using numerical methods, should be the physical substructure and the portion of the mechanical system that is suited for finite element analysis (FEA) or other numerical methods should be the numerical substructure. Next, because stability of the RTHS control loop is critical to the success and accuracy of the experiment, the Robust Stability Analysis method develop by (Botelho R. , 2015) is used to predict the stability of the RTHS control loop. Also, using this analysis, it is determined the level of reference tracking necessary for the transfer system. Knowing this ahead of time ensures successful compensation of the transfer system inherent dynamics in order to achieve a successful RTHS experiment. Next, a multiple inputs multiple outputs (MIMO) system identification and then a model-based feedforward-feedback compensation approach is used to facilitate both stable and accurate RTHS experiments. Finally, the RTHS experiment is performed and verified with a full mechanical system quantitative experiment.

5.3 Partitioning and Boundary Conditions

A RTHS test involves partitioning the whole system into physical and numerical substructures. While testing of mechanical equipment somewhat defines this partitioning, it is important to examine both the effect of this partitioning on the potential stability of the test and the necessary assumptions that will be made regarding chosen boundary conditions. It has been shown in previous chapters that the proportions of mass and stiffness along with the amount of damping, of the RTHS substructures are critical to the stability of the closed loop system (Botelho, Christenson, & Franco, 2013). In a real world application, the physical and numerical are typically predetermined based on the mechanical component which is pre-existing and the mechanical system's support structure which is not realized but only exists as a design, typically as a CAD, which can be leveraged to determine a numerical model. While the mechanical equipment, that will be the physical substructure, is predetermined, the portion of the support structure represented as the numerical substructure in the hybrid test, can be altered to give more advantageous

parameters (i.e. mass and stiffness ratios) that affect the stability of the test since it is a CAD/FEA model and can easily be optimized for better structural vibration mitigation performance.

A typical mechanical system consists of multiple levels of lumped mass and isolation systems. The mechanical equipment is often designed with its own isolation system and the support structure would be design with its own isolation system. In this paper a similar configuration is adopted and the two systems were substructured so each system includes the structure and their respective isolation system. Figure 5.2 shows the substructured layout of this experiment.

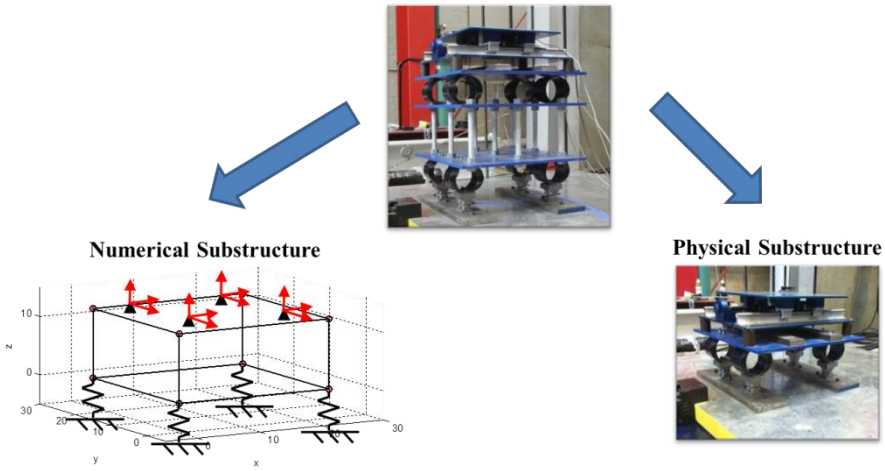

Figure 5.2 – Experimental Substructuring Approach

As in any substructuring method, it is important to couple the necessary degrees of freedom of the substructures in order to accurately represent the desired dynamics. Four tri-axial force sensors placed underneath the isolation system of the physical substructure at the four bottom corners, for a total of twelve axial forces, are used to measure and transmit the reactant forces to the numerical substructure. It should be noted that this was assumed to be sufficient to transmit not only the translational reaction forces, but also the rotational reaction moments.

Earlier chapters have demonstrated that preliminary uni-axial RTHS experiments were able to validate the approach of using RTHS for quantification of mechanical equipment in which the interest was only the lowest frequency resonant frequencies of the system, which were dominated by lateral modes. The research presented here, looks to expand on these experiments by incorporating the system's multi-degree

of freedom dynamics which include multiple directional and cross-coupled modes. Because of this, a six degree of freedom (6DOF) servo-hydraulic actuator system was necessary to achieve the communication between the physical and numerical substructures of the RTHS experiment.

5.4 Notional Mechanical Equipment Real-Time Hybrid Substructuring Test

A notational mechanical system consisting of mechanical equipment and a support structure is used here to demonstrate real time hybrid substructuring for use in predicting system level vibration performance of mechanical equipment. The RTHS test is conducted in the Structures Research Laboratory at the University of Connecticut on the 6DOF shake table. A Quanser Shake Table II, which was treated as the mechanical equipment, was mounted on four linear coil springs spaced 18 inches horizontally and 11 inches laterally. Next, the support structure was constructed and placed on the same four linear coil springs spaced 18 inches horizontally and 11 inches laterally. The support structure is four 24.0 by 24.0 by 0.5 inches horizontal steel plates connected with nine 1 inch diameter threaded rods. Three of the plates are placed at the top of the structure and one of the plates is placed on the bottom, 12 inches apart, vertically. Figure 5.3 shows each of these systems as well as these two systems assembled into the multiple stage system.

(A) (B) (C)

Figure 5.3 – (A) Mechanical Equipment, (B) Foundation Structure, (C) Full Assembled System

The mechanical equipment assembly is supported by four PCB Piezoelectric tri-axial force sensors. The Quanser Shake Table II was commanded a band limited white noise (BLWN) with a roll off at 20Hz. The

roll off at higher frequencies is achieved with an 8th order Butterworth filter. This ensures that low frequency resonances are sufficiently excited but also excites higher frequencies with lower energy so to avoid pushing the Quanser Shake Table II towards its mechanical limits. Auto power spectral densities (PSDs) of the measured force under the four coil springs were recorded using a Data Physics 8 channel dynamic signal analyzer. This represents the response of the first mass-spring oscillator which will later be the physical substructure of the real time hybrid simulation. The lateral force transmitted through the structure as measured during the experiment as well as a numerical model to verify the results are shown in Figure 5.4. The numerical model was derived by using the transfer function equation for reactant force due to displacement excitation derived in previous chapters.

$$TF(s) = (Cs + K)\left[1 - \frac{Cs + K}{Ms^2 + Cs + K}\right] \quad [5.1]$$

To calculate the total force transmitted in this degree of freedom, the magnitude of the PSDs of the transmitted forces at the four sensors at each corner were summed together.

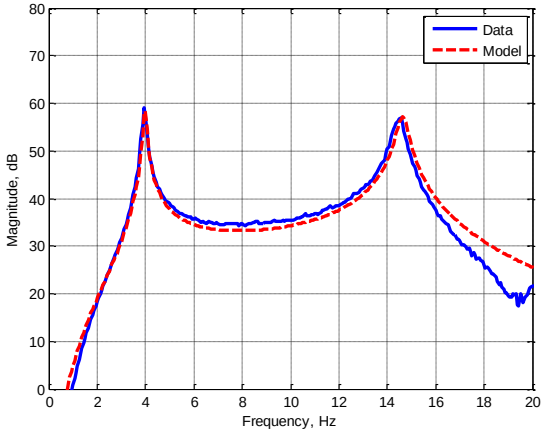

Figure 5.4 – PSD of the Total Force Transmitted to the Base of the Mechanical Equipment in the Horizontal Direction

As in previous work, the support structure is assumed to be linear and a numerical model of this structure is developed. The support structure is assumed linear and an accurate numerical model of this structure is developed. This model was verified by exciting the support structure with an impact hammer at the top portion of the structure and the transmitted force to the base of the structure was experimentally

measured. This portion of the system lends itself well to the numerical substructure of the real time hybrid simulation. The numerical model constructed was a six degree of freedom (DOF) state space model with 12 states. A frequency response function of the total horizontal displacement due to horizontal excitation force was calculated, both numerically and experimentally, and is shown in Figure 5.5.

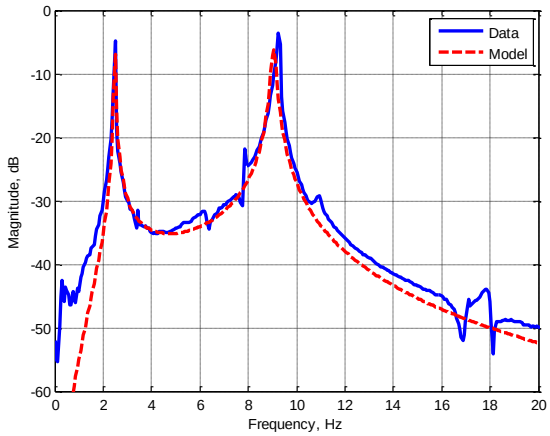

Figure 5.5 – Frequency Response Function of Horizontal Displacement Due to Horizontal Force Excitation.

The complete notational mechanical system (shown in Figure 5.3C) was constructed and the vibration force transmitted through the system to the base was measured below the four corner isolation points using the same four PCB Piezoelectric tri-axial force sensors as in the physical substructure test and the Quanser shake table was commanded the same band limited white noise (BLWN) as in the physical substructure test. Auto power spectral densities (PSDs) of the measured force under the bottom layer of the four coil springs were recorded using a Data Physics 8 channel dynamic signal analyzer. Figure 5.6 shows the force transmitted to the force sensors at the base of the full system. This represents force transmitted through the full system and will later be used to validate the RTHS results. The two lower frequency resonant frequencies are the in-phase and out-of-phase lateral modes of the system. These two resonances are dominated by the lateral dynamics of the system and were the focus of previous work. The two higher frequency resonant frequencies are the in-phase and out-of-phase rotational modes of the system. These two resonances are controlled by the cross-coupling of the lateral and the vertical dynamics

of the system. The simulation results shown are the results of dynamic coupling of the two numerical models shown in Figure 5.4 and Figure 5.5.

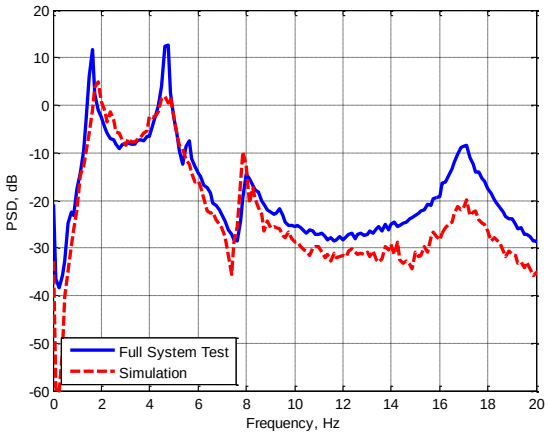

Figure 5.6 – PSD of the Total Force Transmitted to the Base of the Full System in the Horizontal Direction

5.5 Six Degree of Freedom Shake Table

Real Time Hybrid Simulation (RTHS) is the combination of a physical substructure with a numerical substructure. This combination is performed by the use of sensors that transmit reactant forces from the physical substructure to the numerical substructure and servo-hydraulic actuators that transmit displacements, calculated by the numerical substructure, to the physical substructure. Figure 5.7 shows the general layout of a MIMO RTHS test of mechanical equipment at the University of Connecticut using a 6-DOF servo-hydraulic shake table. The real time digital signal processor (DSP) is a dSPACE DS1103 PPC controller board. The numerical substructure, along with the compensation scheme is built in MATLAB Simulink and then downloaded to the DS1103 through dSPACE's real time interface (RTI). The DS1103 has eight BNC D/A channels and twenty BNC A/D channels. The DSP controller sends commanded actuator displacements to the ShoreWestern SC6000 servo valve controller which has an internal analog PID reference tracking controller. Each actuator has an LVDT which measures the displacement. This measured displacement is fed back into the internal PID control loop and the outer RTHS compensation control loop as well as the DataPhysics SignalCalc Mobilizer dynamic signal analyzer.

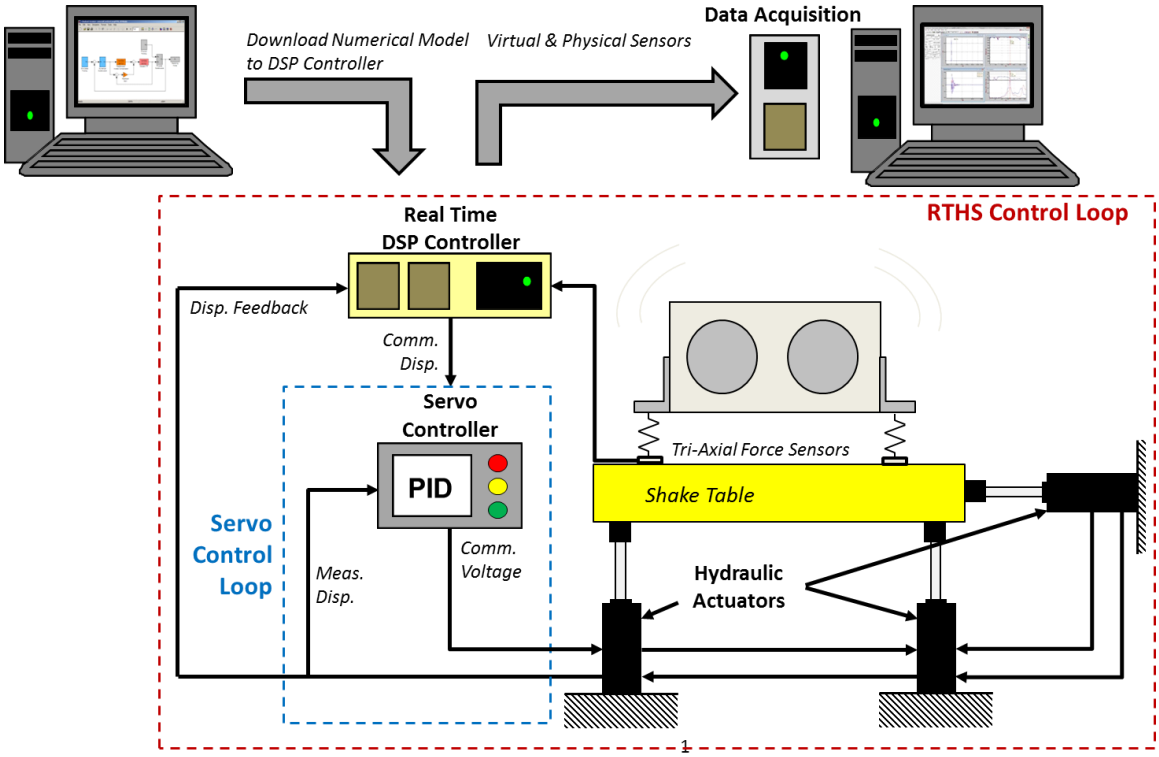

Figure 5.7 – System Diagram of RTHS Substructuring of Mechanical Equipment

A picture of the 6DOF shake table is shown in Figure 5.8.

Figure 5.8 – 6 Degree of Freedom Shake Table

The servo-hydraulic actuators have frequency dependent dynamics that can cause instability in the RTHS feedback loop. These frequency dependent dynamics need to be compensated to provide closed-loop stability and performance.

5.5.1Feedforward Inverse Compensation

The servo-hydraulic control system used to interface the physical and numerical substructures has frequency dependent dynamics that need to be compensated to provide accurate and timely tracking of desired displacements for stability and accuracy of a RTHS. As a result of the physical configuration of the shake table, each of the six actuators in the 6DOF shake table can be treated as independent single input single output (SISO) transfer system (discussed in more detail in previous chapters) and therefore SISO compensation techniques are used to individually compensate the dynamics of each actuator, respectively. Figure 5.9 illustrates the model-based feedforward-feedback control architecture from (Carrion & Spencer, 2007) used for compensating the actuator dynamics. The feedforward compensator is used to cancel the modeled actuator dynamics, while the feedback gain is tuned experimentally to provide robustness due to modeling errors and changes in physical substructure during the experiment.

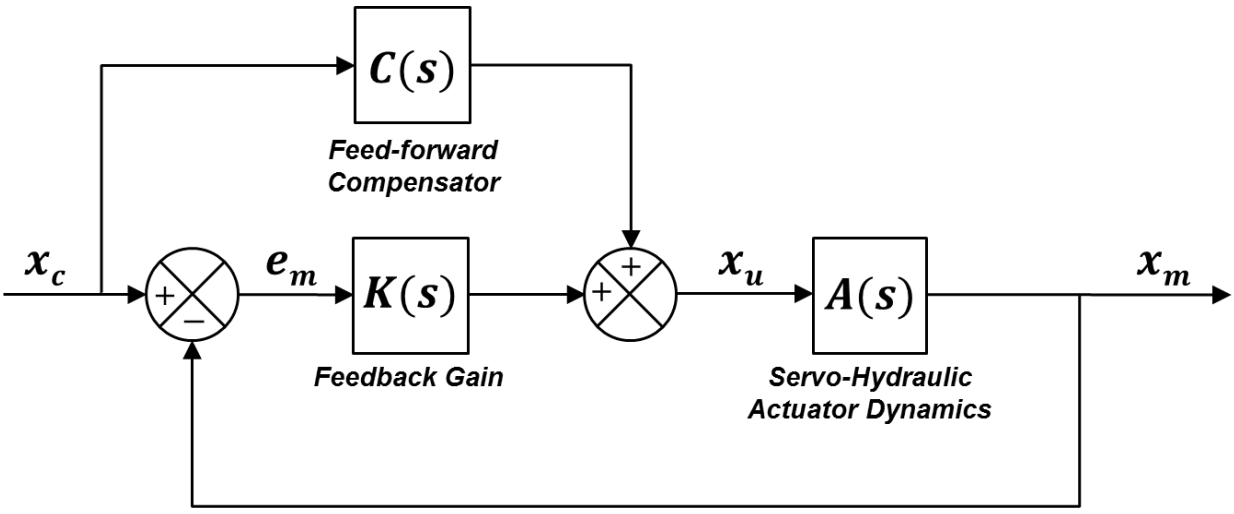

Figure 5.9 – Feedforward-Feedback Control for Actuator Dynamics Compensation

The feedforward inverse compensator is designed to cancel the modeled actuator dynamics of the servo-hydraulic system. Ideally, an exact inverse of the model fit of the servo hydraulic transfer function would

be the perfect compensator. The development of feedforward inverse compensator starts with deriving a Laplace domain transfer function model of the servo hydraulic dynamics from the m^{th} commanded to the n^{th} measured actuator displacement, which can be expressed as

$$A_{y_n x_m}(s) = \frac{\prod_{i=1}^{n}(s - z_i)}{\prod_{i=1}^{n}(s - p_i)} \quad [5.2]$$

The feedforward inverse compensator is determined by

$$C_{y_n x_m}(s) = A_{y_n x_m}(s)^{-1} \quad [5.3]$$

where

$$\mathbb{C}_{y_n x_m} = \begin{bmatrix} C_{y_1 x_1} & C_{y_1 x_2} & \cdots & C_{y_1 x_n} \\ C_{y_2 x_1} & C_{y_2 x_2} & \cdots & C_{y_2 x_n} \\ \vdots & \vdots & \ddots & \vdots \\ C_{y_n x_1} & C_{y_n x_2} & \cdots & C_{y_n x_n} \end{bmatrix} \quad [5.4]$$

If the transfer function model fit has equal number of poles, p_i and zeroes, z_i then an exact inverse can be used. However, in most cases, the model has less zeroes than poles making its inverse an improper transfer function, i.e. having more zeroes than poles. Low pass compensation, as discussed subsequently, can be used to address this issue.

As shown in previous chapters, the dynamics of the actuators are displacement and load dependent and therefore non-linear. To deal with the inherent non-linearity of the actuator system and the frequency dependent dynamics, an approach proposed in previous chapters is the cascaded feedforward inverse compensation method. In this approach, the system identification of the uncompensated system is used to develop an initial compensator. When this compensator is implemented, the commanded displacement can become higher in magnitude at some frequencies to compensate for the frequency dependent attenuation in magnitude. Because the actuators are commanded a significantly larger displacement than the initial system identification, the dynamics of the system change. The initial compensator may no longer be sufficient to achieve the desired actuator dynamics and additional system identification is

necessary. The dynamics of the actuator including the initial compensator is used to develop a second compensator using the same methodology of the initial compensator in order to compensate for the remaining time delay. These two compensators are then used in series as the feedforward compensator. Figure 5.10 illustrates the block diagram of the feedforward-feedback compensation with cascaded feedforward compensators.

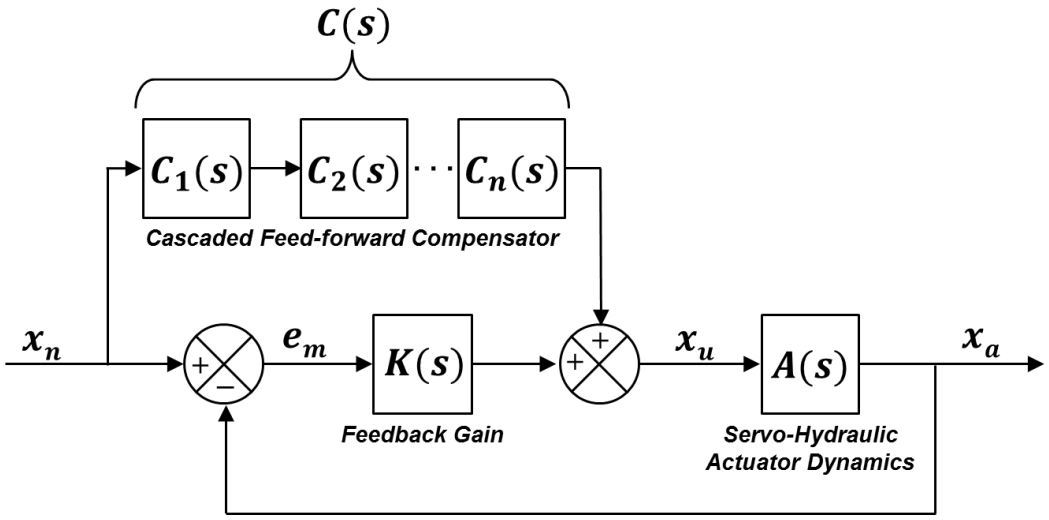

Figure 5.10 – Block Diagram of Cascaded Feedforward Inverse Compensation

The transfer system is observed to be dependent on the level of commanded displacement, i.e., if a feedforward compensator is built with a given commanded displacement level, that compensator does not provide sufficient performance with commanded displacement excitation levels other than was originally used to build the compensator. The method proposed, in previous chapters, to deal with this excitation dependence is referred to as Hybrid System Identification where a frequency based substructuring technique known as Transfer Path Hybrid Substructuring (TPHS) is used to predict the frequency dependent displacement levels that the actuators will be commanded during the RTHS experiment. This method was presented in previous chapters. The governing equation of TPHS is

$$\left\{\frac{F_r}{F_i}\right\} = [I + PN]^{-1} P_i \qquad [5.5]$$

Where F_r is the reactant force between the physical substructure, P and the numerical substructure, N and the system excitation from the physical substructure is represented by P_i. The input force to the system is F_i. To use this approach to determine the displacements transmitted by the transfer system, x_n, Equation [5.5] is transformed into

$$\left\{\frac{x_n}{F_i}\right\} = N[I + PN]^{-1}P_i \qquad [5.6]$$

The FRFs are then curve-fit using the 1-DOF transfer function,

$$TF(s) = \frac{Ms^2\left(2\zeta\omega_n s + \omega_n^2\right)}{s^2 + 2\zeta\omega_n s + \omega_n^2} \qquad [5.7]$$

where ω_n is the natural frequency of the resonance frequency and ζ is the damping coefficient and M is the mass of the system. Since the mass of the system is known, the only unknowns are the natural frequency and the damping coefficient. The natural frequencies and damping coefficients can be estimated by examining the FRF data that is being curve fit and using linear superposition, the transfer functions of each individual pole (resonance) and zero (anti-resonance) of the system can be convolved together to give a continuous function that sufficiently approximates the data shown in Figure 5.11. The blue lines are the experimentally obtained FRFs of each of the six actuators. The red lines are the results of the curve-fitting efforts.

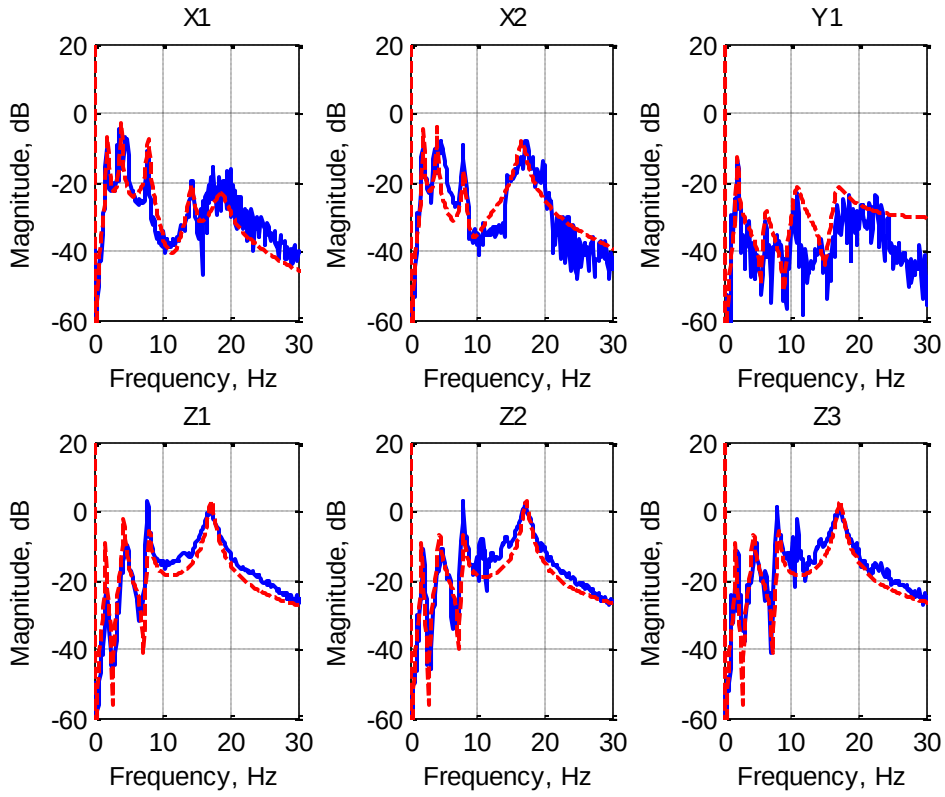

Figure 5.11 – Prediction of Actuator Displacements Using TPHS

The orientation of the six actuators (X1, X2, Y1, Z1, Z2, and Z3) are shown in Figure 5.12.

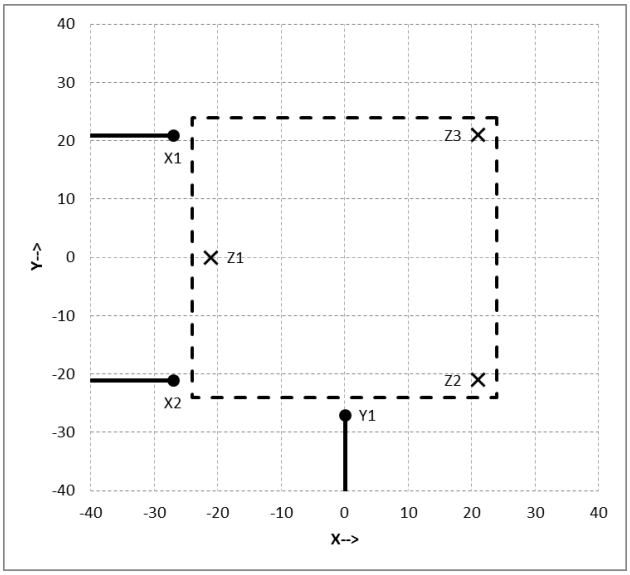

Figure 5.12 – Diagram of Actuator Orientation

Now that there are continuous functions that represent the dynamics of each of the six actuators commanded displacements, these six functions can be converted into one six-input six-output state space

model to be used in the system identification control system. The six continuous functions were assembled into a diagonal matrix and then this system matrix was converted to an equivalent state space model using the MATLAB function *tf2ss* which takes s-domain (Laplace domain) transfer functions and converts them to a state space model.

This state space was then excited with exactly the same excitation as the physical substructure as would be used during the RTHS test. Therefore, the output of the state space is theoretically the same frequency dependent commanded displacement that the actuators will be commanded during the RTHS. This output of the state space is then commanded to the actuators and the transfer system is tested similar to before. Figure 5.13 shows the uncompensated results of the system identification where the blue lines are the measured frequency response functions and the grey lines are the coherence of the respective frequency response function

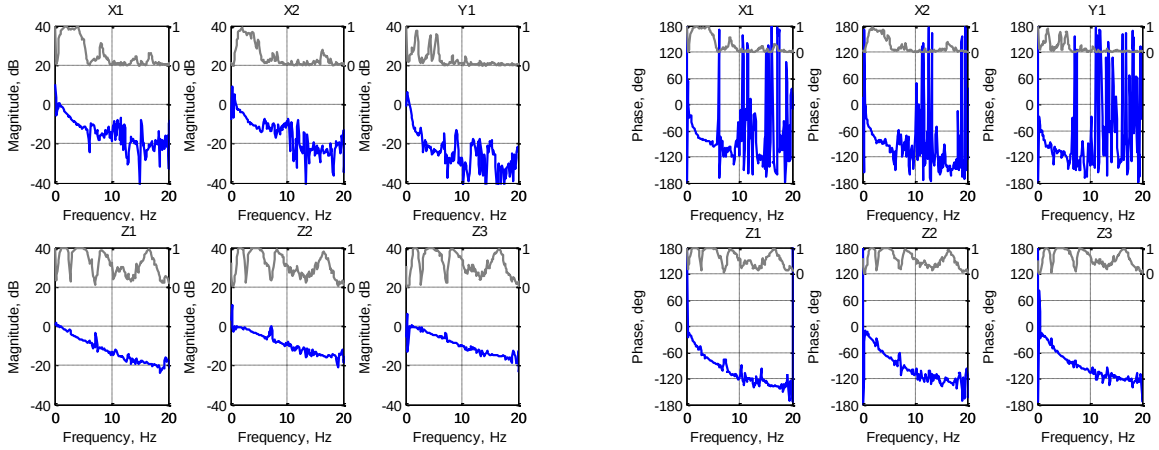

Figure 5.13 - Frequency Response Function Magnitude (A) and Phase (B) of Six Actuators Uncompensated Using the Hybrid System Identification Approach

These results show that there are frequency ranges of low coherence and therefore noisy frequency response function results. These low coherence frequency ranges are caused by lower levels of command excitation which is due to the "valleys" of the commanded displacement frequency response functions shown in Figure 5.11. The commanded displacement in these frequency ranges is so small, the reference tracking is not critical; therefore it isn't an issue that poor results are recorded in these ranges.

5.5.1.1 Low Pass Inverse Compensation

As in previous chapters, the low pass inverse compensator method as described in (Carrion & Spencer, 2007), was used to build the feedforward compensator. This low pass inverse compensation (LPIC) technique involves an alpha scalar value to duplicate the poles of the actuator transfer function as additional poles at higher frequencies. These additional poles are used to create the low pass filter given by

$$L_{y_n x_m}(s) = \frac{\prod_{i=1}^{n} \alpha_i p_i}{\prod_{i=1}^{n} (s - \alpha_i p_i)} \quad [5.8]$$

Multiplying the improper inverse of the actuator model by the low pass transfer functions yields the LPIC transfer function

$$C_{y_n x_m}(s) = A_{y_n x_m}(s)^{-1} L_{y_n x_m}(s) \quad [5.9]$$

Instead of using an alpha scalar to multiply the existing poles, the additional poles here are forced to be a specific frequency. This frequency should be high enough to minimize the effect on the low frequency dynamics over the control band but not too close to the sampling frequency so that accurate numerical integration is possible. The low pass transfer function is represented by

$$L_{y_n x_m}(s) = \frac{\prod_{j=1}^{n} \omega_j}{\prod_{j=1}^{n} (s - \omega_j)} \quad [5.10]$$

An independent inverse compensator was derived for each of the SISO actuator transfer functions. First, each of the input output pairs of the MIMO transfer function were curve fit using the *invfreqs* MATLAB function. A constant (zero order) numerator and a fourth order denominator was found to the best fit of the frequency response data. The form of the curve fit is shown as

$$A_{y_n x_m}(s) = \frac{n_{0i}}{d_{4i} s^4 + d_{3i} s^3 + d_{2i} s^2 + d_{1i} s + d_{0i}} \quad [5.11]$$

Additional zeroes were added to balance each of the SISO transfer functions. These SISO transfer function were place in a MIMO transfer function matrix along the diagonal as

[5.12]

$$\mathbb{A} = \begin{bmatrix} A_1(s) & \cdots & 0 \\ \vdots & \ddots & \vdots \\ 0 & \cdots & A_n(s) \end{bmatrix}$$

Since this MIMO transfer function matrix is diagonal, each SISO transfer function along the diagonal can be independently inverted, which is the same as inverting the MIMO transfer function matrix. The LPIC transfer function matrix is then determined by

$$\mathbb{C} = \mathbb{A}^{-1}\mathbb{L} = \begin{bmatrix} C_1(s) & \cdots & 0 \\ \vdots & \ddots & \vdots \\ 0 & \cdots & C_n(s) \end{bmatrix} = \begin{bmatrix} A_1(s)^{-1}L_1(s) & \cdots & 0 \\ \vdots & \ddots & \vdots \\ 0 & \cdots & A_n(s)^{-1}L_n(s) \end{bmatrix} \quad [5.13]$$

Using Hybrid System Identification and the cascaded low pass inverse compensation method, the dynamics of the transfer system were sufficiently compensated. Figure 5.14 shows the results of the compensation efforts using the hybrid system identification approach where the blue lines are the compensated measured FRFs and the black lines are the uncompensated FRFs.

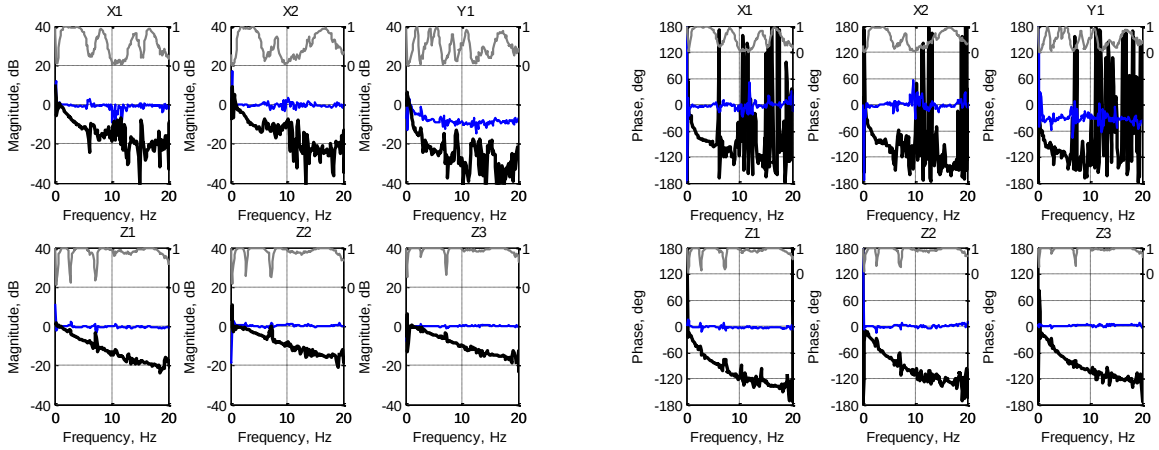

Figure 5.14 – Frequency Response Function Magnitude (A) and Phase (B) of Six Actuators Using the Hybrid System Identification Approach

These results show sufficient reference tracking for all the actuators except the Y1 actuator. The Y1 actuator commanded displacement is significantly less than the rest of the actuators which results from

the excitation of the system being in the X direction. The X direction excitation cross-couples to the Z direction because of rotation of the system but the X direction excitation doesn't couple to the Y direction, therefore the levels of displacement are significantly less. This causes low coherence almost over the entire frequency range of interest. This makes the compensation of the dynamics of the Y1 actuator very difficult. But, since the displacements are almost negligible, its dynamics may not be of concern. Other than the Y1 actuator, all the actuators show sufficient reference tracking with generally less than ±1dB of amplification/attenuation and generally less than one millisecond of time delay which is adequate for the planned RTHS testing of lightly damped structures.

5.5.1.2 High Frequency Amplification

Up until this point, the focus of the compensation efforts has been exclusively the low frequencies of interest (0-20Hz). However, because of the high sampling rates necessary for real-time processing, the entire frequency range of the RTHS test is important to consider. This RTHS experiment is sampled at 1024Hz which means that the entire frequency range is 0-512Hz. The RTHS is excited by BLWN from 0-20Hz so it was therefore assumed that there is negligible excitation at frequencies between 20Hz and the Nyquist frequency (512Hz) and therefore the commanded displacements at frequencies between 20Hz and the Nyquist frequency would be negligible. However, because the feedforward compensators developed from the LPIC method are continuous, they have characteristic performance at all frequencies. APPENDIX B documents the approach to address and reduce the high frequency amplification.

5.6 Stability and Performance Analysis

Presence of apparent time delay and magnitude attenuation in the real time hybrid substructuring feedback loop due to servo hydraulic actuator dynamics can lead to unwanted instability and loss of accuracy during RTHS testing. There are basically two causes for instability: inherent instability and feedback instability. Inherent instability is when the system is naturally unstable meaning even an open loop representation would be unstable. The second cause for instability is feedback. This source of instability works like a viscous circle, where the feedback signal causes the numerical substructure to

command increasingly higher and higher displacements to the servo hydraulic transfer system. In the design of mechanical systems, any system design that has inherent instabilities would not be an adequate design and therefore the instability concerns with real time hybrid substructuring are those of feedback stability.

The robust stability analysis methodology developed by (Botelho R. , 2015), is used to provide insight on acceptable time delay for stable closed-loop testing by casting stability analysis as an uncertainty problem. Figure 2.11 shows how the robust stability analysis methodology sets up the RTHS feedback loop in order determine whether the loop will be stable or not.

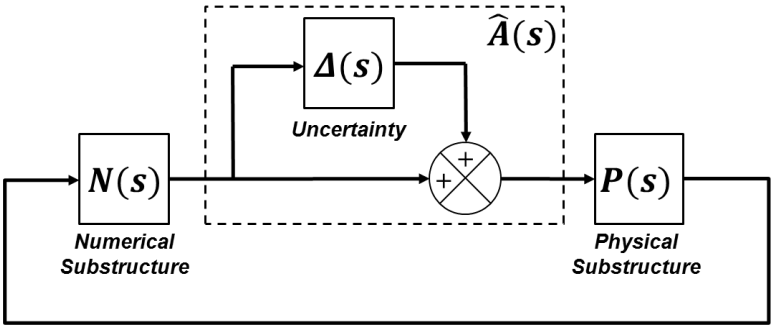

Figure 5.15 – Schematic of Robust Stability Analysis Feedback Loop

The robust stability analysis methodology says the sufficient condition for robust stability is

$$\|\Delta(s)T_0(s)\|_\infty < 1 \qquad [5.14]$$

Where:

$$\Delta(s) = \hat{A}(s) - I = [I - A(s)C(s)K(s)]^{-1}\{A(s)C(s)\} - I \qquad [5.15]$$

$$T_0(s) = [I + P(s)N(s)]^{-1}P(s)N(s) \qquad [5.16]$$

The robust stability analysis methodology was used to provide insight on acceptable time delay for the RTHS test of the notional mechanical equipment. Figure 2.19 shows the results of this analysis for the uncompensated transfer system, the compensated transfer system using just the feedforward compensator.

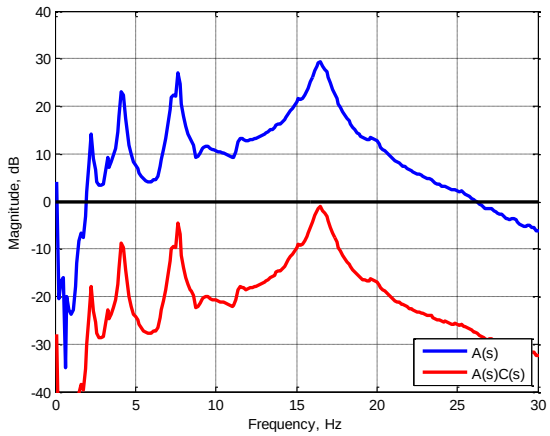

Figure 5.16 – Robust Stability Analysis for the Uncompensated and Compensated Transfer System.

These results show that the RTHS feedback loop is marginally stable with the feedback compensator. These results are shown up to a slightly higher frequency in order to check the trend of the stability curve as frequency increases. In these results, it's shown that the stability curve reduces in magnitude as frequency increases which is satisfactory.

5.7 Real Time Hybrid Simulation Results

The RTHS is conducted in the Structures Research Laboratory at the University of Connecticut. The mechanical equipment was placed on the linear springs mounted to the tri-axial force sensors (as shown in Figure 5.3A). This setup was placed on the 6DOF servo hydraulic actuator shake table. The Quanser Shake Table II was driven with the same band limited white noise as in the previous mechanical equipment tests. The forces from the tri-axial sensors are sent through the dSPACE controller into the numerical model. These forces drove the numerical model of the steel support structure. The response of the steel support structure is calculated and then communicated to the transfer system which displaced the base of the component in all six translational and rotational directions. The transmitted force was calculated at the base of the steel foundation structure numerical model using virtual sensors. This calculated transmitted force was then compared to the full system test results.

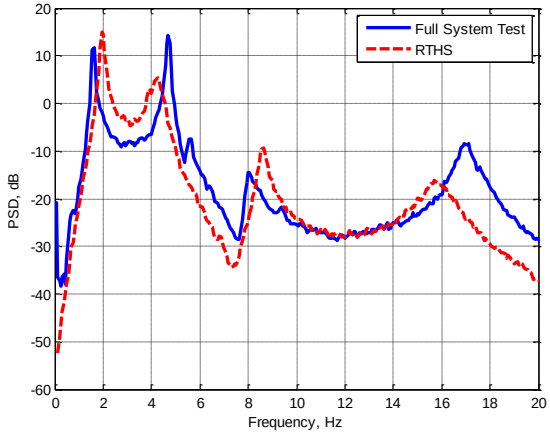

Figure 5.17 – Comparison of RTHS vs. Experimental Test Results

The results from the RTHS experiment show favorable correlation with the full system experiment response. This proves that RTHS can accurately represent the phase relationship of the coupled system. It is thought that the remaining discrepancies are either caused by either poor reference tracking of the transfer system or idealizations made in the RTHS numerical substructure. Considering that Figure 3.16 shows that good correlation between the TPHS results and the full system test results, and that the numerical model used in the TPHS approximation and the RTHS experiment are the same, it leads to the conclusion that the discrepancies between the RTHS results and the full system test results shown in Figure 5.17 are not related to numerical model inaccuracies.

Concerning potential poor reference tracking, (Botelho R. , 2015) describes potential degradations in performance due to marginally stable systems such as this one as seen in Figure 5.17. The robust stability analysis methodology says the sufficient condition for robust stability is given in Equation [5.14] but the condition for robust performance, i.e., accurate results is given as

$$\|\Delta(s)T_0(s)\|_\infty \ll 1 \qquad [5.17]$$

In (Botelho R. , 2015), it is assumed that $\|\Delta(s)T_0(s)\|_\infty$ being an order of magnitude less than one (-20 in decibel scale) is desired for robust performance. The stability analysis of this system shown in Figure 5.16 shows that there exist frequency ranges in which this criterion isn't met, therefore it is possible that this insufficient stability caused the inaccuracies of this RTHS experiment. These frequency ranges in

which insufficient stability exists show good correlation to the frequency ranges in which there are inaccuracies of the RTHS experiment. What appears to be a frequency shift, between the full system test and the RTHS results is also potentially explained by (Botelho R. , 2015). This research describes critical frequencies at which a system will oscillate when marginally stable. These critical frequencies, in lightly damped systems are typically relatively close to the natural frequencies of the system. The system oscillations, due to marginal stability will correspond to these critical frequencies instead of the natural frequencies of the system. Since, these critical frequencies are typically very close to the natural frequencies of the system, the results can misleadingly show what seems to be a frequency shift in resonance when compared to system dynamics without time delay i.e., the full system test shown in Figure 5.17.

Transfer Path Hybrid Substructuring can be used to further demonstrate the relationship between transfer system reference tracking accuracy and the accuracy of the RTHS experiment. The TPHS results shown Figure 3.16 assumes ideal reference tracking of the transfer system. However, if the transfer system is not assumed to be unity, then the sensitivity of the system to transfer system dynamics can be simulated using the governing equation of TPHS as described in previous chapters.

$$\left\{\frac{F_r}{F_i}\right\} = [I + PAN]^{-1} P_i \qquad [5.18]$$

where A is the transfer system dynamics which is typically assumed to be unity i.e., an identity matrix. This A matrix was calculated to include a pure time delay calculated using the equation

$$A_i = e^{-i\omega\tau} \qquad [5.19]$$

where A_i is the transfer function of the i^{th} actuator of the transfer system and τ is the amount of time delay in seconds. A variety of time delays were simulated and for simplicity purposes, all actuators of the transfer system were assumed to have equal time delay. Figure 5.18 shows the results of these analyses.

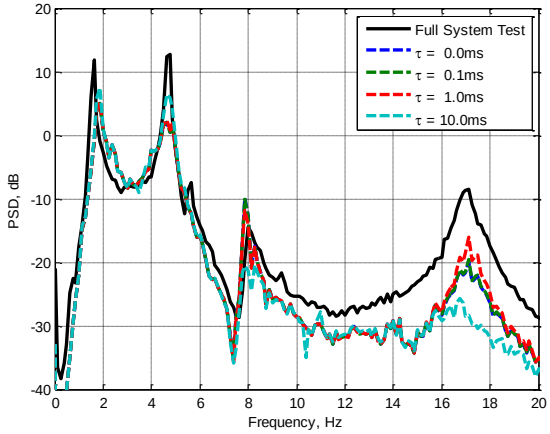

Figure 5.18 – Transfer Path Hybrid Substructuring Results including Pure Time Delay

It is shown that as the accuracy of the transfer system decreases, and therefore the stability of the RTHS loop decreases, the accuracy of the simulations decreases as well.

5.8 Conclusion

This paper describes the development and implementation of RTHS for quantification of system level vibration of mechanical equipment systems using the example of a multiple degree of freedom multi stage mechanical system. RTHS was used to interface a physical substructure, notional mechanical equipment, to a notional foundation structure which was represented numerically forming a multi stage system. This was accomplished by closed-loop RTHS testing using a model-based feedforward-feedback actuator tracking controller with a low pass inverse compensator (LPIC). The RTHS experiment shows encouraging results, however there are remaining inconsistencies. These results show there are limitations of RTHS for lightly damped mechanical systems which are controlled by the stability of the control loop. However, the promising comparison of the results of the RTHS with the full system experimental test proves that RTHS could accurately represent the dynamics of the coupled system as well as provide insight into the design of mechanical systems using system level mechanical vibration.

5.9 References

Botelho, R. (2015). *Real-Time Hybrid Substructuring for Marine Application of Vibration Control and Structural Acoustics.* University of Connecticut.

Botelho, R. B., Christenson, R., & Franco, J. (2013). Exact Stability Analysis for Uniaxial Real Time Hybrid Simulation of 1-DOF and 2-DOF Structural Systems. *Engineering Mechanics Institute Conference.*

Bouscayrol, A. (2008). Different types of hardware-in-the-loop simulation for electric drives. *Industrial Electronics*, pp. 2146-2151.

Carmeli, M. S., Castelli-Dezzaa, F., Mauri, M., & Marchegiani, G. (2013). Novel Mechanical Hardware in the Loop Platform for Distributed Generation Systems. *Distributed Generation and Alternative Energy Journal, 28*(3), 7-27.

Carrion, J. E., & Spencer, B. (2007). Model Based Strategies for Real Time Hybrid Testing. *NSEL Report No NSEL-006*.

Chen, C., & Ricles, J. M. (2010). Tracking Error Based Servohydraulic Actuator Adaptive Compensation For Real Time Hybrid Simulation. *Journal of Structural Engineering, 10*, 432-440.

Darby, A. P., Blakeborough, A., & Williams, M. S. (1999). Real Time Substructure Test Using Hydraulic Actuator. *Journal of Engineering Mechanics, 125*(10), 1133-1139.

Dimig, J., Shield, C., French, C., Bailey, F., & Clark, A. (1999). Effective Force Testing: A Method of Siesmic Simulation for Structural Testing. *Journal of Structural Engineering, 125*(9), 1028-1037.

Fathy, H. K., Ahlawat, R., & Stein, J. L. (2005). Proper powertrain modeling for engine-in-the-loop simulation. *ASME 2005 International Mechanical Engineering Congress and Exposition*, 1195-1201.

Filipi, Z., & Kim, Y. J. (2010). Hydraulic hybrid propulsion for heavy vehicles: Combining the simulation and engine-in-the-loop techniques to maximize the fuel economy and emission benefits. *il & Gas Science and Technology–Revue de l'Institut Francais du Petrole, 65*(1), 155-178.

Filipi, Z., Fathy, H., Hagena, J., Knafl, A., Ahlawat, R., Liu, J., . . . Stein, J. (2006). Engine-in-the-loop testing for evaluating hybrid propulsion concepts and transient emissions-HMMWV case study. *AE Technical Paper*.

Gao, X., Castaneda, N., & Dyke, S. J. (2013). Experimental validation of a generalized procedure for MDOF real-time hybrid simulatio. *Journal of Engineering Mechanics, 140*(4).

Hanselmann, H. (1993). *Hardware-in-the loop simulation as a standard approach for development, customization, and production test of ECU's.* SAE Technical Paper.

Horiuchi, T., Inoue, M., Konno, T., & Namita, Y. (1999). Real Time Hybrid Experimental System With Actuator Delay Compensation and It's Applications to a Piping System With Energy Absorber. *Earthquaker Engineering and Structural Dynamics, 28*(10), 1121-1141.

Isermann, R., Schaffnit, J., & Sinsel, S. (1999). Hardware-in-the-loop simulation for the design and testing of engine-control systems. *Control Engineering Practice, 7*(5), 643-655.

Jung, R. Y., & Shing, P. B. (2006). Performance Evaluation of a Real Time Pseudodynamic Test System. *Earthquake Engineering Structural Dynamics, 35*(7), 789-810.

Marienfeld, H. (1965). Flugsimulation. *Dissertation TU Darmstadt*.

Mitra, S. K. (2011). *Digital Signal Processing: A Computer-based Approach.* McGraw-Hill.

N.N. (1964). Schulung und Praxis mit Flugsimulator. *INTERAVIA,* 1104-1107.

Nakashima, M., & Masaoka, N. (1999). Real Time On-Line Test for MDOF Systems. *Earthquake Engineering and Structural Dynamics, 28*, 393-420.

Phillips, B. M., & Spencer Jr., B. F. (2012). Model-based multiactuator control for real-time hybrid simulation. *Journal of Engineering Mechanics, 139*(2), 219-228.

Phillips, B. M., & Spencer, B. F. (2011). *Model Based Servo Hydraulic Control For Real Time Hybrid Simulation.* University of Illinois, Urbana-Champaign, IL: Newmark Structural Engineering Laboratory Report Number NSE-028.

6 CONCLUSION

This dissertation presents the efforts and case studies to extend and demonstrate RTHS for system level vibration testing of mechanical systems. These efforts include: analysis of mechanical system dynamics comparing low frequency linear superposition approximation method with the exact solution and system identification and compensation of a MDOF servo-hydraulic actuator shake table using feedforward-feedback compensation methods. Significant efforts consist of analysis of mechanical system dynamics comparing low frequency linear superposition approximation method with the exact solution, single degree of freedom RTHS with lightly damped physical and numerical substructures of a mechanical system as well as system identification and compensation of a MDOF servo-hydraulic actuator shake table using feedforward-feedback compensation methods. In addition, two case studies were constructed to demonstrate RTHS for mechanical systems. The first case study consists of experimental verification of a nominal mechanical system using RTHS consisting of a uni-axial transfer system. The second case study is an extension of RTHS for MDOF transfer system using RTHS testing of the same physical substructure coupled to a MDOF numerical substructure. Experimental results demonstrate that RTHS accurately captures the system-level response in a laboratory setting and allows for repeatable tests of various dynamic conditions and potential system improvements to be efficiently examined. The following sections summarize the significant findings and key contributions of each chapter followed by potential directions for future research.

6.1 Significant Findings and Key Contributions

Chapter 2 demonstrated the development and implementation of RTHS for quantification of system level vibration of mechanical equipment systems using the example of a simplified multi stage mechanical system. RTHS was used to interface a physical substructure, notional mechanical equipment, to a notional support structure which was represented numerically forming a multi stage system. This experiment was accomplished by closed-loop RTHS testing using a model-based feedforward-feedback actuator tracking controller with a low pass inverse compensation (LPIC). The consistent results of the RTHS with the full

system experimental test prove that RTHS can accurately represent the dynamics of the coupled system as well as provide insight into the design of mechanical systems using system level mechanical vibration.

Chapter 3 demonstrated a new frequency based substructuring method referred to as Transfer Path Hybrid Substructuring. It was demonstrated that this method is mathematically equivalent to traditional dynamic substructuring. In addition, it was shown that this method can be used to accurately couple physical loading with unknown vibration excitation, with the dynamics of a numerically modeled support structure. This is the main advantage of this method over other substructuring methods since typically it is very difficult to quantify the exact source of the system excitation.

This method does have required conditions. The physical loading should be measured with the physical substructure having a perfectly rigid interface to the test base in the frequency range of interest. This method also requires that the physical substructure transfer function (reactant force due to an applied base motion excitation) can be measured using linear signal processing techniques. This obviously assumes that this substructure is a stationary, ergodic system. In the case study presented in this paper, this was true and the physical substructure transfer function was able to be measured because of the availability of a 6DOF shake table which could be used to apply a base motion and record the reactant forces of the physical substructure. This will typically be cost and time prohibitive so other methods to achieve this transfer function could be a subject of further research.

Chapter 4 described MIMO system identification and model-based feedforward feedback compensation of a six degree of freedom shake table for conducting stable RTHS testing of lightly damped mechanical systems. First, the nonlinear transformation matrix relating the Cartesian degrees of freedom of the shake table to the six individual actuators was linearized. This allowed compensation of the actuator dynamics of the six individual actuators of the shake table to provide effective displacement tracking of the six Cartesian degrees of freedom (i.e., x, y, z translations and rotations) of the shake table. This compensation was accomplished by calculating a MIMO transfer function quantifying the frequency dependent magnitude and time delay. Initial proof of principle test cases show once the actuator dynamics was

quantified, a cascaded feedforward inverse compensation was successfully developed to linearize the actuator dynamics and reduce the inherent time delay.

However, these initial results still showed a significant dependence on commanded displacement levels. Digitally supplemental PID controller proportional gain was added to attempt to reduce this dependence without success. But a new system identification method was introduced, which leverages displacement predictions using frequency based substructuring technique known as Transfer Path Hybrid Substructuring, to mimic the commanded input to the actuators, during the RTHS, during the system identification of the transfer system. This eliminates the concern of the displacement excitation level dependence. Using the same compensation methods used in preliminary test cases, the transfer system was linearized and reduced the inherent time delay. The cascaded feedforward inverse compensation and linearized transformation can be used to perform multiple degree of freedom RTHS testing of lightly damped mechanical systems using the six degree of freedom shake table as part of future research.

Chapter 5 describes the development and implementation of RTHS for quantification of system level vibration of mechanical equipment systems using the example of a multiple degree of freedom multi stage mechanical system. RTHS was used to interface a physical substructure, notional mechanical equipment, to a notional foundation structure which was represented numerically forming a multi stage system. This was accomplished by closed-loop RTHS testing using a model-based feedforward-feedback actuator tracking controller with a low pass inverse compensator (LPIC). The RTHS experiment shows encouraging results, however there are remaining inconsistencies. These results show there are limitations of RTHS for lightly damped mechanical systems which are controlled by the marginal stability of the control loop. However, the promising comparison of the results of the RTHS with the full system experimental test proves that RTHS could accurately represent the dynamics of the coupled system as well as provide insight into the design of mechanical systems using system level mechanical vibration.

6.2 Future Research Directions

The research performed in this dissertation provides a strong foundation for continued advancements of RTHS for mechanical systems. The following are potential future research directions that could be pursued to expand the range of applications for RTHS:

- Servo-hydraulic actuator based transfer systems inherently are limited to a low frequency bandwidth. Therefore, other forms of transfer systems could be examined to increase the practical frequency range of RTHS. Electro-dynamic and piezoelectric actuation offers potential alternatives to hydraulic actuation for increasing the RTHS control band. In addition, an RTHS framework using force-based actuator control with electro-dynamic inertial actuators and accelerometers should be investigated to increase RTHS control band. Another potential advancement from developing force-based RTHS with electro-dynamic inertial actuators and accelerometers could be enabling RTHS of free-free dynamic systems.
- Current stability and performance analysis methods should be advanced to understand the effects of not only absolute stability of feedback systems but also marginal stability of these systems. This research has shown that even though a system is stable doesn't necessarily mean that it is accurate. Research to understand the constraints of marginal stability will help to improve the capabilities of RTHS as well as understand it's accuracy and limitations.
- Since RTHS allows for physical testing of mechanical systems, non-linear physical phenomena can be incorporated into the complete system. However, existing practices of using linear signal processing techniques can negate or remove these non-linear effects due to time segmenting and averaging. Advanced non-linear techniques could be investigated to fully take advantage of the opportunities of RTHS.
- Also, incorporating probabilistic approaches into RTHS could be explored. These methods could be used for evaluating the system-level response of physical hardware components. By using reliability based methods, a probabilistic approach could lead to more robust hardware designs that better

account for potential system variability as well as non-linarites captured by the numerical substructure. In addition, probabilistic methods could be used to include uncertainty from a) measurement noise in the displacement and force feedback signals, b) system identification errors of the actuator dynamics and physical substructure, and c) neglected dynamics of the numerical substructure. Being able to quantify the variability could lead to better transfer system compensation methods which would make RTHS more robust against these uncertainties, and therefore would lead to more reliable test results.

- RTHS could also be expanded to mechanical systems with multi-transmission paths, such as large span structures and systems with multiple attachment supports. This expansion will require multi-actuator and shake tables systems with improved MIMO control algorithms to properly enforce the displacement conditions onto a physical substructure with multi-paths.
- Since the attachment conditions of the physical substructure with the actuator transfer system can influence the stability and accuracy of a RTHS test, new methods should be investigated to remove these effects. The transmission simulator technique being developed for experimental dynamic substructuring should be evaluated as a means to remove the dynamic effects of the attachment conditions from the RTHS feedback loop.

The above topics could lead to further advancements of RTHS, further making it an advantageous method for system level vibration testing of complex hardware components for many different engineering applications. With the above research, RTHS could grow to support various fields of vibration engineering from hardware development to prototype and qualification testing to enable system level testing of critical components and subsystems earlier in the development process prior to full-system verification testing.

7 APPENDIX A – SIMO VS. MIMO SYSTEM IDENTIFICATION

7.1 SIMO System Identification

The cross-coupling of the six-actuators can be calculated and quantified by sending a single actuator a signal and measuring the output of each of the actuators in the MIMO system. Coherence between each of the output signals and the input signal can be calculated. If there is a significant amount of coherence between the input signal and the output signals would indicate if there is cross-coupling or not. This is done by driving each of the actuators one at a time and measuring the output of all the actuators during each test. Each one of these tests creates a column array of transfer functions representative of the SIMO system.

Let G_{xx} be the input auto spectral density, G_{yy} the column array of output auto spectral densities, G_{yx} the column array of cross spectral densities between the input and the outputs, H_{yx} the column array of transfer functions, γ_{yx} the column array of coherences, $\mathbf{H}_{\mathrm{yx}}$ the transfer function matrix and $\boldsymbol{\gamma}_{\mathrm{yx}}$ the coherence matrix.

For n number of inputs and m number of outputs:

$$H_{yx} = \frac{G_{yx}}{G_{xx}} = \begin{Bmatrix} G_{y_1 i}/G_{ii} \\ G_{y_2 i}/G_{ii} \\ \vdots \\ G_{y_m i}/G_{ii} \end{Bmatrix} \qquad \gamma_{yx}^2 = \frac{|G_{yx}|^2}{G_{yy}G_{xx}} = \begin{Bmatrix} |G_{y_1 i}|^2/G_{y_1 y_1}G_{ii} \\ |G_{y_2 i}|^2/G_{y_2 y_2}G_{ii} \\ \vdots \\ |G_{y_m i}|^2/G_{y_m y_m}G_{ii} \end{Bmatrix}^2 \tag{7.1}$$

$$\mathbf{H}_{\mathrm{yx}} = \sum_{i=1}^{n} H_{yx} = \sum_{i=1}^{n} \begin{Bmatrix} H_{y_1 i} \\ H_{y_2 i} \\ \vdots \\ H_{y_m i} \end{Bmatrix} = \begin{bmatrix} H_{y_1 1} & H_{y_1 2} & \cdots & H_{y_1 n} \\ H_{y_2 1} & H_{y_2 2} & \cdots & H_{y_2 n} \\ \vdots & \vdots & \ddots & \vdots \\ H_{y_m 1} & H_{y_m 2} & \cdots & H_{y_m n} \end{bmatrix} \tag{7.2}$$

$$\boldsymbol{\gamma}_{\mathrm{yx}}^{2} = \sum_{i=1}^{n} {\gamma_{yx}}^{2} = \sum_{i=1}^{n} \begin{Bmatrix} \gamma_{y_1 i} \\ \gamma_{y_2 i} \\ \vdots \\ \gamma_{y_m i} \end{Bmatrix}^{2} = \begin{bmatrix} \gamma_{y_1 1} & \gamma_{y_1 2} & \cdots & \gamma_{y_1 n} \\ \gamma_{y_2 1} & \gamma_{y_2 2} & \cdots & \gamma_{y_2 n} \\ \vdots & \vdots & \ddots & \vdots \\ \gamma_{y_n 1} & \gamma_{y_n 2} & \cdots & \gamma_{y_n n} \end{bmatrix}^{2} \quad [7.3]$$

7.2 MIMO System Identification

Consider **X** to be a column vector of the Fourier transforms of *n* the inputs to the system, the commanded actuator displacement, and **Y** is a column vector of the Fourier transforms of the *n* outputs of the system, the measured actuator displacement.

$$\mathbf{X} = \begin{bmatrix} X_1 \\ X_2 \\ \vdots \\ X_n \end{bmatrix} \quad \mathbf{Y} = \begin{bmatrix} Y_1 \\ Y_2 \\ \vdots \\ Y_n \end{bmatrix} \quad [7.4], [7.5]$$

Let $\mathbf{X}^*$, $\mathbf{Y}^*$ be the complex conjugate vectors of **X**, **Y,** respectively, $\mathbf{G}_{\mathrm{xx}}, \mathbf{G}_{\mathrm{yy}}$ the input and output auto spectral density matrices, respectively, $\mathbf{G}_{\mathrm{yx}}$ the cross spectral density matrix between the input and outputs can be determined as

$$\mathbf{G}_{\mathrm{xx}} = E\left\{ \begin{bmatrix} X_1^* \\ X_2^* \\ \vdots \\ X_n^* \end{bmatrix} [X_1 \quad X_2 \quad \cdots \quad X_n] \right\} = \begin{bmatrix} G_{x_1 x_1} & G_{x_1 x_2} & \cdots & G_{x_1 x_n} \\ G_{x_2 x_1} & G_{x_2 x_2} & \cdots & G_{x_2 x_n} \\ \vdots & \vdots & \ddots & \vdots \\ G_{x_n x_1} & G_{x_n x_2} & \cdots & G_{x_n x_n} \end{bmatrix} \quad [7.6]$$

$$\mathbf{G}_{\mathrm{yy}} = E\left\{ \begin{bmatrix} Y_1^* \\ Y_2^* \\ \vdots \\ Y_n^* \end{bmatrix} [Y_1 \quad Y_2 \quad \cdots \quad Y_n] \right\} = \begin{bmatrix} G_{y_1 y_1} & G_{y_1 y_2} & \cdots & G_{y_1 y_n} \\ G_{y_2 y_1} & G_{y_2 y_2} & \cdots & G_{y_2 y_n} \\ \vdots & \vdots & \ddots & \vdots \\ G_{y_n y_1} & G_{y_n y_2} & \cdots & G_{y_n y_n} \end{bmatrix} \quad [7.7]$$

$$\mathbf{G}_{\mathrm{yx}} = E\left\{ \begin{bmatrix} X_1^* \\ X_2^* \\ \vdots \\ X_n^* \end{bmatrix} [Y_1 \quad Y_2 \quad \cdots \quad Y_n] \right\} = \begin{bmatrix} G_{y_1 x_1} & G_{y_1 x_2} & \cdots & G_{y_1 x_n} \\ G_{y_2 x_1} & G_{y_2 x_2} & \cdots & G_{y_2 x_n} \\ \vdots & \vdots & \ddots & \vdots \\ G_{y_n x_1} & G_{y_n x_2} & \cdots & G_{y_n x_n} \end{bmatrix} \quad [7.8]$$

The frequency response function matrix, H_{yx} the and the coherence matrix, γ_{yx}, can then be determined as

$$\mathbf{H}_{yx} = \mathrm{G}_{xx}^{-1}\mathrm{G}_{yx} = \begin{bmatrix} H_{y_1x_1} & H_{y_1x_2} & \cdots & H_{y_1x_n} \\ H_{y_2x_1} & H_{y_2x_2} & \cdots & H_{y_2x_n} \\ \vdots & \vdots & \ddots & \vdots \\ H_{y_nx_1} & H_{y_nx_2} & \cdots & H_{y_nx_n} \end{bmatrix} \quad [7.9]$$

$$\boldsymbol{\gamma}_{yx}^2 = \left[\mathrm{G}_{yy}\mathrm{G}_{xx}\right]^{-1}\left|\mathrm{G}_{yx}\right|^2 = \begin{bmatrix} \gamma_{y_1x_1}^2 & \gamma_{y_1x_2}^2 & \cdots & \gamma_{y_1x_n}^2 \\ \gamma_{y_2x_1}^2 & \gamma_{y_2x_2}^2 & \cdots & \gamma_{y_2x_n}^2 \\ \vdots & \vdots & \ddots & \vdots \\ \gamma_{y_nx_1}^2 & \gamma_{y_nx_2}^2 & \cdots & \gamma_{y_nx_n}^2 \end{bmatrix} \quad [7.10]$$

Using linear superposition, these SIMO systems are assembled into a square transfer function matrix that represents the MIMO system. Figure 7.1 shows the measured diagonal terms of the frequency response matrix of measured to commanded actuator displacement obtained from both SIMO and MIMO system identification testing where the blue line is the MIMO test and the dotted red line is the SIMO test.

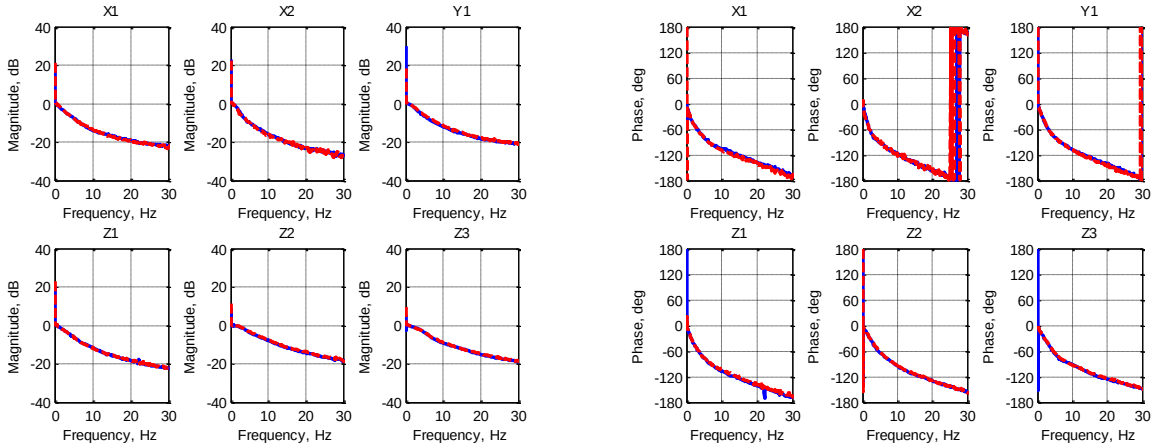

(A) **(B)**

Figure 7.1 - SIMO vs. MIMO System Identification Frequency Response Function Magnitude (A) and Phase (B) Comparison

This comparison proves that the SIMO system identification method is a sufficiently accurate method for quantifying the dynamics of multiple actuators.

8 APPENDIX B

The results of the compensation efforts shown in Figure 5.14 include the following efforts to remove high frequency amplification due to LPIC transfer system compensators. Figure 8.1 shows the results of the initial compensation efforts.

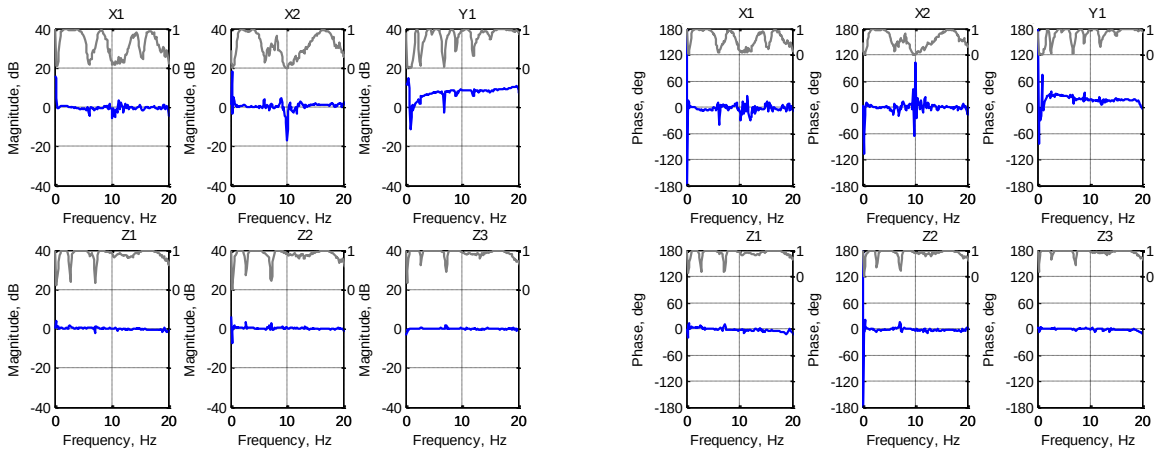

(A) **(B)**

Figure 8.1 - Frequency Response Function Magnitude (A) and Phase (B) of Six Actuators Initially Compensated Using the Hybrid System Identification Approach

These results show encouraging magnitude tracking and minimum time delay. These were initially found to be adequate for the RTHS case study. However, when the high frequency amplitudes were measured, they were found to be significantly larger than expected. Figure 8.2 shows the high frequency response function magnitudes of the six actuators feedforward compensators.

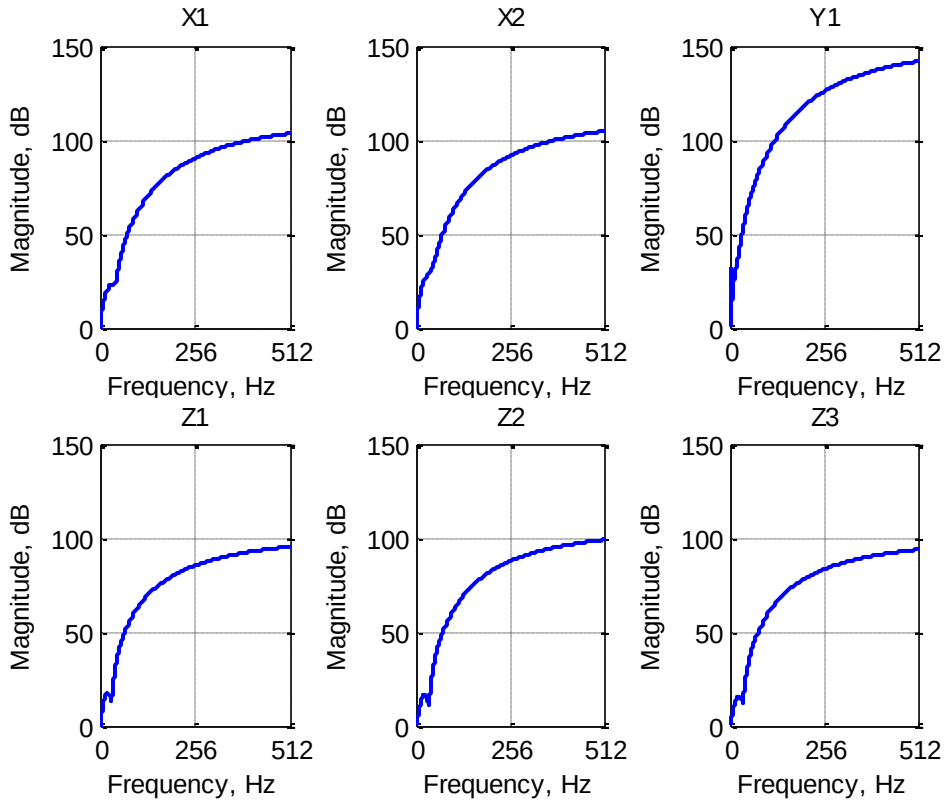

Figure 8.2 – Frequency Response Function Magnitude of Six Actuators Initial Feedforward Compensators

These results show significant amplification outside of the 0-20Hz frequency range that most previous compensation studies as a part of this research have been focused on. As stated before that it has been assumed, since there is negligible BLWN excitation to the physical substructure during the RTHS, this application would also be negligible. However, because of instrumentation noise, there is a certain level of energy at all frequencies within the Nyquist frequency range, referred to as the noise floor. During the system identification of the transfer system, this noise floor was recorded up to the Nyquist frequency and the results of this are shown in Figure 8.3.

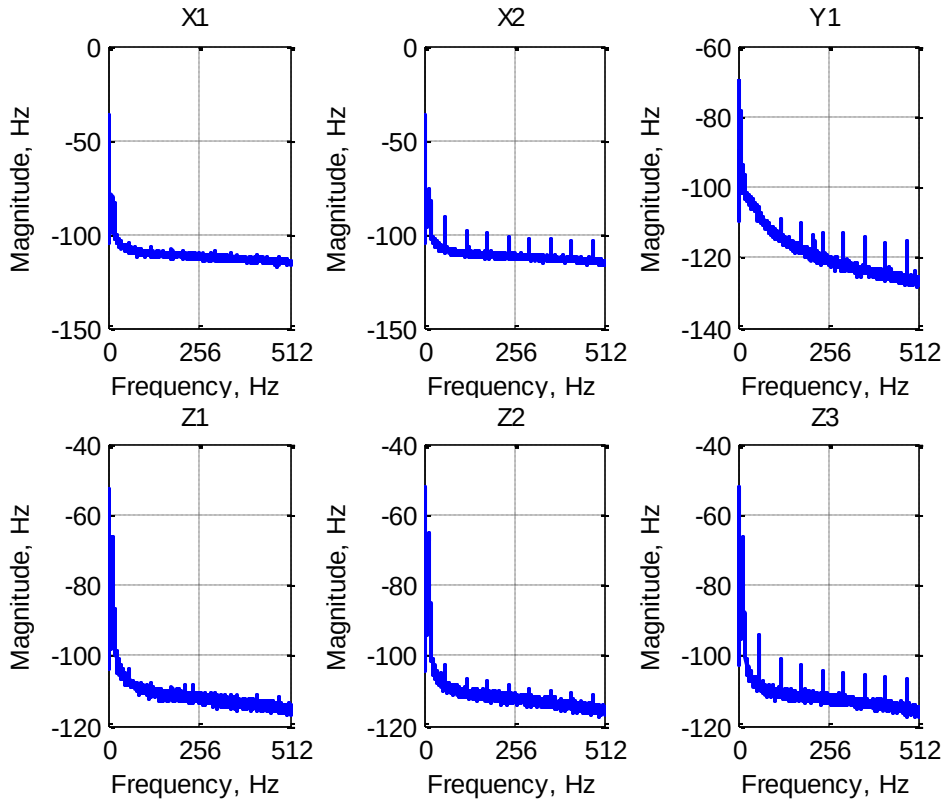

Figure 8.3 –Noise Floor Measurements Up to Nyquist Frequency

Considering this noise floor, combined with the significant amplification of the feedforward compensator, the energy and the high frequency range becomes substantial. Generally, it seems that the energy at these higher frequencies would actually be greater than the energy at the low frequency range of interest. Because of this, the existing LPIC compensators were abandoned and further effects were made to minimize the high frequency energy while mimicking the low frequency compensation performance.

Previously, the curve fit the data with a Laplace domain transfer function, the MATLAB function *invfreqs* was used which uses a least-mean-square optimization algorithm to find the best numerator and denominator of a transfer function that best fits the data input into the function. The practice has been to input only the data from the frequency range of interest to ensure the best fit for that set of data. As previously, stated it was assumed that the transfer function performance outside this frequency range could be ignored. Because of this assumption, the given transfer functions typically had high frequency

performance as shown in Figure 8.2. In order to have more control over the control curve fitted Laplace domain transfer function, a manual curve fitting approach was adopted.

Based on previous research, it was generally assumed that a transfer function with a constant numerator and a third order denominator would give a sufficient Laplace domain curve fit. The form of the curve fit is given as

$$A(s) = \frac{a}{s+a} \cdot \frac{\omega_n^2}{s^2 + 2\zeta\omega_n s + \omega_n^2} \qquad [8.1]$$

Through trial and error, suitable values for a, ω_n, and ζ were selected for each actuator. According to the feedforward low pass inverse compensation method, this expression for A is inverted and then convolved with a low pass filter, L in order to balance the inverse of A. L was of the same form as shown in Equation [5.9] but the values for each of the parameters weren't necessarily the same as the values used for A, respectively. However, this L has its own dynamics which affect the performance of the system. Since L has been designed, its dynamics are obviously known so they can be accounted for. Figure 8.4 shows the uncompensated system identification data along with the curve fits of the data.

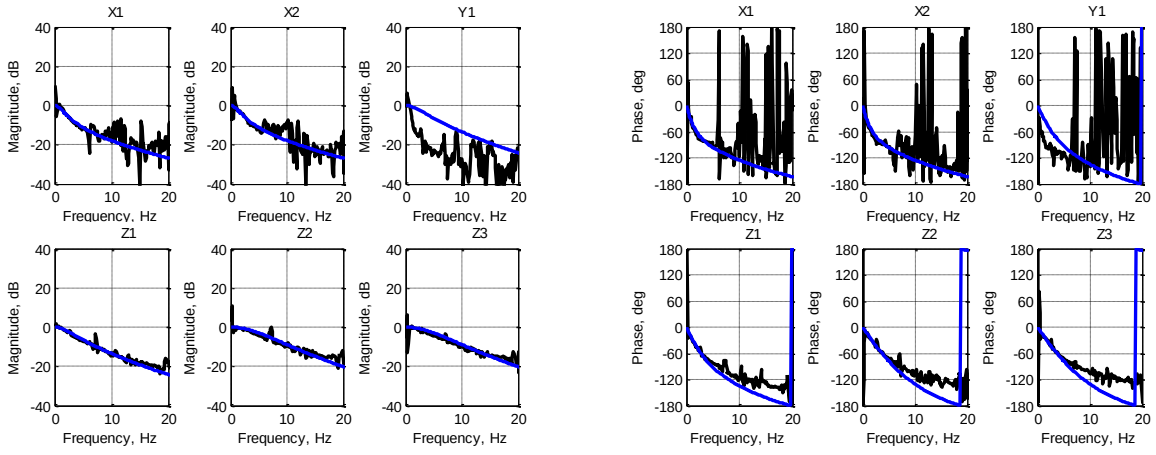

(A) **(B)**

Figure 8.4 – Frequency Response Function Magnitude (A) and Phase (B) of Six Actuators Uncompensated Along with Curve Fit Results

The curve fits shown include the known dynamics of L. The effect of L on the magnitude is negligible, therefore the curve fits line up with the data fairly well. However, the effect of L on the phase is more

significant, therefore it can be seen that the curve fits shown do not match the test data. This is because the curve includes the dynamics of L so when the curve fit is inverted and then convolved with L; the dynamics of L are essentially cancelled out. The high frequency content of this compensator was then examined and is shown in Figure 8.5.

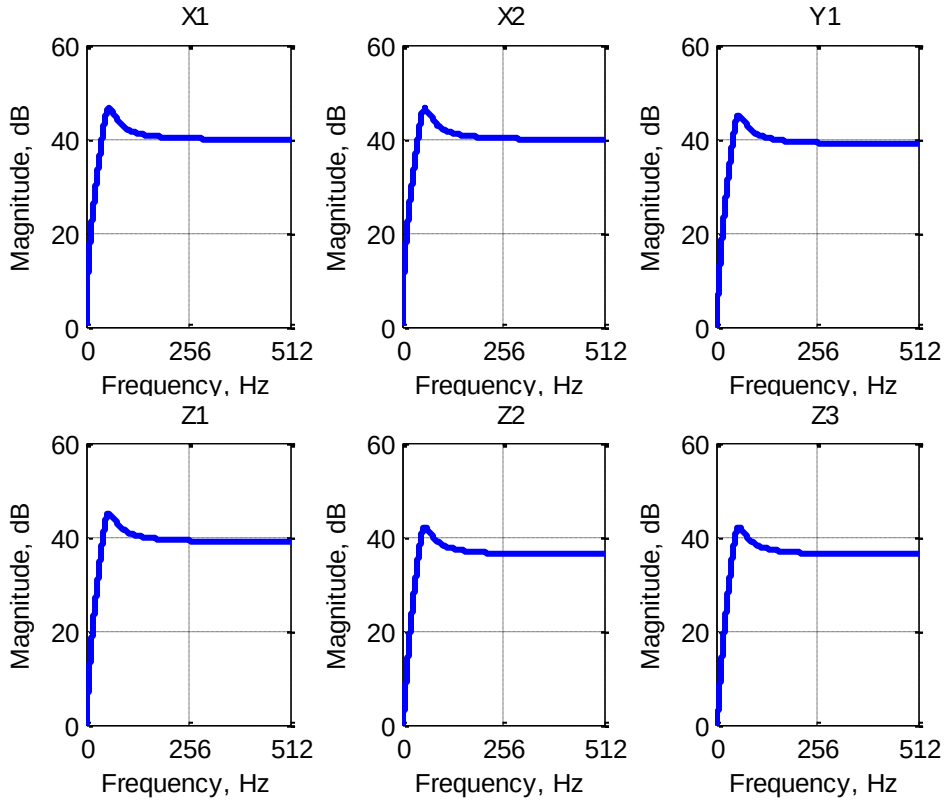

Figure 8.5 – Frequency Response Function Magnitude of Six Actuators Updated Feedforward Compensators

These results show an improvement in the high frequency content of the feedforward compensators over the results shown in Figure 8.2. 40dB of amplification was considered sufficiently low because when combined with the noise floor of the actuators shown in Figure 8.3, the high frequency levels were still relatively low amplitude compared to the low frequency amplitudes. The dynamics of the transfer system were retested with this compensator present and the results of this test are shown in Figure 8.6.

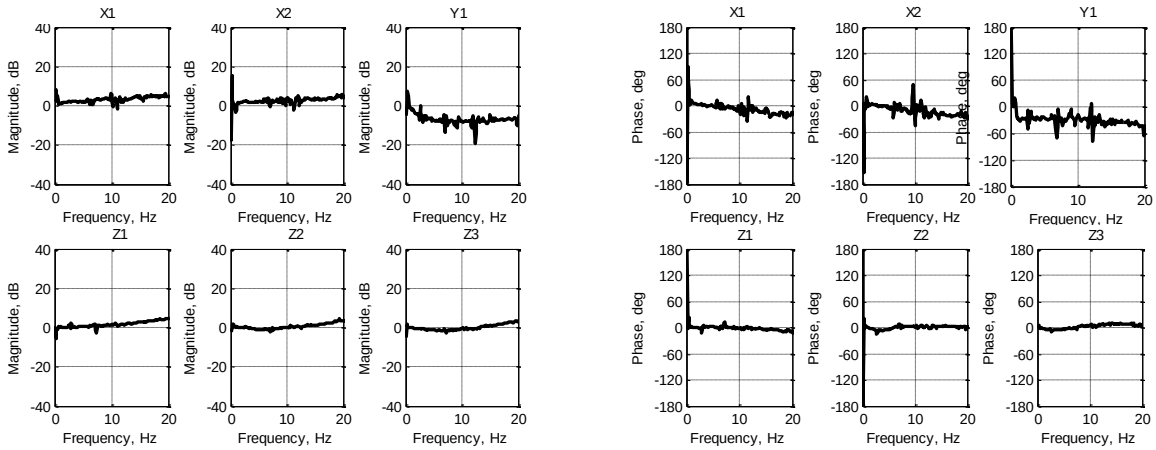

Figure 8.6 – Frequency Response Function Magnitude (A) and Phase (B) of Six Actuators Compensated Using the Hybrid System Identification Approach

As with previous compensation efforts with this transfer system, an iterative compensation method is necessary. This is due to the commanded displacement becoming a lot larger in at some frequencies to compensate for the frequency dependent attenuation in magnitude. Because the actuators are commanded a significantly larger displacement than the initial system identification, the dynamics of the system change. The initial compensator may no longer be sufficient to achieve the desired actuator dynamics and additional system identification is necessary. With the cascaded feedforward compensation method, typically multiple feedforward compensators are convolved together to achieve the desired reference tracking results. This issue with this approach is that when there are multiple feedforward compensators, each one contains its own high frequency amplification and when multiple compensators are convolved together, this becomes multiplication in the frequency domain and addition in the frequency domain decibel scale, i.e., the high frequency amplification of each of the multiple feedforward compensators is summed together to give even greater high frequency amplification. It would be better to iteratively replace the feedforward compensator instead of adding to it.

The results shown in Figure 8.6 are a measure of the amount of magnitude and phase by which the original compensator needs to be adjusted. Since the original compensator is known, it can be removed from the data by dividing (or subtracting decibels) the measured data by the compensator's transfer

function in the frequency domain. This theoretically gives an updated measure of the uncompensated transfer function of the transfer system. The results of this calculation are shown in where the black lines are the same data shown in Figure 8.6 and the blue lines are the result of removing the original compensator from the data shown in black.

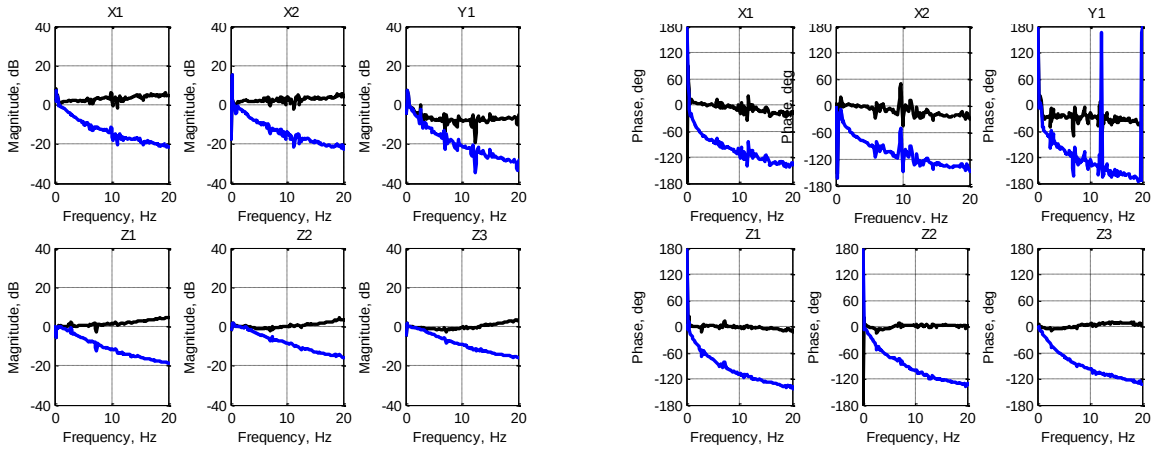

(A) **(B)**

Figure 8.7 – Frequency Response Function Magnitude (A) and Phase (B) of Six Actuators Compensated and Updated Uncompensated

These updated measurements of the uncompensated dynamics of the transfer system are used to build a new feedforward compensator to replace the original. As before, a low pass filter, *L* is built to balance the inverse of the curve fit of this data. Again, this *L* affects the dynamics of the compensator and since these dynamics are known, they can be compensated for by convolving L with this data shown in

(A) **(B)**

Figure 8.7. This was done and the resulting data is shown in Figure 8.8 where the black lines are the original measured data, the blue lines are the result of removing the original compensator from the data shown in black and the red lines are the blue lines convolved with the transfer function of *L*.

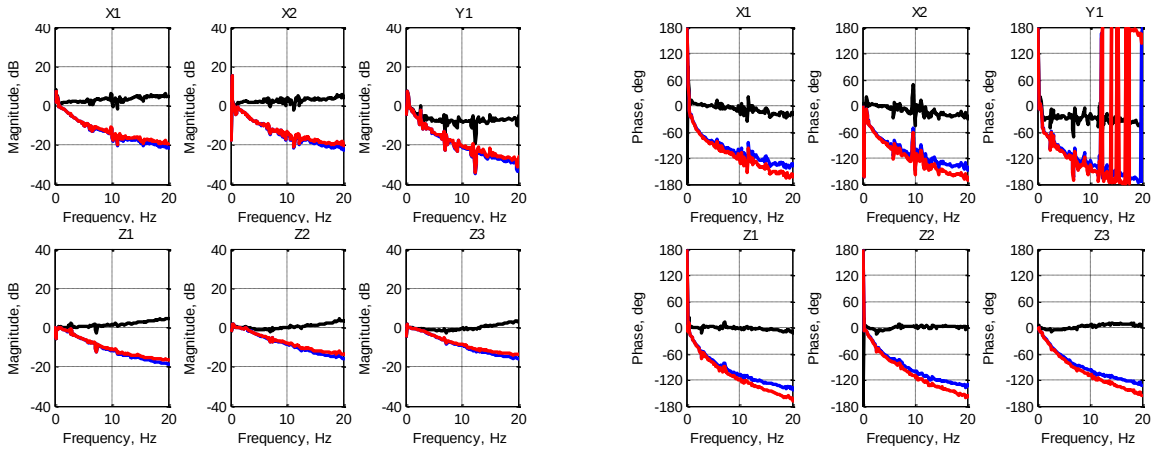

(A) **(B)**

Figure 8.8 – Frequency Response Function Magnitude (A) and Phase (B) of Six Actuators Compensated and Updated Uncompensated

The red data shown in Figure 8.8 was curve fit, inverted, and then convolved with the low pass filter as before. Also, as before, the high frequency content was examined and is shown in Figure 8.9.

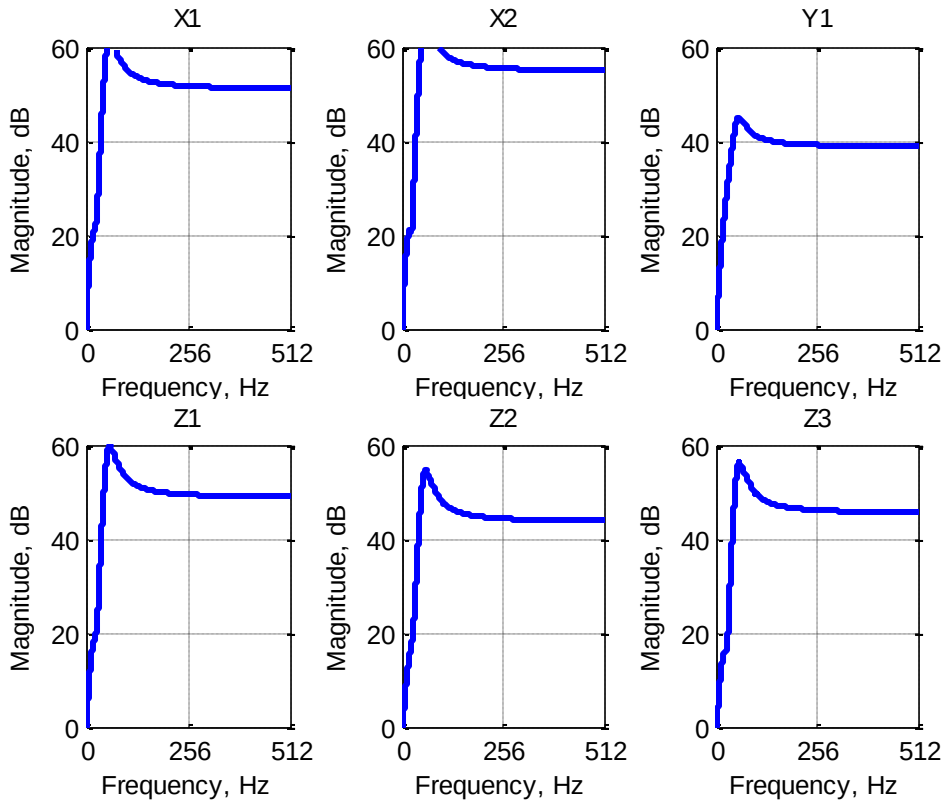

Figure 8.9 – Frequency Response Function Magnitude of Six Actuators Updated Feedforward Compensators

This data shows an increase in the high frequency amplitude of this compensator over the original compensator; however it is still sufficiently low, considering the noise floor of the transfer system. This new compensator was used in the re-testing of the transfer system and the new measured dynamics are shown in Figure 8.10 where the blue lines are the measured FRFs and the black lines are the uncompensated FRFs.

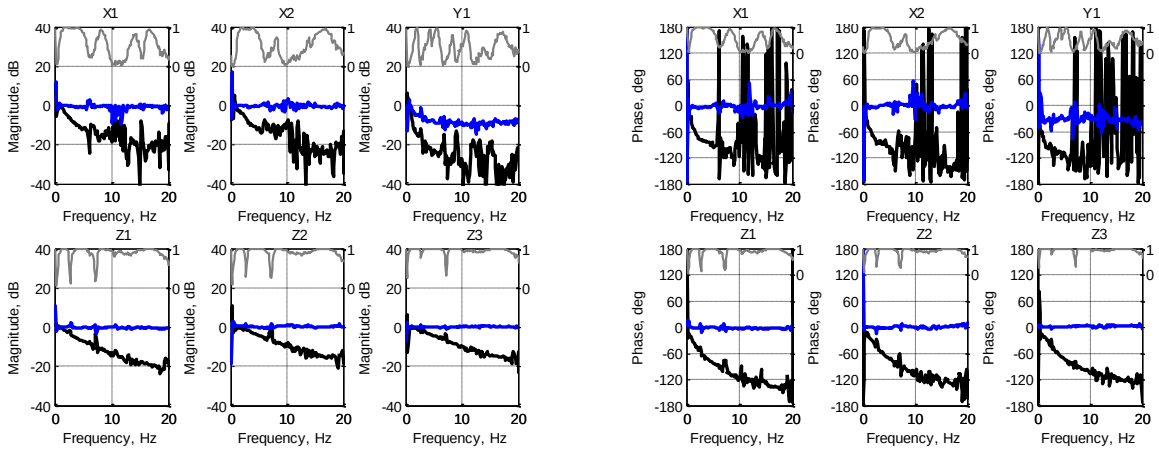

(A) **(B)**

Figure 8.10 – Frequency Response Function Magnitude (A) and Phase (B) of Six Actuators Compensated with Payload Using the Hybrid System Identification Approach

Also, to verify sufficiently low amplitude high frequency content, the spectrums of the measured displacements of the transfer system were recorded and examined and are shown in Figure 8.11.

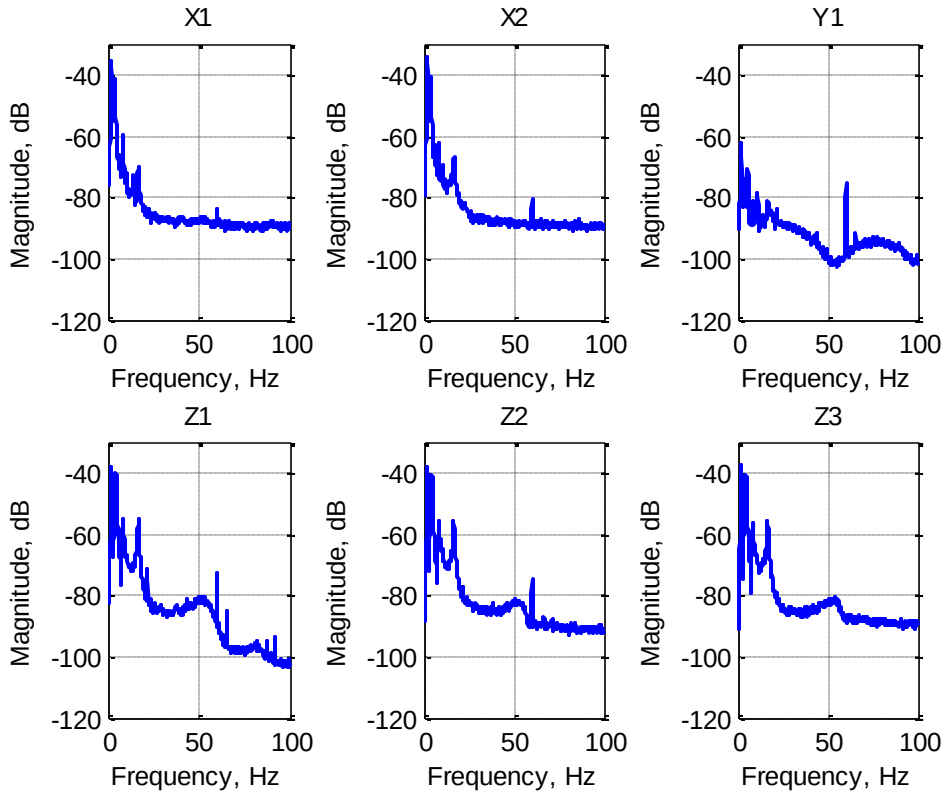

Figure 8.11 - Frequency Response Function Magnitude of Six Actuators Measured Displacements

The results, shown in Figure 8.10 and Figure 8.11 show sufficient transfer system performance after two iterations of system identification and compensation. Figure 8.10 shows sufficient reference tracking with magnitude tracking within ±1dB and time delay less than 1ms. Figure 8.11 shows some high frequencies over the noise floor shown in Figure 8.3, however, the relative level to the low frequency amplitudes is sufficiently lower so this performance is also seen as sufficient for RTHS experimentation. The results shown in Figure 8.10 show the magnitude and phase of the final compensator used during the RTHS test and are the same results shown in Figure 5.14.